GRAPHENE-BASED TEXTILE FIBRE SENSORS

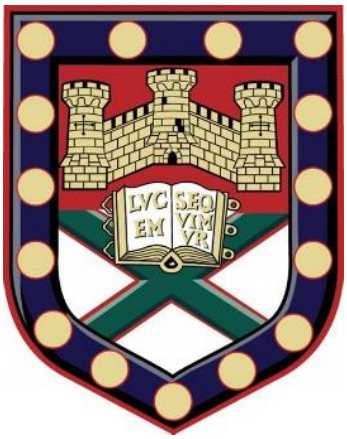

Submitted by Gopika Rajan to the University of Exeter as a thesis for the degree of Doctor of Philosophy in Engineering, April 2021

Supervised by Dr. Ana Neves & Prof. Monica Craciun

I certify that all material in this thesis which is not my own work has been identified and that no material has previously submitted and approved for the award of a degree by this or any other university.

……

Gopika Rajan

ABSTRACT

The challenges of conventional wearable technology have been overcome to a vast extent by the rapid strides in flexible technology. However, the integration of the flexible devices in the textile industry still includes challenges like the heaviness and rigidity of electronic components, lack of washability, and high operating power. In this thesis, these challenges have been addressed with the fabrication of textile-based devices consisting of lightweight, flexible, washable, and bendable materials. Here, graphene-coated monofilament polypropylene (PP) textile fibres have been presented for their use as textile-based temperature and humidity sensors. A detailed analysis of the transient response of temperature and humidity on the resistance of different types of graphene-coated fibres is presented. These include chemical vapour deposition (CVD) of graphene and graphene produced from the shear exfoliation of graphite (SEG). Trilayer graphene (TLG) grown on copper by CVD along with carbon paste as contacts displays better sensitivity and reliability in response to temperature. These TLG-sensors show a negative thermal coefficient of resistance (TCR) in the human body temperature range of 30-45 °C. The TLG-coated PP fibres also show better mechanical stability, washability, and transparency as compared with SEG-coated PP fibres. The TLG and SEG-based sensors show increase and decrease in conductivity with the increase in humidity levels, respectively, with TLG exhibiting faster response and recovery than a commercial humidity sensor. The demonstrated textile-based sensors can function in operating voltages as low as 0.5 V, suggesting low operating power applications. The presented results demonstrate flexible and lightweight temperature and humidity sensors which can be used to continuous monitoring of temperature and humidity levels and can be seamlessly integrated into most of the textile-based applications especially clothing or upholstery with no heavy, fragile, or toxic materials and components involved in the fabrication process.

“I would rather have questions that cannot be answered than answers which can’t be questioned”

Richard Feynman

Dedicated to:

Ana Neves

&

George Crosland

Two of the most honest, compassionate, and wise humans I have ever met. I am forever indebted to the two of you.

ACKNOWLEDGMENTS

Isaac Newton once said,

'If I have seen further than others, it is by standing on the shoulders of giants.'

A Ph.D. is not just about the thesis we submit or the papers we publish as often perceived by those around us. To me, it is the years of constant climbing on a lonely steep path like a mountain goat who, to avoid falling, keeps going. The journey is not without fear, pain, loss, and despondency. The repeated failures make us constantly underestimate our intelligence and strength. However, if we look around, we find that we are not alone on the path. There are many who help us get to the top of the hill. All we need to do is ask. Everyone acknowledged in this section have been responsible for this thesis in more ways than mentioned. They are the ones who happily shared their experiences and wisdom without hesitating or looking at the clock. I am a better scientist, a better student, a better teacher, and a better person because of each one of them.

A million thanks:

To the **University of Exeter**, for granting me the Ph.D. studentship, without which none of this would have been possible.

To my sister, **Padmeeca Rajan**, for supporting me in and out.

To **Ajay Dhar**, for always being available whenever I needed a fatherly advice.

To **George Crosland**, who taught me the skill of logical and critical thinking, asking the right questions, and not giving up until I find the right answer.

To **Monica Craciun**, who was not only one of my supervisors throughout and was always available despite being very busy, but also who taught me how to be humble yet proud of my accomplishments, be calm and keep smiling when we hit a wall.

To **Peter Armitage**, who showed me how to embrace my inner creativity and keep creating, inventing, designing new things in addition to helping me design the measuring setups in this thesis.

To **Hong Chang**, who taught me the value to diligent communication no matter how smaller the task is.

To **Mark Heath**, who was always be willing to help with any experimental modifications in the clean room.

To **Ellen Green,** who taught me the value of soft yet powerful speech and would always take time out of her busy schedule to help me with the Raman spectroscopy measurements.

To **Chris Forrest**, who would always solve any IT issues I would face.

To **Joe, Elias, Shin, Kieran, Jessica, and Conor**, who are not only my co-authors in the published papers but were always available to help me with all sorts of weird scientific questions I would get stuck up with.

To **Anna Ott**, for teaching me how to listen without defending and speak without offending, with whom I spent very little time, but it felt as if we had known each other forever.

To **all the project students** I had the privilege of working with, who turned me into a team-leader and team-player.

To **Victoria García Rocha, Junning Chen, and Aziz Mustafa**, for making me comfortable during the scariest examination of my life (viva exam).

Finally, and the most importantly to **Ana Neves**, who is the best supervisor I could have hoped for, who encouraged me to overcome my speech constraints that led me to engage in scientific public speaking, who taught me the art of working with others instead of against them, who taught me how to use well what we have and find alternatives for what we don't, who was more than patient with me than I could have asked for and gave me more chances than I deserved, who helped me deal with all the personal struggles a doctoral researcher deals with, who always encouraged me to connect with my peers and not be afraid of expressing my emotions, who taught me how to teach others while learning from them, who taught me the importance of acknowledging our limited knowledge and willingness to learn a new skill, who showed me the perfect balance between informality and formality, who pushed me to be detail-oriented, who trained me in the art of writing official emails, who taught me how to be

grateful and humble enough to thank when helped and gracious enough to apologise when we do something wrong, who taught me the art of note-taking and proper documentation, who was always available for a chat, who always replied to my emails even while being extremely busy, who has been the greatest critic to my work, eventually shaping me into the scientist I am today.

Gopika Rajan

TABLE OF CONTENTS

ABSTRACT……iii

ACKNOWLEDGMENTS……...ix

TABLE OF CONTENTS……xiii

LIST OF ACRONYMS……..xvi

LIST OF PUBLICATIONS AND
CONFERENCES……xviii

1 INTRODUCTION **1**

2 LITERATURE REVIEW **5**

2.1 WEARABLE TECHNOLOGY 5

2.1.1 E-TEXTILES…… 6

2.1.2 POLYPROPYLENE……10

2.2 GRAPHITE, GRAPHENE & GRAPHENE OXIDE 12

2.2.1 INTRODUCTION, PROPERTIES, AND APPLICATIONS 12

2.2.2 GRAPHENE PRODUCTION 14

2.2.3 GRAPHENE TRANSFER 21

2.2.4 RAMAN SPECTROSCOPY FOR
GRAPHENE CHARACTERISATION 24

2.3 PREVIOUS WORK ON GRAPHENE-COATED
POLYPROPYLENE FIBRES 27

2.4 TEMPEATURE SENSORS 31

2.5 HUMIDITY SENSORS 36

3 METHODOLOGY **41**

3.1 INTRODUCTION 41

3.2 TEXTILE FIBRES 41

3.3 GRAPHENE PRODUCTION 42

3.3.1 CHEMICAL VAPOUR DEPOSITION 42

3.3.2 SHEAR EXFOILATION OF GRAPHITE 45

3.3.3 GRAPHENE OXIDE 46

3.4 GRAPHENE TRANSFER 46

3.4.1 CVD-GRAPHENE TRANSFER 47

3.4.2 TRANSFER OF GRAPHENE FROM SHEAR EXFOILATION OF GRAPHITE 50

3.4.3 TRANSFER OF GRAPHENE OXIDE 51

3.5 PATTERNING OF GRAPHENE 51

3.6 CHARACTERISATION TECHNIQUES 53

3.6.1 RAMAN SPECTROSCOPY 53

3.6.2 ELECTRICAL CHARACTERISATION 54

3.6.3 RESILIENCE TESTS 56

3.6.4 ATOMIC FORCE MICROSCOPY 57

3.6.5 SCANNING ELECTRON MICROSCOPY 57

3.6.6 TRANSMITTANCE STUDIES 58

3.7 TEXTILE HUMIDITY SENSOR: FABRICATION AND SENSING TESTS 59

4 CHARACTERISATION OF GRAPHENE-COATED TEXTILE FIBRES **61**

4.1 INTRODUCTION 61

4.2 CHARACTERISATION OF GRAPHENE 61
4.2.1 SINGLE-LAYER GRAPHENE 61
4.2.2 TRILAYER GRAPHENE 63
4.2.3 FEW-LAYER GRAPHENE 67
4.2.4 GRAPHENE FROM SHEAR EXFOILATION OF GRAPHITE 67
4.3 GRAPHENE-COATED PP FIBRES 71
4.4 ATOMIC FORCE MICROSCOPY 72
4.5 ELECTRICAL CHARACTERISATION 75
4.6 RESILIENCE TESTS 76
4.7 SUMMARY 79
5 BODY WEARABLE TEMPERATURE SENSORS 81
5.1 INTRODUCTION 81
5.2 FABRICATION AND MEASUREMENT METHODOLOGY 82
5.3 RESULTS AND DISCUSSION 83
5.4 SUMMARY 94
6 TEXTILE FIBRE-BASED HUMIDITY SENSORS 95
6.1 INTRODUCTION 95
6.2 FABRICATION AND MEASUREMENT METHODOLOGY 96
6.3 RESULTS AND DISCUSSION 100
6.4 SUMMARY 105
7 CONCLUSION AND OUTLOOK 107
BIBLIOGRAPHY 111

LIST OF ACRONYMS

AFM	Atomic force microscopy
APCVD	Atmospheric pressure chemical vapour deposition
ASTM	The American Society for Testing and Materials
B2B	Batch-to-batch processing
CNTs	Carbon nanotubes
CVD	Chemical vapour deposition
DIW	De-ionised water
$FeCl_3$	Iron(iii) chloride
FLG	Few-layer graphene
FWHM	Full width at half maximum
GO	Graphene oxide
IPA	Isopropanol
IDT	Isopropanol direct transfer
LED	Light-emitting diode
LPCVD	Low pressure chemical vapour deposition
LPE	Liquid-phase exfoliation
NMP	N-methyl-2-pyrrolidone
PDMS	Polydimethylsiloxane
PE	Polyethylene

PEDOT:PSS	Poly(3,4-ethylenedioxythiophene) polystyrenesulfonate
PET	Polyethylene terephthalate
PLA	Polylactic acid
PMMA	Poly(methyl methacrylate)
PP	Polypropylene
PTFE	Polytetrafluoroethylene
R2P	Roll-to-roll processing
R_C	Contact resistance
RTD	Resistance temperature detector
RF	Radio-frequency
RFID	Radio frequency identification
R_G	Resistance of graphene
rGO	Reduced graphene oxide
RH	Relative humidity
SEG	Shear exfoliation of graphite
SEM	Scanning electron microscope
SiO_2/Si	Silicon dioxide/silicon
SLG	Single-layer graphene
TCR	Thermal coefficient of resistance
TLG	Trilayer graphene
UVO	Ultraviolet-ozone

LIST OF PUBLICATIONS AND CONFERENCES

Publications:

1. Rajan, G, Morgan, JJ, Murphy, C, Torres Alonso, E, Wade, J, Ott, AK, Russo, S, Alves, H, Craciun, MF, and Neves, AIS, Low Operating Voltage Carbon-Graphene Hybrid E-textile for Temperature Sensing, 2020, *ACS Appl. Mater. Interfaces* 12 (26), 29861- 29867. https://doi.org/10.1021/acsami.0c08397.
2. Torres Alonso, E., Shin, DW., Rajan, G., Neves, AIS., Russo, S., and Craciun, MF., Water-Based Solution Processing and Wafer-Scale Integration of All-Graphene Humidity Sensors, 2019, *Adv. Sci.* 6 (15), 1802318. https://doi.org/10.1002/advs.201802318.
3. Rajan, G, Guillotel, S, Torres Alonso, E, Ott, AK, Craciun, Neves, AIS, Low operating voltage carbon-graphene hybrid e-textile for humidity sensing, 2022. [Unpublished work]

Conferences:

1. Rajan, G, Graphene-based textile temperature and humidity sensors, *innoLAE 2020: Innovations in Large-Area Electronics,* January 2020 held at Cambridge, UK (Poster).
2. Rajan, G, Graphene-based textile devices, *13th International Symposium on Flexible Organic Electronics*, July 2019 held at Thessaloniki, Greece (Oral).
3. Rajan, G, Graphene-based textile sensors, *International Women in Engineering Day*, June 2019 held at Exeter, UK (Poster).

4. Rajan, G, Graphene-based textile sensors, *Materials for Clean Energy Conference*, April 2019 held at National Physical laboratory, UK (Poster).
5. Rajan, G, Graphene-based textile devices, *International Women in Engineering Day*, June 2018 held at Exeter, UK (Poster).
6. Rajan, G, Graphene-based textile devices, *Royal microscopical society*, April 2018 held at Exeter, UK (Poster).
7. Rajan, G, Graphene based conductive textile fibres, *Recent Appointees in Material Science*, September 2017 held at Exeter, UK (Poster).
8. Rajan, G, Graphene-based conductive fibres, *11th International Nanoscience Student Conference*, August 2017 held at Bristol, UK (Poster).
9. Rajan, G, Graphene-based conductive fibres, *International Women in Engineering Day*, June 2017 held at Exeter, UK (Poster).

Chapter 1

INTRODUCTION

1.1 MOTIVATION AND OBJECTIVES

Wearable technology has become an important part of our everyday lives, from the watches worn on the wrist to the blood pressure monitor on the arm. With the end user industries of this technology including sports, military, fashion, medical and entertainment, the cost of production and operation, the environmental impact, comfort of the user, durability and reliability are the major factors to be considered before commercialising a certain wearable device. The current challenges of this quickly emerging field include the lack of flexibility and washability, high cost of production and operation, fragility and use of toxic materials to manufacture the devices. Over the last few years, significant improvement in flexible technology, especially e-textile technology, has paved a way to overcome most of the mentioned challenges. However, the cost of operation, environmental concerns, and resilience of the wearable devices remain an important concern in the industries.

The motivation for this thesis began as the investigation into the use of graphene as a conductive material for the purpose of sensing in textile fibres, a foundation laid by the work done by Neves *et al*.[1,2] and Torres Alonso *et al.*[3,4] towards the production of graphene-based conductive textile fibres and their application as various sensors. This began with the literature review of the most studied sensors based on graphene, the other materials required in fabricating the sensors and the substrates. Graphene is highly conductive, lightweight, and flexible which are the essential qualities required for the success of e-textile technology. It was found that there are not many reports for textile-based temperature and humidity sensors which are based on graphene. Although graphene oxide (GO)[5] and reduced graphene oxide (rGO)[6] have been used in several reported temperature and humidity sensors, their production requires the use of toxic chemicals and are not easily scalable without the production of large amounts of chemical waste. Furthermore, the fabrication of most of these sensors often requires multiple steps, which would affect the cost-effectiveness of the finished

e-textiles. The reduction of the production steps of textile sensors became the first objective of the work conducted. This approach required a detailed study of different types of graphene (produced by various scalable methods) to find out the best type to be used as the sensing layer in the temperature and humidity sensors.

Although graphene has high electronic mobility and high electrical conductivity for a single-atom thick material, its conductivity is often not sufficient for large area sensing applications and might require high operating voltages which are not ideal for wearable technology especially for the application in close contact to the human skin. Textile sensors with low operating voltage, thus, became the second objective which was obtained by purposely producing graphene by chemical vapour deposition (CVD) process with more than a single layer of graphene. The third objective was to produce washable and durable e-textiles which has been one of the hindrances for the successful commercialisation of e-textiles. Most of the reported e-textiles required heavy, rigid, and fragile electronic components mounted on them which are not washable, durable aesthetic or comfortable. Neves *et al.* produced conductive fibres based on graphene which do not require mounting of separate electrical components, electrodes, conductive threads, or wires[1]. This meant that these conductive fibres are the entire electronic device on their own, entirely removing the need to use rigid electronics components, making fourth objective to produce sensors which are lightweight, flexible, and completely integrated within the clothing or the apparel.

1.2 CONTRIBUTIONS

The work carried out in this thesis makes a key improvement towards the development of textile-based temperature and humidity sensors. In this section the problems associated with the successful commercialisation of the e-textiles and the author's contribution to the potential solutions have been mentioned below:

(1) High operating voltage requirement: The sensors demonstrated in this thesis requires very low voltage which would ease their integration into the clothing and reduce the overall cost of operation.

(2) Complex fabrication process: The demonstrated sensors have a simple device architecture without using any toxic or rare material or additional complex techniques

such as soldering or lithography steps, which simplifies the fabrication process as well as reduces the cost of production of these sensors.

(3) Durability and washability of e-textiles: The graphene-coated textiles fibres were subjected to a series of resilience tests and exhibited long term washability and durability.

(4) Use of heavy and rigid electronic components: Due to the lightweight and flexible nature of graphene-coated textile fibres, the studied textiles are themselves the sensors without the need of additional electrodes or wiring and can seamlessly be incorporated in the clothing, linen, or apparels.

1.3 THESIS STRUCTURE

This thesis has been structured in the following manner.

Chapter 2 provides a detailed account of the background and review of literature to the work undertaken in this thesis. The chapter begins with an overview of wearable technology and the drawbacks of the current wearable electronic devices, followed by an overview of flexible electronics and e-textiles as a potential alternative to the conventional wearable devices, including the fundamental issues and possible solutions in the integration of electronics in textiles. The next section introduces graphene, reviews its production by various methods and techniques often used to use graphene to produce conductive textiles. The chapter ends with a detailed literature review of the previously reported temperature and humidity sensors along with their limitations.

Chapter 3 describes all the tools and methodologies employed to produce graphene-based textile fibres and their further application in the fabrication of textile-based temperature and humidity sensors. The methods employed for the characterisation of graphene-coated fibres by spectroscopic, electrical, microscopic, and resilience-testing have also been mentioned in the chapter.

The next three chapters provide the characterisation and applications of the studied conductive textile fibres, solely carried out by the author. Each of these chapter begins with a brief introduction and motivation of the work carried out, followed by the results

obtained from the experimentation and ends with a detailed discussion of the obtain results.

Chapter 4 includes the bulk of the experimental work carried out in this thesis and provides a detailed characterisation of different types of graphene and the graphene-coated textile fibres.

One of the applications of graphene-coated textiles fibres have been demonstrated in Chapter 5 as textile-based temperature sensors as an alternative to the conventional rigid temperature sensors available for sensing the temperature of the human body. The temperature sensing behaviour of the temperature sensors fabrication by using different types of graphene produced by CVD and shear exfoliation of graphite (SEG) have been compared. Two different contact materials have also been compared for their flexibility and durable adhesion to the textile fibres.

Chapter 6 reports another potential application of graphene-coated textile fibres as textile-humidity sensors. The humidity sensing behaviour of graphene produced by CVD and SEG has been compared. The chapter emphasis on the simple device architecture which leads to cost-effective production of these devices in terms of commercialisation as opposed to the flexible humidity sensors reported in the literature.

To conclude the thesis, Chapter 7 contextualises and reiterates the findings of this work along with the future scope.

Chapter 2

LITERATURE REVIEW

2.1 WEARABLE TECHNOLOGY

Wearable technology is one of the current revolutionary advancements which relates to devices that are small and light enough to be carried on one's body as hands-free gadgets, fixed firmly on the skin or embedded in the clothing to facilitate the everyday life. This new industrial sector has numerous applications in the field of healthcare, military, sports, security apparel, consumer electronics, and fashion[7]. For instance, in the case of healthcare, the innovations include wearable technology for rehabilitation[8], fall detection[9], and activity recognition[10]. These wearable devices, or wearables, have distinctive features such as the hands-free function, portability, comfort and multifunctionality in addition to immediate and remote services with a greater degree of accuracy[11].

The global market for wearables was valued at 32.63 billion US dollars in 2019 and is expected to expand from 2020 to 2027 at an compound annual growth rate of 15.9%[12]. The increasing concerns of chronic diseases, including obesity, has driven to the adoption of wearable products as activity trackers, and other body monitors which can offer real-time information about the overall health of the user. These include blood pressure and sugar levels, oxygen levels, quantity and quality of sleep, cholesterol level, and pulse rate among other required information[12]. Wrist bands such as Samsung Gear S2[13], FitBit Sense[14], chest straps such as Wahoo TICKR X[15], eyewear such as Google Glass[16], and footwear such as LECHAL GPS[17] are few examples which assist the users to understand their sleep cycles, move and eat better.

The adoption of conventional wearable devices for daily use is not without various barriers such as high cost, rigidity, short battery life, discomfort, heaviness while being cold to touch. There is a drive now to directing resources towards developing wearables with flexibility, reasonable cost, and comfort. This target has been supported

greatly by the emergence of flexible technology which involves the use of flexible substrates and materials.

The wide variety of applications of flexible technology includes flexible light-emitting devices[18], flexible memory[19], e-skin[20] in biomedical technology, sensors[21], electrodes[22], and conformable RFID tags[23]. By the simple substitution of rigid materials for deformable and flexible materials, flexible technology solves some of the drawbacks of the conventional wearable technology. Flexible devices are relatively light, and entail the ability to undergo large mechanical deformation, such as twisting, bending, folding, stretching, and deforming into more complex shapes still maintaining the high performance of the devices. These properties require materials which can be used to fabricate devices that offer great flexibility and durability.

One of the common materials used in traditional electronic industry is silicon which is intrinsically rigid. Therefore, finding materials to substitute silicon is of great importance. Some of the silicon replacement materials include conductive polymers[24], and carbon-based materials such as carbon nanotubes (CNTs)[25] and graphene[26]. The most investigated flexible substrates for the thin-film deposition are paper and different types of polymers (e.g., polyimide (PI), polyethylene terephthalate (PET), polydimethylsiloxane (PDMS) and polypropylene (PP)). Different architectures have been studied to improve the bendability and stretchability of flexible devices; some of them include the planar structure and fibre-based for the fabrication of flexible devices. One of the examples of the planar structure strategy involves fabricating wrinkled semiconductor nanoribbons to accommodate applied strains using lithographic processing and then bonding them to flexible materials PDMS[27]. The other designs of deformable structures include fractal[28] and serpentine[29] designs. These designs prevent the strain induced by human body's motions on the performance of the electronic devices. The next section focuses on fibre-based architecture that lays a foundation for the next generation of flexible wearable technology.

2.1.1 E-TEXTILES

E-textiles, or electronic textiles, are textiles with a wide spectrum of electronic functions. Textiles mainly include fibres, filaments, and yarns (woven, knitted, or non-

woven). These electronic functions are either from the electronic components/interconnections mounted/woven in or are intrinsic to the textile[30].

The American Society for Testing and Materials (ASTM) considers a textile fibre as a 'unit of matter that is characterised by having a length at least 100 times its diameter or width and which can be spun into a yarn or made into a fabric by interlacing in a variety of methods, including weaving, knotting, etc.'[31]. Textile fibres can be monofilament or multifilament. A monofilament textile fibre is defined by ASTM as 'a single filament which can function as a yarn in commercial textile operations, i.e., it must be strong and flexible enough to be knitted, woven, or braided, etc.'[31]. On the other hand, a multifilament yarn is composed of a bundle of thin but long threads of infinite length[32]. These textile fibres can also differ on shape (tape-shaped, cylindrical, space contour (rough, smooth, serrated)), feltability, which is the ability of a fibre to mat together which also assists in spinning or weaving, the amount of static electricity built on its surface, resilience, pilling (ball-like structure on materials after washing), abrasion resistance, elasticity, specific gravity, absorbency, lustre (amount of light reflected from a surface), density and the basic material[33]. There are key attributes that play a significant role in the design of wearable textile devices. The requirements are that the e-textiles should be mainly soft, durable, stretchable, be twisted or bent, breathable, washable (maintain integrity), flexible, lightweight, environment friendly, cost-effective, intrinsically warm, achieve good electrical performance together with the comfort of the end-users and thus overcome the shortcomings of the conventional wearable electronic devices.

In recent years, fibres with built-in or add-on electronic functions have presented possibilities for flexible circuits[34], sensors (temperature[35], humidity[36], touch[3], and strain[37]), light-emitting devices[3], antennas[38], antistatic functionality[39], electromagnetic interference shielding[40], energy harvesting devices[41,42]. The hierarchical nature of these fibres from fibre to yarn to fabric, makes them suitable for the fabrication of wearable electronics[43]. Materials such as nano-scale, organic, carbon, inorganic and polymeric materials have been frequently used and investigated for wearable devices. Conducting polymers have been considered one of the suitable candidates because of the intrinsic flexibility and ability to get blended in the fibres to make composite materials. An example includes poly-(3,4-ethylenedioxythiophene) polystyrene

sulfonate (PEDOT:PSS)[44]. PEDOT:PSS has been explored to make electrodes for flexible and wearable temperature sensors because of the high conductivity and easy solution processing[45]. Conducting polymers have stability issues that have limited their application in wearable light emitting diodes (LED) and solar cells[24]. Carbon-based materials (0D, 1D & 2D) have been demonstrated as promising materials for flexible electronics due to their unique properties such as environmental and mechanical stability, porosity large surface area, electrical conductivity, and high intrinsic carrier mobility[46]. CNTs and graphene have become the most explored for wearable applications. It has been demonstrated that coating cotton threads with CNTs leads to smart yarns which can be used as strain sensors[21]. Nickel[47] and gold-plated Kevlar® fibres[48], nylon fibre mats coated with tungsten[49] are a few examples of metals being employed in wearable electronics. These fibres, however, are rough and unstable. A recent report about a novel all-fibre piezoelectric nanogenerator, using a stretchable silver coated polyamide fabric as fabric electrodes (as compared to thin metal electrodes) resulted in high durability and good power generation[50] .

The incorporation of the above-mentioned materials into the textiles can be done by various methods such as sewing[41], knitting[51], embroidering[52], weaving[53], braiding[54], coating[1] or laminating[55], spinning[56], and printing[57]. One of the techniques used for the fabrication of e-textiles includes the use of conductive inks and has also been reported for fabricating conductive textiles. These inks must contain a highly conductive material that can be printed onto a variety of substrates to create conductive patterns. This leads to preservation of the flexibility of the bare fabric. The porous nature of the textile facilitates the fabrication process. One such example is screen-printing of silver-based ultraviolet-curing conductive ink to print circuits on a textile substrate[58] (Figure 2.1a and b). The ink was cured by exposing to ultraviolet light. Conductive threads made up of metal wires produced by mechanical wire drawing which are then incorporated into textile yarns. A fabric called PETEX® (Figure 2.1c) is an example of the use of conductive threads[59]. PETEX® consists of woven polyester monofilament fibres and copper alloy wires with an interconnection created with conductive adhesive and encapsulation by epoxy resins assists with electrical and mechanical protection[59]. These threads can be electrically insulated by coating individual wire with polyurethane varnish. Thermoplastic adhesives have been used to attach thin film-based devices to

the textile fabrics[60]. Flexible fabric patches have also been fabricated by depositing circuits on a fabric patch by sputtering, placing an electronic component such as integrated circuits on the fabric and then wire-bounding the integrated circuits on the patterned electrodes[61].

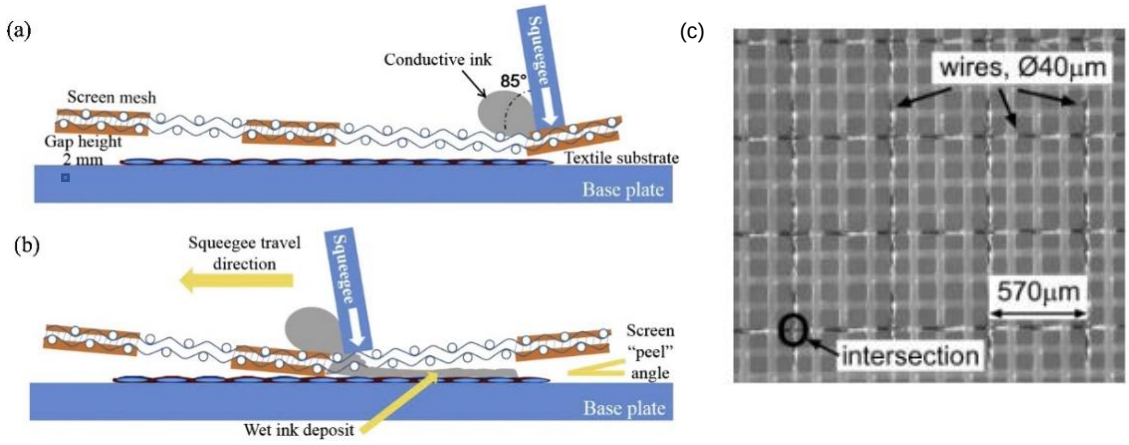

Figure 2.1. (a, b) Screen printing process of silver-based ink on textile substrate[58]. Reprinted with permission from Elsevier and (c) PETEX consists of woven polyester monofilament fibres and copper alloy wires[59]. Reproduced with permission from SAGE Publications.

Despite the significant advancements in e-textile technology, the reported devices do not fulfil all the application requirements. For conductive threads, this could be due to the loss of contacts caused by the removal of the conductive material because of the movement during washing which causes the devices to stop functioning[62]. The electronic components and the interconnections are often visible and susceptible of being stuck or tangle with the surrounding objects, which is inconvenient to the users[63]. Some of the processes used to fix the electronic components, such as LEDs on the textile fibre, include soldering on a textile substrate (Figure 2.2a) or using a silver adhesive (Figure 2.2b). In 2017, Tao *et al.* demonstrated an approach to protect the conductive threads and the electrical contacts with the flexible printed circuit board by encapsulating the assembly with a thin film of thermoplastic polyurethane[62] (Figure 2.2c). Most of the experimental wearable textile devices are not ready to be commercialised because of the lack of washability which reduces their durability and

reliability. Breathability is another significant concern for e-textiles to maintain the user comfort, and the use of adhesives or planarisation layers can reduce the breathability[63].

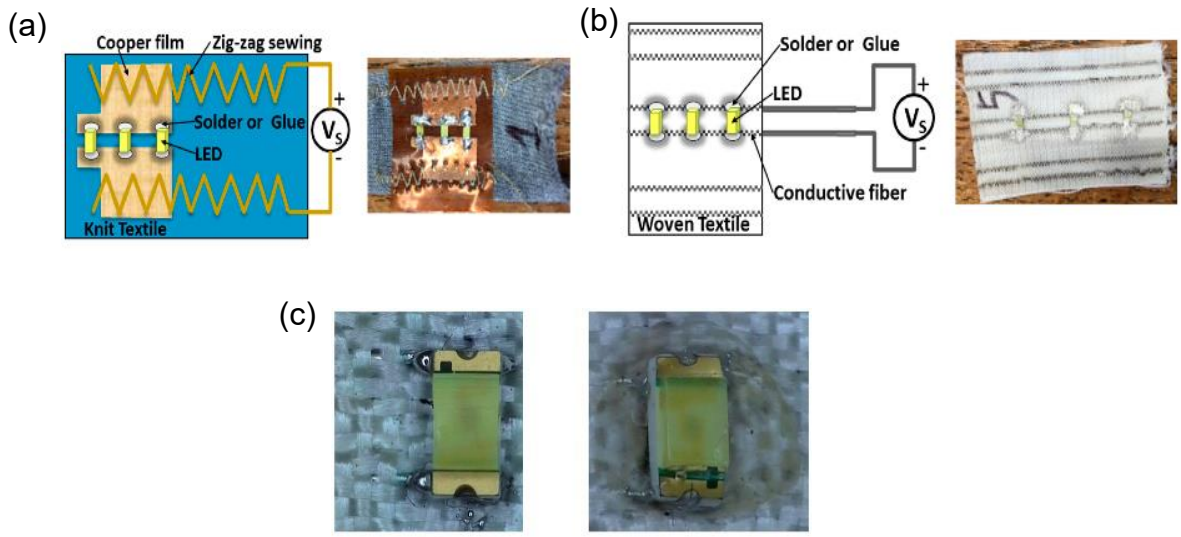

Figure 2.2. (a) Soldering of LEDs on textile substrate, (b) LEDs fixed with silver adhesive on conductive thread, and (c) textile with array of LEDs[62]. Reproduced with permission from MDPI (CC-BY).

To overcome these shortcomings, a more practical strategy to produce conductive e-textiles was used by Neves *et al.*, by directly coating insulating fibres with a graphene layer[1]. Only the surface of the textile fibres, made by the extrusion of PP, are coated with graphene. This is one of the techniques used in this thesis to produce conductive textile fibres.

2.1.2 POLYPROPYLENE (PP)

Polypropylene was first successfully polymerised in 1954[64], whose monomer is propylene with the chemical formula C_3H_6. This polymer is often denoted by the abbreviation, 'PP'. PP is known to be a thermoplastic polymer which softens upon heating and can, therefore, be easily remoulded. It is non-polar and has a partially

crystalline structure[255]. It is produced with propylene as a raw material which is one of the gases liberated during crude-oil refining. PP-based textiles have been used in a variety of applications such as production of lightweight fabrics[65], geotextiles[66], industrial sacks for packaging (e.g. sacks for fruits and vegetables)[67], and marine ropes[68]. PP textile fibres are usually considered in textile applications where the cost of the raw materials represents a significant share in the net manufacturing cost. The low cost of PP when compared to nylon, acrylic fibre, and high-density polyethylene, is the result of easily obtainable raw materials and easy manufacture[69]. PP has a greater resistance towards heat as compared to PE. It has a high heat distortion temperature, excellent rigidity, electrical insulation, ease of moulding and resistance to folding. The density of crystalline PP is 0.946 g/cm^3 and amorphous PP is 0.855 g/cm^3. The Young's modulus of PP is between 1300 and 1800 N/mm^2 [255]. PP is mostly inert which allows it to withstand chemical exposure, including acids, alkalis, and many organic compounds. For this reason, PP fibres are more resistant to staining than polyester or nylon fibres[70]. The low density and specific gravity of PP makes PP cheaper and lightweight. PP fibres are non-toxic, a poor bacterial host and mildew resistant, which adds to the advantages while using them in applications involving humid or wet environments such as bathroom curtains or rugs[71]. This is the due to the quick moisture transport through the PP fabrics as compared to polyester which allows them to remain dry in a high humid environment, leading to hygienic medical or next-to-the-skin uses. The PP fibres have been replacing natural fibres such as jute, hemp, and sisal since mid-1960s as well as reinforcing them due to lower risk of contamination by foreign textile fibres, damp-resistance, high strength to weight ratio, and consistent manufacture process[64,72,73]. The PP is not readily transparent as other plastics but can be made translucent by reducing the turbidity by increasing the fraction of amorphous phase, to reduce the size of the spherulites or by destroying the spherulite texture by stretching[255].

The melting point of PP occurs in a range which makes it essential to perform differential scanning calorimetry analysis to find out the melting point of a particular PP sample. The differential scanning calorimetry curves for PP shows an endothermic peak due to the PP melting around 160 °C. The tacticity of the polymer also has been observed to have an effect of the melting point of the polymer. PP can be isotactic, atactic or syndiotactic. A perfect isotactic PP would have a melting point of 170 °C,

while the commercial isotactic PP has the melting point that ranges from 160-166 °C. The syndiotactic PP has the melting point of 130 °C[255].

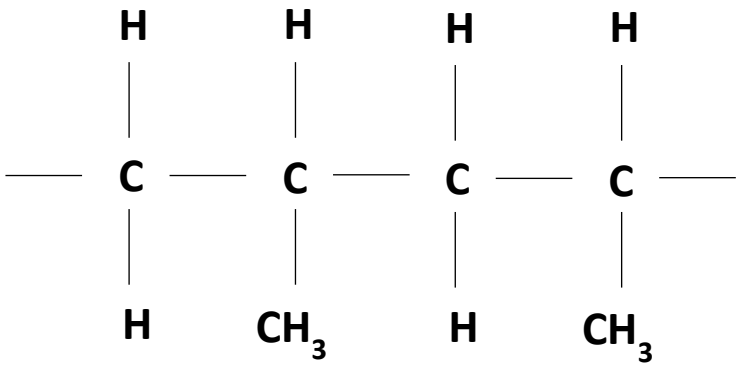

Figure 2.3. Chemical structure of Polypropylene

The Fourier transform infrared spectroscopic analysis of PP which gives information about the interaction between infrared radiation and PP leads to peaks at 808 cm^{-1} which is related to the stretching mode of the C-C bond, peak at 840 cm^{-1} is attributed to the rocking mode of the C-H mode, 996 cm^{-1} peak to the rocking mode of the functional group of CH_3, 1456 cm^{-1} to the symmetrical bending of the CH_3 group, 2920 and 2950 cm^{-1} to the asymmetrical stretching of the CH_3 group[261].

2.2 GRAPHITE, GRAPHENE AND GRAPHENE OXIDE

2.2.1 INTRODUCTION, PROPERTIES, AND APPLICATIONS

Graphite is a hexagonally bonded allotrope of carbon in which each carbon atom is bonded to three others to make a large plane molecule. These planes are stacked together relatively loosely to make graphite[259]. It is a good conductor of heat and has highly electronic conductivity, making it very useful in electronic applications such as electrodes and solar panels. The graphite crystals are highly anisotropic. Graphite is known as one of the softest substances. Graphite is stable at high temperatures in the absence of oxidising agents due to the strong carbon-carbon bonds in the planes.

There is a weak binding (Van der Waals bonds) between the planes which allows graphite to be used in several applications[259].

Even though it is well known that GO is an infinitely thin sheet of oxidized graphite, there is no accurate model currently to describe the chemical structure of GO. This could be due to the amorphous and non-stoichiometric atomic composition and there are no precise analytical techniques available to well characterise the GO. There have been several structural models suggested to describe the structure of GO. The most acceptable configuration is the Lerf-Klinowski model which contains sp^2 and sp^3 hybridized carbon atoms and various substituents such hydroxy, epoxy or carboxylic groups[262].

Graphene is a two-dimensional layer of sp^2-hybridised carbon atoms with a hexagonal lattice[74]. It is the building block of carbon nanotubes ('rolled up' graphene) and graphite (graphene sheets stacked and held together by van der Walls forces). Since its discovery by Novoselov and Geim (Nobel prize in physics in 2010) by what is now known as the 'Scotch-tape' method[75,76], graphene, a semimetal, has attracted world-wide attention owing to its exceptional physical properties, such as excellent mechanical strength, a large surface area (2630 m^2g^{-1}), high electronic conductivity, good thermal stability and flexibility which suggests it can bend, twist, compress, stretch and deform while upholding its performance and reliability[76,77]. All the atoms, in graphene, are covalently bonded by three in-plane σ-bonds from sp^2 orbitals and one π-bond from the 2p orbital perpendicular to the base plane. The graphene edges can take the form of a zigzag structure or sometimes an armchair structure Even though the zigzag form exhibits superior stability, in most forms of the synthesized graphene, both configurations are present at the same time and have different properties which can be intentionally tuned for applications[262].

The International Organization for Standardization (ISO TS 80004-13: Nanotechnologies) defines the single-layer graphene (SLG) as 'Single layer of carbon atoms with each atom bound to three neighbours in a honeycomb structure, bilayer graphene as the 'Two-dimensional material consisting of two well-defined stacked graphene layers' and few-layer graphene as the 'Two-dimensional materials consisting of three to ten well-defined stacked layer[78]. Graphene also has a high optical transparency of up to 97.7%. A single layer of graphene absorbs about 2.3% of visible

light at 550 nm and when another layer is added to the first layer, the amount of white light absorbed also increases by approximately the same value (2.3%)[79,80].This property can be applied in the fabrication of graphene-based transparent electronic devices, important for applications such as transparent electrodes in solar cells[19]. The above-mentioned properties make graphene highly attractive to a wide range of applications (rigid and flexible), including sensors (temperature[81], gas[82], humidity[83], and touch[3]), flexible light-emitting diodes[3], energy storage devices (graphene electrodes in solar cells[84]), energy harvesting[85], and even in the construction industry for reinforcement of concrete[86].

2.2.2 GRAPHENE PRODUCTION

The quality of graphene plays an important role as the presence of impurities[87], structural disorders[88], grain boundaries[89] or wrinkles[90] in the graphene layer could have an adverse effect on its properties. Single-crystalline graphene possessing minimal to no structural defects, high electronic and thermal conductivity as well as excellent optical transparency is desired for the best electronic device performance. Hence, the most appropriate method of production should be selected for the purpose. There are five methods widely used: (i) liquid-phase exfoliation (LPE)[85]; (ii) growth on transition metals by chemical vapour depostion[91,92]; (iii) epitaxial growth on silicon carbide by thermal decomposition[93]; (iv) micromechanical exfoliation of graphite[94]; (v) chemical exfoliation (reduction of graphene oxide)[95]. The micromechanical exfoliation technique is a top-down process, was the first discovered technique using a Scotch tape and has been widely used high-quality graphene flakes[76]. Despite being reliable, quick and easy, the number of exfoliated layers is not always easily controlled along with the isolation of only small amounts of graphene. The process is also quite labour-intensive since it requires a flake by flake exfoliation and study the number of layers[96]. Therefore, other above-mentioned methods were developed. Only the first two methods (CVD and LPE) will be presented and compared next, as they are the ones used in this thesis. The other methods have been explained and compared by Randviir *et al.*[92] *and* Backes *et al.*[96,97]*.*

Chemical vapour deposition (CVD)

CVD is a chemical process to produce thin films by exposing a substrate to volatile precursors which react with the surface of the substrate to decompose and produce a thin film of desired composition. Usually, the process is accompanied by the formation by-products (e.g. hydrogen) which are removed by the bulk gas flow[91]. There are different types of CVD processes for graphene growth which can be categorised based on the chamber pressure (low-pressure CVD or LPCVD, atmospheric pressure CVD or APCVD), substrate heating mode (hot-wall CVD, cold-wall CVD), or on the energy source (photo-thermal, plasma-enhanced CVD and thermal CVD). The synthesis of graphene by CVD, a bottom-up process, has been one of the most widely used methods to produce graphene. This method is scalable and reliable and enables producing large-area and high-quality graphene[98]. The large-scale graphene films typically are polycrystalline. Hence, efforts have been made to control the domain size, defects, and number of graphene layers to achieve large domain size, fast growth, and low growth temperature[91].

Among the various catalytic metal substrates used for the graphitic growth by CVD, Cu and Ni are the most widely used metals for graphene growth due to their stability, good homogeneity, abundance, and easy availability[91]. The CVD growth of graphene on Ni (Figure 2.4a) substrate has three major steps: (i) *decomposition*, where the hydrocarbon gas molecule contacts the heated metal surface and decomposes to a metal-stable carbon; (ii) *surface segregation*, where above 800 °C the decomposed carbon atoms diffuse into the Ni bulk since the solubility of carbon in Ni strongly depends on the temperature i.e. high temperature leads to high solubility and low temperature leads to low solubility of carbon in Ni; (iii) *precipitation*, where the carbon atoms diffuse out of the Ni bulk to the surface when the Ni substrate is cooled down rapidly. The growth process of Ni leads to non-uniform few-layer to multilayer graphene. The preparation of uniform single-layer graphene requires very accurate cooling rate[99].

In contrast to Ni, the solubility of carbon in Cu is quite low. For the CVD growth of graphene on Cu (Figure 2.4b), one of the proposed mechanisms suggests that the graphene layer is formed along the surface of the Cu substrate by the adsorption of decomposed carbon atoms[100]. Li *et al.* observed there is limited diffusion of carbon into

the bulk Cu[101]. It was suggested that the instant the substrate is exposed to the carbon precursor, the nucleation begins, and the number of islands increases with the longer carbon precursor exposure. The islands continue growing while some coalesce with the other islands at high temperature to form a single-layer graphene. This causes the growth process to get terminated, after the first layer of graphene since no catalytic surface is available, due to the self-limiting nature of the Cu substrate[102]. However, Bhaviripudi *et al.* found that under atmospheric pressure, the mass transport rate of the carbon source is low, causing precursor saturation and formation of multilayer graphene[103,104]. It has also been proposed that the graphene grain boundaries provide nucleation sites for additional layer of graphene[105].

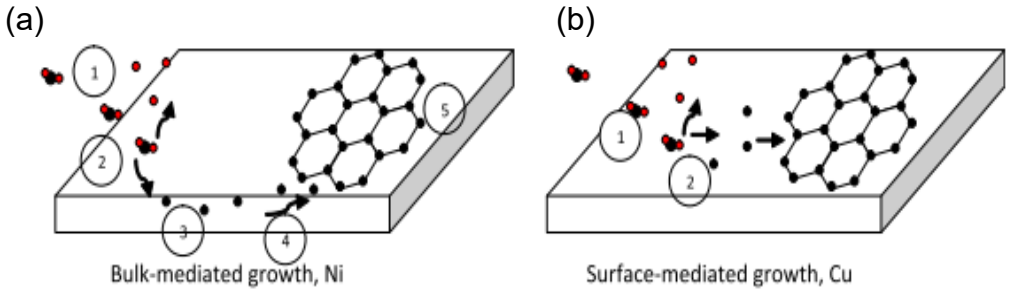

Figure 2.4. Schematic of mechanism behind graphene growth on (a) Ni:(1) hydrocarbon that chemisorbs on the Ni surface, (2) dissociation through dehydrogenation, (3) diffusion of carbon atoms into the bulk Ni, (4) cooling step where the carbon atoms diffuse to the surface, (5) graphene formation and (b) Cu: (1) decomposition, (2) graphene formation. Reprinted with permission from Elsevier[91].

The critical parameters that require optimisation before the CVD process are the catalytic substrates, temperature, pressure, precursor material and gas flow. The dissociation of the carbon precursor is a highly endothermic process requiring temperatures that can be as high as 1200 °C for methane[106]. The decomposition of the carbon precursor can also be achieved at a lower temperature using plasma enhancement to provide the necessary energy for the process. Although methane requires high temperatures, it is still the most widely used carbon precursor for graphene growth as compared to ethane, benzene, toluene, ethanol (liquid carbon source) and PMMA (solid carbon source) which required much lower temperatures (as

low as 300 °C) where the quality of the graphene produced is much lower with more defects than methane. In addition to the carbon precursors, hydrogen and argon are the two commonly used gases. Although the role of hydrogen in CVD graphene growth is disputed, it plays a crucial part in reducing the native oxides on the surface of the substrate and reduces the residual oxygen[107] while the argon is used to dilute the gases[108] or control the chamber pressure. For the mass production of graphene, there have been attempts to find an alternative for hydrogen, which has safety concerns, and argon, which is expensive. These attempts include pre-treatment of the Cu substrates, graphene growth in CO_2-enriched atmosphere and using nitrogen as the carrier gas[109].

In terms of pressure, in LPCVD there is fast diffusion of the carbon source to the Cu surface which causes self-limited growth, leading to 95% single-layer coverage with a wide range of methane concentrations. In contrast, APCVD allows the growth of a monolayer at low methane concentration and the growth of multiple domains on a monolayer at higher methane concentration. The decomposed carbon atoms increase in quantity while moving downstream along the chamber, which produces thicker graphene layers deposit on the monolayer to form multilayers[91]. It has also been suggested that it is possible for some carbon atoms to get trapped between the first layer and the substrate to form adlayers during the catalytic decomposition[110]. The coverage of the graphene is larger for higher pressures due to the higher partial pressure of the methane[96].

Two types of processes have been widely investigated for the mass production of CVD-graphene: continuous or roll-to-roll (R2R) and batch-to-batch (B2B) processing. The B2B process is commonly used in laboratory research and uses flexible catalytic substrates which are loaded inside a quartz tube (in the case of thermal-CVD) to produce homogeneous graphene. The substrates could be several thin Cu foils which are stacked to fit the tube separated by graphite foils as spacers to prevent Cu adhesion to each other at high temperatures. The graphene growth takes place in a controlled gas atmosphere, at around 1000 °C. This configuration was used to grow large-area high quality graphene by using LPCVD[111] and APCVD[112]. Although the B2B process allows high stack density of graphene, the size is still limited and with the increase of the substrate stack density, simple gas exchange is also a problem. The R2R process (Figure 2.5), is an automated process for producing functional devices

such as solar cell on a roll of flexible substrates. In addition to B2B, R2R is also used for industrial production. A report by Polsen *et al.* includes Cu strips wrapped on a pair of rollers and continuously subjected to the CVD processes (heating, growth, and cooling) in a concentric tube[113]. The movement of the Cu foil is controlled by a pair of motors. *Deng et al.* produced graphene with dimensions of 5 × 5 cm before transferring the graphene onto a plastic by electrochemical method to reuse the Cu foil, which is helps with the low-cost production[114].

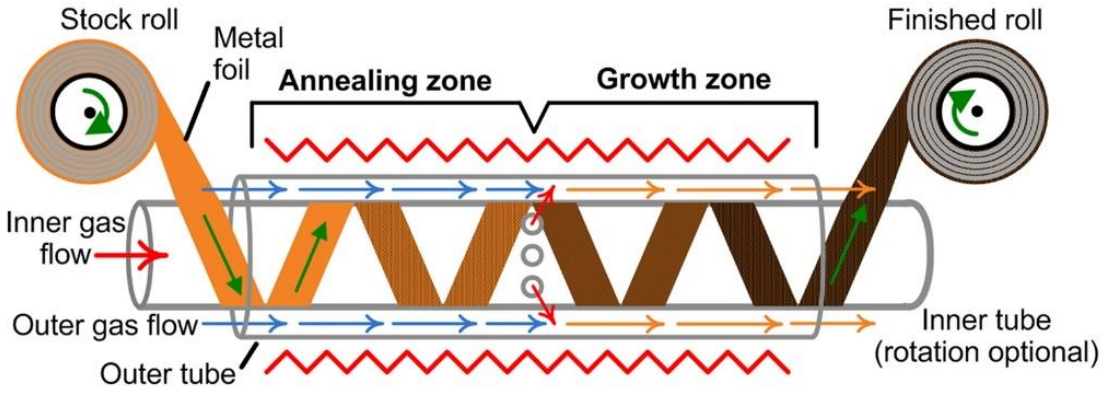

Figure 2.5. Schematic representation of the CVD growth setup of a roll-to-roll system[113]. Reproduced with permission from Nature Research [CC BY 4.0].

Liquid-phase exfoliation (LPE)

LPE is one of the top-down processes to obtain stable dispersions of single to few-layer graphene which involves the exfoliation of natural graphite by ultra-sonication or shear mixing in a suitable solvent[115]. LPE has a high potential for the mass production of graphene due to the mild operating conditions without requiring vacuum or high temperature systems. There have been several reports demonstrating different techniques for LPE such as high-shear mixing[116], jet cavitation[117], and microfluidisation[118]. Even a kitchen blender has been used along with household detergents to prepare graphene dispersions[119]. In this thesis, only LPE by high-shear mixing will be presented. The other LPE methods have been explained in a review paper by Xu *et al.*[120].

There are many devices which can offer high-shear to exfoliate graphene such as rotor-stator mixer[121], Taylor-Couette flow reactor[122] and rotating blade mixer[119]. In 2014, Paton *et al.* reported the use of L5M mixer Silverson model, a rotor-stator mixer which generates high-shear in the gap between the rotor and the stator[121]. This work included the use of organic solvents, namely NMP (*N*-methyl-2-pyrrolidone) and aqueous solutions in the presence of a surfactant, sodium cholate. The high-speed rotation of the rotor blades exerts a powerful suction and hence drawing the graphite upwards from the bottom of the vessel into the stator and centrifugal force drives them towards the edge of the rotor blades and the inner wall where they are subjected to fragmentation. Further follows hydraulic shear as the materials are forced out of the perforations in the rotor head into the mixture at high velocity. The graphite is successfully exfoliated because of the continual rotation of the rotor[121].

The most investigated media includes organic solvents such as NMP[123], γ-butyrolactone[123], *N,N*-dimethylformamide[124], and ortho-dichlorobenzene[125].The organic solvents are more effective polar solvents than water which is why using them leads to better exfoliation rate. Xu *et al.* performed a detailed study of the liquid-phase exfoliation of graphene in organic solvents. It was found that the production yield of graphene sheets dispersed in these organic solvents was 0.8 mg/ml in the case of NMP, 0.04 mg/ml for 1,3-dimethyl-2-imidazolidinone, 0.5 mg/ml for cyclohexanone, 0.02 mg/ml for benzylamine, and 0.01 mg/ml in the case of propylene carbonate. The addition of naphthalene to organic solvents has been demonstrated to further increase the graphene concentration by 2-4 times. The naphthalene acted as a ‘molecular wedge; to intercalate into the edge of graphene, facilitating the exfoliation of graphite during sonication, thus improving the production yield of graphene significantly[256]. NMP is soluble in water, ethanol, acetone and several other organic solvents, cyclohexane on the other hand is miscible and is soluble in all organic solvents. On the other hand, polypropylene carbonate is only soluble in water. These organic solvents are not only expensive but also not volatile and have a high boiling point for example, the boiling point of NMP is 202-204 °C, cyclohexane requires 155.65 °C, and propylene carbonate requires 242 °C[257], which makes it difficult to remove the solvent residues during subsequent processing. To solve this, the use of solvents with low boiling points, including acetone (miscible in water with boiling point of 56 °C), isopropanol (miscible in water with boiling point of 82.6 °C), and chloroform (soluble in water with boiling

point of 61.15 °C)[257], was suggested, which lead to a defect-free graphene dispersion. However, the graphene concentration was still lower when compared to previously studied organic solvents[126]. Choi *et al.* demonstrated an exfoliation method using volatile solvents such as 1-propanol which could be removed easily by air drying[127]. Other methods have also been reported such as the use of ionic liquids[128]. However, ionic liquids are quite expensive and difficult to remove in addition to having high viscosity which would affect the exfoliation process[120]. Recently, more environmentally friendly, or 'green' dispersions such as alkali lignin[129], black tea[130] and ammonia solution[131] have been used to produce graphene dispersions.

Usually, water has been an ideal medium for dispersion of a material[132]. Understanding the interaction between graphite and water is critically important to optimize the exfoliation process. Though by various water contact angle tests and due to the non-polar nature of the sp^2 carbon, it is well accepted that graphite is hydrophobic in nature. However, recent results have shown that the graphitic surfaces are intrinsically mildly hydrophilic and the adsorbed hydrocarbon contaminants from the ambient air render the graphite hydrophobic[258]. There were several facile methods to remove hydrocarbon contaminants from the graphite surface, these methods have not yet been widely studied to produce graphene by shear exfoliation method. Therefore, due to the hydrophobic nature of graphite and graphene as well as the high surface tension of water than the organic solvents, a surfactant is required to better disperse the flakes in an aqueous medium, to produce high concentration graphene dispersion and to ensure the graphene does not agglomerate[133]. Some of the surfactants reported are sodium dodecylbenene sulfonate[133] and sodium cholate[121]. The disadvantage of using surfactants over organic solvents is the tendency of surfactants to get adsorbed onto the graphene surface. The adsorption process prevents the re-aggregation of graphene sheets via hydrophilic interactions; they also affect the conductivity of the graphene[120]. Shin *et al.* suggested an extra processing step by immersing the graphene-coated substrate in de-ionised water (DIW) for a few hours to remove the residual surfactant. The surfactant used in that work was sodium cholate[85]. Another research effort demonstrated the production of graphene dispersion using just pure water without the use of surfactants. However, this method requires higher temperature to exfoliate and stabilise the graphene dispersion[134] .

One of the advantages of graphene suspensions produced by LPE of graphite is that they can be easily mass-produced by scaling up the materials and the solvents used. Several of litres of graphene suspensions can be produced easily with a laboratory scale exfoliation system, and this can be further increased with an industrial shear mixer allowing the production of more than 100 L/h. External pressure and temperature are not required for the processes which adds to the cost-effectiveness of LPE.

2.2.3 GRAPHENE TRANSFER

After the production of graphene, a transfer step to transfer it to another substrate is required for most applications. A transfer without damages and contaminations is essential in order maintain the quality of graphene.

In the case of CVD, the graphene layer needs to be (1) completely separated from the growth substrate and (2) protected from any physical or chemical changes, for the fabrication and characterisation of the graphene-based devices. CVD transfer usually relies on dissolving the growth substrate with an appropriate etchant. Graphene can be transferred with or without a support layer (Figure 2.6). The conventional and efficient support layer methods are polymer-based (poly(methyl methacrylate) or PMMA-assisted[135], PDMS-assisted[136], thermal release-tape assisted[137] and natural polymer-assisted[138]), or non-polymer-based (metal-assisted, small-molecules-assisted[139], hexane-assisted[140] and static-charge-based[141]). A review by Chen *et al.* suggests that an efficient graphene carrier must be flexible, sufficiently strong to protect the graphene from fragmentation by the etchant's surface tension, and it should be easy to remove without leaving any residues[142]*.* PMMA meets the first two requirements, and therefore PMMA-assisted graphene transfer is widely used due to process simplicity and reliability. The PMMA-coated graphene is placed at the surface of a solution consisting of either ammonium persulfate or iron(III) chloride and de-ionised water until the metal (Cu or Ni) is etched away. The PMMA-coated graphene is rinsed with DIW before lifting off with a target substrate, which is then which is then dried in air, under vacuum, or through baking on a hot plate, to remove any water residues trapped between the graphene and the substrate. The final step is removal of PMMA in acetone, in which it is highly soluble. However, PMMA inevitably leaves

residues behind which can affect the conductivity of the graphene[143]. To solve this issue, several developments, such as laser treatment[144] and electrolyte cleaning[145], have been made, but none can fully remove the PMMA residues. Nonetheless, it is possible to transfer graphene without the use of a support layer, but the surface tension of the etching solution could tear the graphene. An alternative approach is the modification of the surface tension of the etchant. Lin *et al.* reported that by mixing 0.1 M ammonium persulfate with isopropanol (IPA) (10:1) reduces the surface tension of the etchant[146] and the transfer can be done without the need for a support layer. In the literature, several other ways of metal etching have been suggested. These can be divided into acidic etching and alkaline etching processes. The acidic method is used to etch the copper and includes the use of cupric chloride which accurately etches off smaller features. However, the maximum etching rate is obtained from a combination of cupric chloride[263] and HCL. The use of a strong acid and an additional component makes the process inconvenient. On the other hand, the alkaline process which uses cupric chloride and hydrogen peroxide is fast but an expensive process[264]. The parameters for this process must be diligently followed since a longer contact with the sample can damage the sample. Some other combinations of etchants include sulfuric acid + hydrogen peroxide, alkaline ammonia, sulfuric acid -chromic acid[265]. Iron chloride is an etchant commonly used to etch copper. This is due to the easy availability and quick etching time (less than two hours)[229]. Ammonium persulfate is another etchant that takes more than 8 hours (depending on the concentration used) to etch same size of copper foil[1].

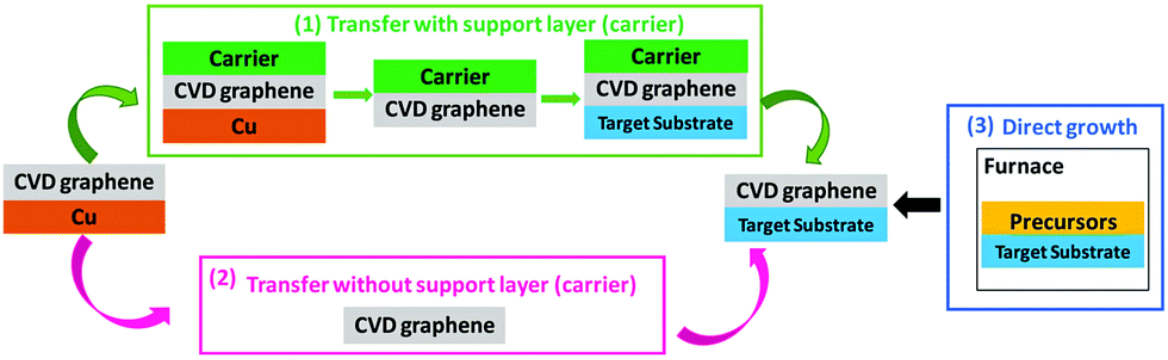

Figure 2.6. Schematic of different routes to transfer CVD graphene onto target substrates Republished with permission of Royal Society of Chemistry from Materials Horizons, Advances in transferring chemical vapour deposition graphene: a review, Chen et al.,4, 2017; permission conveyed through Copyright Clearance Center, Inc[142].

Graphene suspensions are versatile in their method of transfer to a desirable substrate. They can be used as inks with the conventional coating methods such as drop-casting of graphene suspension for flexible strain sensor[147], spray-coating[148], spin-coating of graphene suspension as transparent electrode for organic photovoltaics[149], and dip and dry for various applications such as anti-corrosion barrier on aluminium[150]. Vacuum filtration has been used widely for the deposition of graphene[136] and carbon nanotubes on various substrates[85,151]. The filtration of the dispersion can be done by using different filter membranes (e.g., Teflon, cellulose) with the desired pore size. However, controlling the thickness and the transfer efficiency is challenging. To solve this issue, Shin *et al.* developed a versatile way to assemble graphene dispersions. This method is called isopropanol direct transfer (IDT)[85], is reproducible and can be employed to a wide range of rigid and flexible substrates (Figure 2.7). In this method, the films obtained by filtering graphene dispersions were transferred from the membrane to the target substrate by adding about 0.5 ml of IPA on the target substrate, flipping the graphene/filter in such a way that the graphene is in contact with the substrate and IPA and heating the assembly from room temperature to 90 °C. The IPA slowly evaporates which leads to the release of graphene from the filter membrane. This happens due to the properties of IPA such as high-water miscibility and low surface tension which makes it easier to wet the graphene sheets around by water molecules and the release of the graphene away from the filter and towards the target substrate. Graphene was transferred to a variety of substrates such as glass, paper, PP textile fibres, Si/SiO_2 and PET.

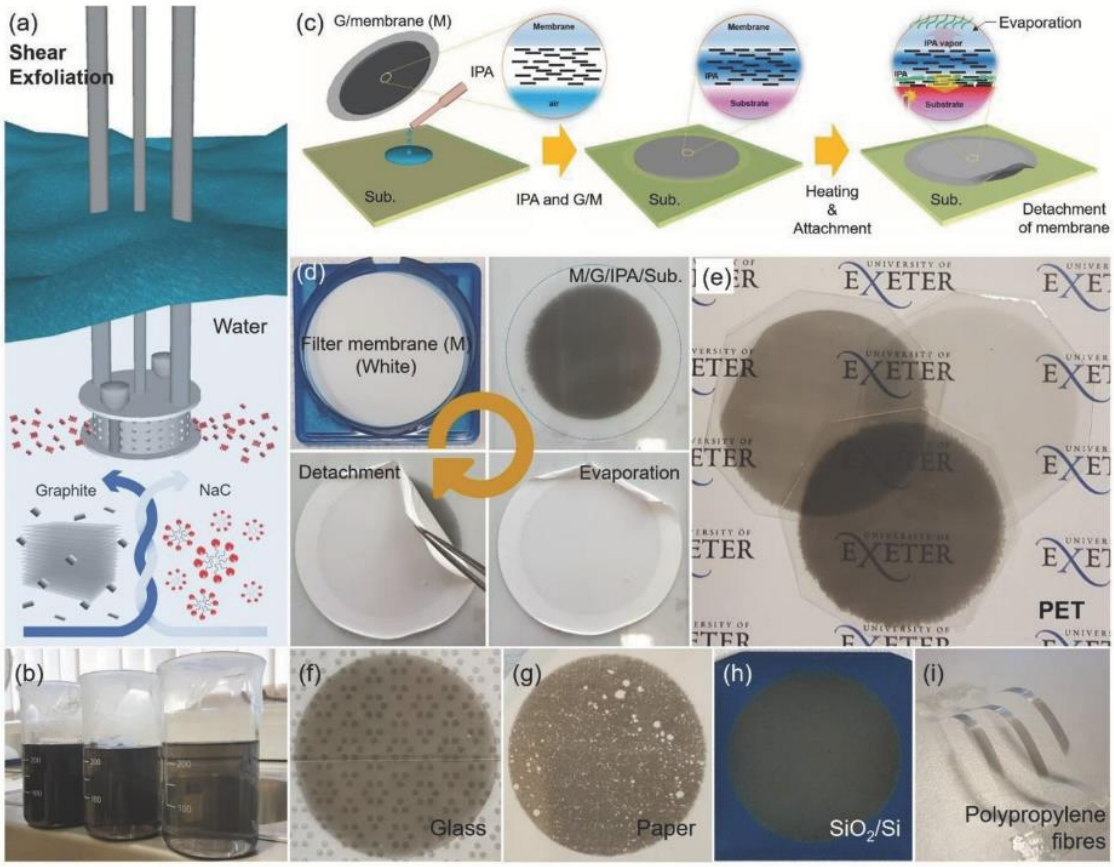

Figure 2.7. (a) Schematic of shear exfoliation of graphite flakes in water with sodium cholate by high-speed rotation of shear mixer head, b) Photograph of graphene suspensions with different concentrations, controlled by shear exfoliation time (10, 30, and 60 min), (c) Schematics, and (d) photographs of IDT method, graphene transfer on different substrates: (e) PET, (f) glass, (g) paper, (h) Si/SiO_2, and (i) PP fibres[85]*. Reproduced with permission from WILEY-VCH Verlag GmbH & Co. KGaA, Weinheim [CC BY 4.0].*

2.2.4 RAMAN SPECTROSCOPY FOR GRAPHENE CHARACTERISATION

The graphene produced by the methods detailed above needs to be characterised to assess the quality (number of layers, crystallinity, defects) before the fabrication of graphene-based devices. This is usually performed after the transfer step. In terms of imaging, SEM provides a clear surface morphology to identify the areas with different voids, cracks, wrinkles, and different number of layers. Transmittance studies can be

done to study the transparency of graphene in addition to obtaining the number of layers. Raman spectroscopy is one of the widely used techniques to characterise the quality of graphene such as crystallinity, defects and the number layers, and the details of its use to characterise graphene are given below.

Raman spectroscopy is a fast and non-invasive characterisation method based on the scattering by molecules on interaction with a monochromatic light. Among the numerous forms of light-matter interactions, Raman scattering, by atoms or phonons, is one of the examples where the wavelength of the light changes matter (i.e., the energy of the scattered photon is unequal to that of the incident photon)[152]. This effect has been named after Chandrasekhara Venkata Raman who was the first to publish experimental observations in 1928[153]. An extensive knowledge of both classical and quantum physics is required to fully explain the physics behind the Raman effect. However, this is beyond the scope of this thesis. For more details, Long[152] and Malard *et al.*[154] have written a comprehensive book and review on Raman spectroscopy, respectively.

In Raman spectroscopy, which is a measurement and quantification of Raman effect, a laser of a certain wavelength is used to induce Raman scattering within a material so that a detector collects the scattered light and determine the subsequent Raman shift. The Raman signatures are unique to each material which helps in the characterisation of the material. Raman spectroscopy can be used to indicate the presence of graphene on a substrate, differentiate graphene based on the number of layers, and to assess the quality of the graphene produced. The next paragraph gives a highlight of the standard practices of presenting Raman spectra and using it for characterising graphene.

It is standard practice to use the change in wavenumber of photons (units of cm^{-1}) to quantify the scattered photon's energy shift. The x-axis of a Raman spectrum is usually designated 'Raman shift' and the y-axis 'Raman intensity', which is the count of the number of photons that hit the detector in the spectrometer. The numerical values of the Raman spectra are not considered since they greatly depend on the laser (power, age of the laser) and are given in arbitrary units. Typically, a Raman spectrum of graphene is measured in the range of 1200-2900 cm^{-1}. There are three main distinctive peaks in the Raman spectrum of a graphene: G-peak corresponds to the primary in-

plane vibration (1580 cm^{-1}) and is present in all forms of carbon; D-peak which is the disorder induced peak (1350 cm^{-1}) which could be missing carbon atoms, grain boundaries or sp^3 hybridisation; 2D-peak: an overtone of the D-peak at 2690 cm^{-1}[154–156].

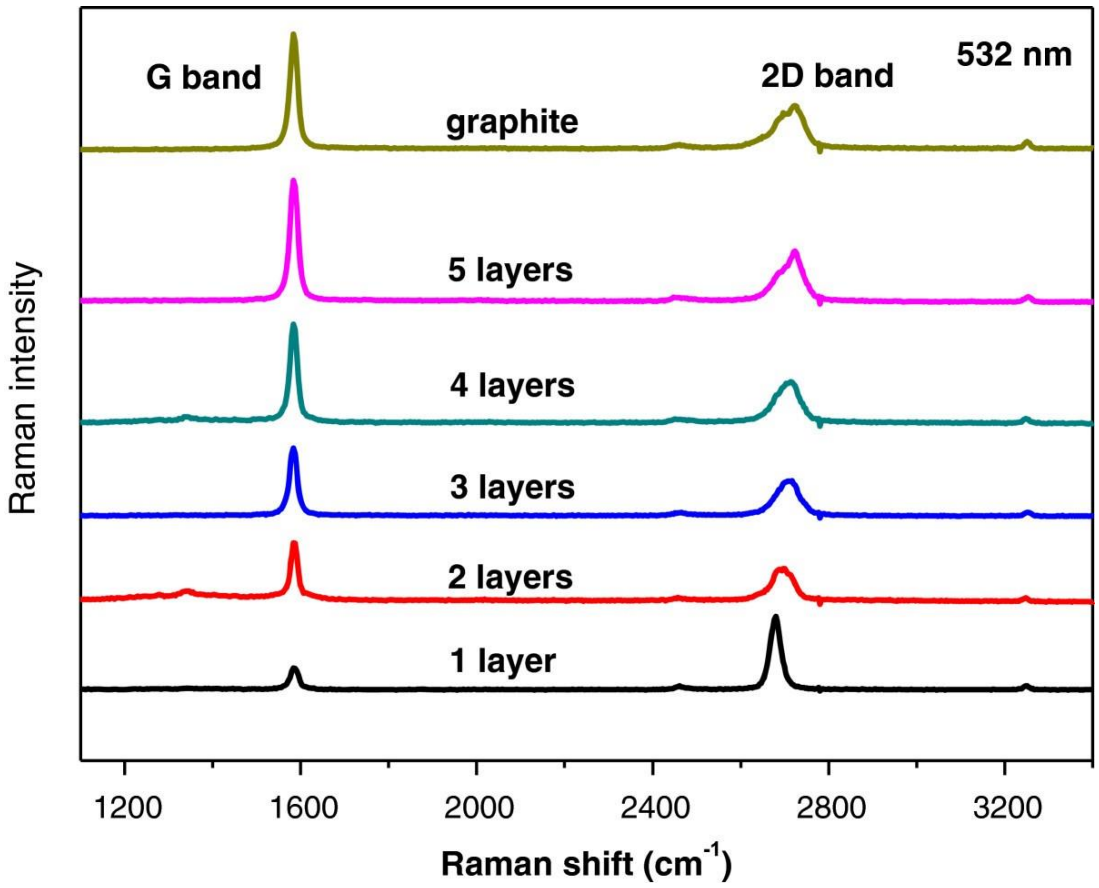

Figure 2.8. Comparison of Raman spectra of different number of layers of graphene at 532 nm. Reproduced with permission from SpringerOpen [CC BY 2.0][266].

These peaks provide information about the number of graphene layers, their orientations, disorders, strain, and doping. The D-peak is not present if the lattice is pristine. However, in the CVD grown graphene, the D peak is used to assess the quality of the graphene produced as it is a measure of the defects present. Low I_D/I_G indicates better electronic properties with minimum defects and/or grain boundaries. The G-peak can be shifted due to strain or doping in the graphene. The ratio of the intensity of G and 2D-peaks are considered to extract the number of layers. The higher the number

of layers get, the more intense the G peak would be. In mechanically exfoliated graphene samples, the expected I_G/I_{2D} = 0.5 for SLG, I_G/I_{2D} = 1 for bi-layer and more than one layer, I_G/I_{2D} > 1. The G-peak represents the planar configuration sp^2 bonded carbon that constitutes graphene. The G-peak position is independent of the excitation laser wavelength and is used to determine the graphene layer thickness. As the layer thickness increases, the peak position shifts to lower energy representing a slight softening of the bonds as the layer thickness increases. It should be noted that the G-peak position is sensitive to doping and even minor strain. The 2D band is sometimes referred to as G'-band. The 2D-peak is also very sensitive to graphene folding. In a single layer graphene, it is the most pronounced. However, it broadens and reduces in intensity in a multilayer graphene. When successive layers of graphene are added to single layer of graphene, the 2D-peak splits into several overlapping modes due to the added forces. The splitting going from single layer graphene to multilayer graphene arises from symmetry lowering that takes place when the number of layers is increased. In the case of SLG, the 2D-peak can be fitted with a single Lorentzian and there is only one component to the 2D-band. Fitting with more than one Lorentzian signifies increasing number of layers as the 2D-peak split. To determine whether the graphene is single-layer or greater than one, full width at half maximum (FWHM) of 2D-peak is also used. It is a second order of the D-band but doesn't represent the defects. It is a result of a two-phonon lattice vibrational process, but unlike the D-band, it does not need to be activated by proximity of a defect. There is a shift to higher wavenumbers as the number of layer increases. One of the similarities between the D- and 2D-band is that their shape and position can be significantly different with various excitation laser wavelengths. [152-158].

2.3 PREVIOUS WORK ON GRAPHENE-COATED POLYPROPYLENE FIBRES

As mentioned in section 2.1.1, one of the most effective ways of developing conductive textiles is coating the PP fibres with graphene. The seminal work by Neves *et al.*[2], that motivated this thesis, consisted of using tape-shaped thermoplastic monofilament PP textile fibres with a width of 2.4 mm, thickness of 0.03 mm that could be cut to desired length. The monolayer graphene was produced by a cold-wall CVD process at low pressure[2] and transferred to the bare PP fibres using PMMA-assisted graphene

transfer and then characterised using different techniques. Single-layer graphene was also transferred to another monofilament textile fibres made up of polylactic acid (PLA) with thickness of 0.1 mm in this work. It was demonstrated that an ultraviolet-ozone (UVO) treatment of the PP and PLA fibres prior to the graphene transfer, can improve the graphene adhesion. After the UVO treatment, the graphene conformed to the fibre scaffold without any tears. The sheet resistance was calculated for the graphene-coated PP and PLA fibres and was between 1 and 12 $k\Omega sq^{-1}$. However, the untreated fibres were found to have better bendability. It was found that the UVO pre-treatment can cause some damage to the fibres. The same graphene was also transferred to Si/SiO_2 substrate and the sheet resistance was found to be only slightly lower than on PP, suggesting the transfer process does not have any significant impact on the electrical properties of graphene.

The above-mentioned research was further carried on by coating various other polymer textile fibres (two types of PP, two types of PLA, polyethylene, and nylon) with single-layer graphene[1] (Figure 2.9a). The PMMA-assisted transfer method was found to be suitable for coating tape-shaped and cylindrical textile fibres. The graphene-coated PP fibres were found to lose only 2% of transparency over the wavelength range of 430-900 nm which agreed with the 2.3% absorbance of monolayer graphene[77]. The Raman spectra indicated the presence of graphene G band at 1585 cm^{-1}, as expected. Atomic force microscopy (AFM) and scanning electron microscopy (SEM) suggested that the cracks seen in the graphene were due to the manipulation during the transfer process which causes mechanical stress leading to minor changes in the sheet resistance. The bending tests, to check the mechanical resilience, had no significant effect on the resistance value even after 1000 bending cycles. The sheet resistance of the graphene-coated PP fibres was found to be in the order of 1 kΩ/sq. The authors also coated PP fibres with few-layer graphene (FLG) produced by CVD on a Ni substrate. This type of graphene has been produced using CVD but has higher conductivity than the single-layer graphene due to the increased number of layers. The use of FLG was an effort to prove the potential of PMMA-assisted transfer method in transferring not only single-layer graphene but also all other types of graphene and other 2D materials on textile fibres. Once again it was found that, though the UVO pre-treatment increased the conductivity of graphene, it often made the fibres more prone

to damage. It is still possible to achieve good graphene coverage without the pre-treatment.

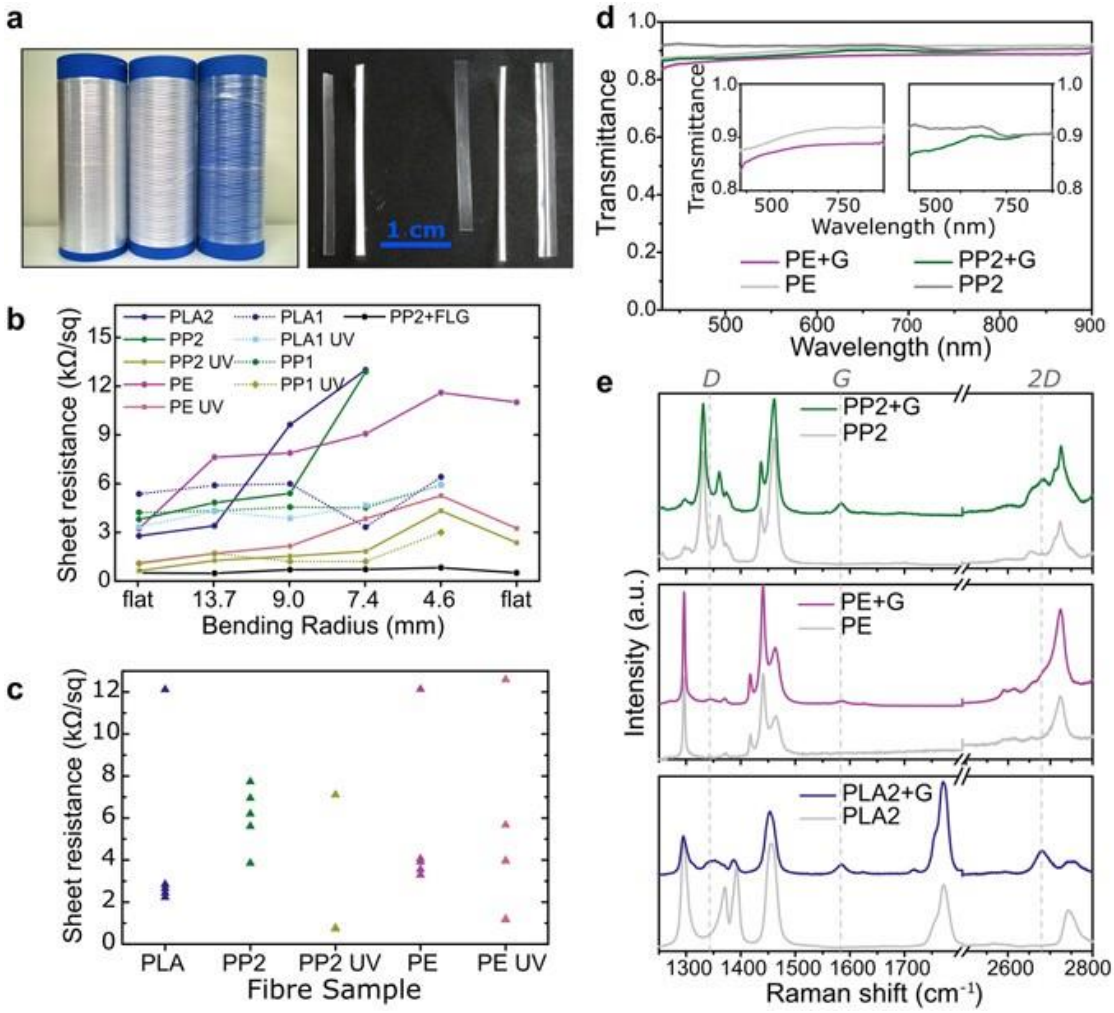

Figure 2.9. (a) Photo of the fibres in reels, left to right: PP, PE, PLA (left) and of the fibres cut to ca. 3 cm length, left to right: PP1, PLA1, PP2, PLA2, PE (right). (b) Sheet resistance as a function of bending radius for samples of each graphene-coated fibre. (c) Distribution of sheet resistance values for multiple graphene-coated samples of each fibre. (d) Transmittance as a function of wavelength for bare PP2 and PE, and graphene-coated PP2 and PE fibres. (e) Raman spectra of the bare fibres and graphene-coated fibres. Reproduced with permission from Nature Research [CC BY 4.0][1].

The PP fibres can also be coated with graphene produced by shear-exfoliation of graphite in water medium and transferring the graphene on PP using the IDT-method[85]. The average lateral size of the graphene sheets produced by Shin *et al.* using shear exfoliation and IDT methods, transferred onto PET, was about *ca.* 110 nm with an

average thickness of four layers (≈ 50 % containing one, two, or three layers). Depending upon the thickness of the graphene layer, which can be easily modified by varying the amount of filtered suspension, the sheet resistance as low as 152.7 kΩ/sq and the transparency was between roughly 45 % and 80 %.

Torres Alonso *et al*. used these graphene-coated PP fibres (SLG, FLG & LEG), where LEG is the graphene produced by liquid-exfoliation of graphite, to fabricate graphene-enabled functional devices such as textile touch sensors and light-emitting devices which are compatible with roll-to-roll techniques[3] (Figure 2.10).

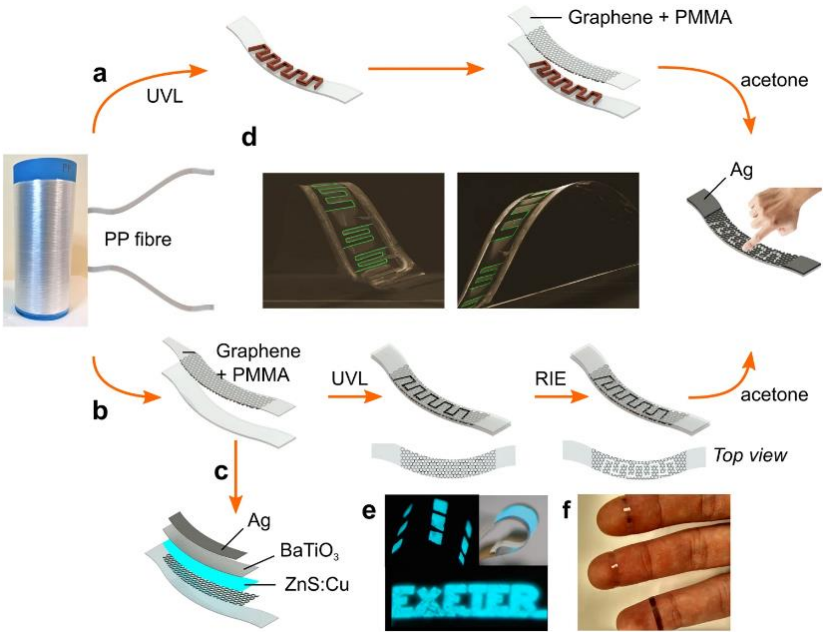

Figure 2.10. Photo of PP textile fibre rolled in a bobbin, (a, b) schematics of the step-by-step process of fabrication of touch-sensing devices by conventional lithography and etching process, (d) SEM pictures of the bent touch sensors with the gap between graphene electrodes highlighted in green (c, e) Schematic and photo of light emitting devices, and (f) textile-based touch sensors using graphene produced by different methods[3]. Reproduced with permission from Springer Nature [CC BY 4.0].

The touch sensors can be fabricated by either patterning the fibres by UV-lithography before the transfer of graphene or the other way around. In both the cases, acetone is used to remove PMMA, or the polymer used in UV-lithography. The capacitive touch sensors use interdigitated graphene electrodes (feature size ranging from 50 µm to 100 µm), produced by lithographic patterning and the measurement of impedance to

detect finger touch. The impedance drops (ON state) and increases (OFF state) when the finger is pressed and lifted-off, respectively. Even after 500 touch and bending cycles, it was observed that the device retained its performance. The light-emitting devices were fabricated on individual graphene-coated PP fibres with graphene serving as the bottom electrode. The graphene was covered with commercially available Cu-doped zinc sulfide as emitter, barium titanate as an insulating layer and silver as the top electrode. It was observed that the light is emitted from the Cu-doped zinc sulfide upon excitation with an AC voltage[3]. The emission peak was around 500 nm and the light intensity depended on the applied voltage.

This thesis focusses mainly on using this platform, graphene-coated PP textile fibres, to demonstrate two types of devices: temperature sensors and humidity sensors. The following sections will review different approaches on both fields.

2.4 TEMPERATURE SENSORS

Temperature is an important parameter that plays a crucial role in the health, aerospace, agricultural, industrial, food, scientific research, and automotive sectors. Temperature is one of the most measured variables which is expected since most physical, chemical, mechanical, biological, and electronic systems are affected by temperature. For instance, the stable body temperature usually ranges between 35-37 °C, a low core body temperature in humans, below 35 °C leads to hypothermia and a high core temperature leads to hyperthermia[159]. There are several applications where maintaining a specific temperature is critical, for instance, if a product or an environment must be kept at a certain temperature, the accuracy and responsiveness of the temperature sensor is vital. The temperature sensor applications frequently incorporate instances where the other components in a system may not be able to function at certain temperatures so the temperature must be monitored within the system. A temperature sensor is a device that measures and monitors the temperature of its environment and records it[160]. Temperature sensing can be done either through a direct contact with the heating source (contact sensors) or indirect contact with the source (non-contact sensors).

There is a wide variety of temperature sensors commercially available today, including thermocouples, thermistors, resistance temperature detectors (RTDs), infrared, semiconductor, and sensors. The relationship between the electrical conductivity and temperature is often used in temperature sensing. A linear relation is observed in RTDs like metals while a non-linear relationship is observed in thermistors, like semiconductors or ceramics. In temperature sensing, temperature coefficient of resistance or TCR is considered an essential parameter:

$$TCR = \frac{R_b - R_a}{R_a(T_b - T_a)} \quad (3.1)$$

where R_a and R_b are the initial and final resistance, respectively and T_a is the initial temperature and T_b is the final temperature. A higher TCR means higher sensitivity[81]. The sensitivity of a temperature sensor is usually defined as the ratio of the change in resistance to the initial resistance[161]:

$$Sensitivity = \frac{R_b - R_a}{R_a} \quad (3.2)$$

Despite providing with high resolution and accuracy, most of the available temperature sensors are rigid and share the same drawbacks as the other rigid electronic devices. The advantages flexible temperature sensors offer have gained tremendous interest due to their compatibility to curvilinear and irregular surfaces, mechanical robustness, multi-functionality, and biocompatibility along with comfort[162,163]. An overview of the types of flexible temperature sensors along with the sensing materials and fabrication has been shown in Figure 2.11. The most investigated materials for flexible temperature sensors include carbon-based materials and inks; metals, including metal-based inks; conductive polymer-based materials. Some of the flexible substrates used in the literature for temperature sensors include PI[164], PDMS[165], PET[166], paper[167] and textiles[168]. These flexible temperature sensors can be fabricated using printing technology (e.g., inkjet[45], screen[169] and gravure[170]), coating and deposition techniques (e.g., spin-coating, spray-coating, dip-coating, doctor-blading, magnetron sputtering, and drop-casting)[163] and using textiles as substrates.

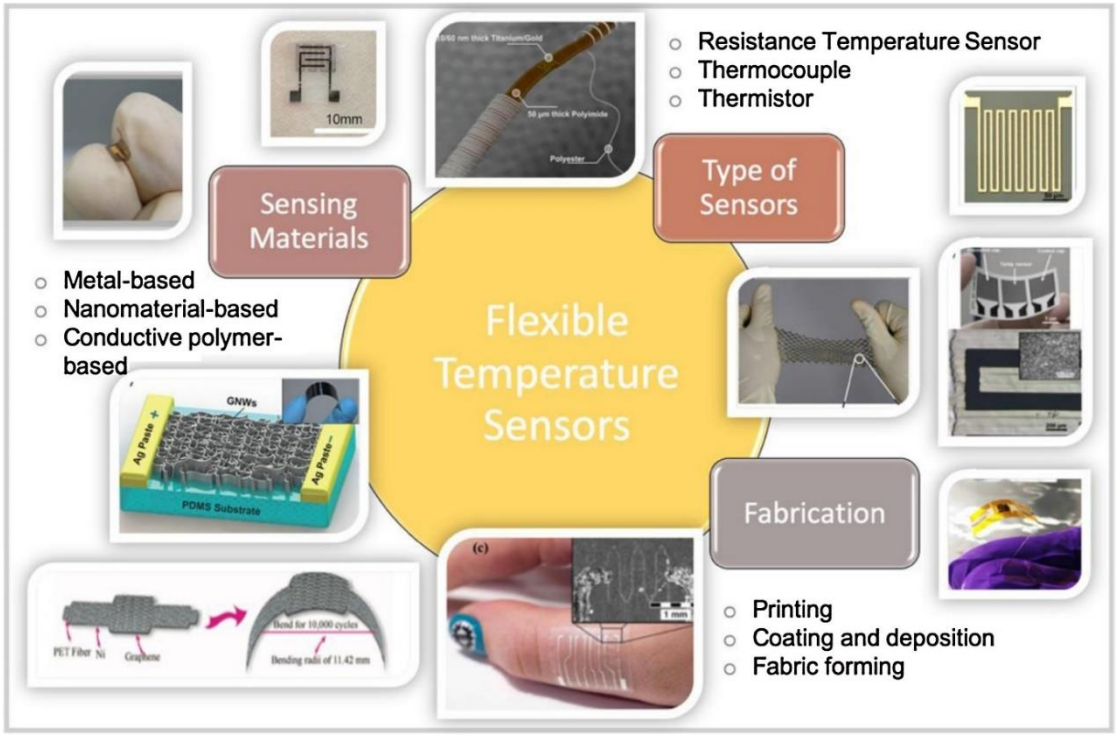

Figure 2.11. Schematics of types and methods to deposit sensing materials onto the substrates for temperature sensors. Reprinted with permission from Elsevier[163]*.*

Printing technology, especially inkjet printing, has been used widely to produce printed temperature sensors. Courbat *et al.* designed a sensor by inkjet printing with silver nanoparticles printed structures on paper[171], while Dankoco *et al.* used organic silver ink on Kapton tape[172]. In a different study, graphene/PEDOT:PSS was printed on a skin-conformable polyurethane plaster using inkjet printing. Li *et al.* showed that conductive copper and nickel lines could be easily printed on the paper using the inkjet technology[173]. Paper-based temperature sensor has produced by dip-coating the paper substrate with PEDOT:PSS based aqueous solution. This sensor exhibited sensitivity in the range of 30-42 °C and is body-attachable. However, the structural integrity of the paper can be compromised by moisture which affects the sensor's performance and limits the application[174]. Ni-microparticles filled PE and polyethylene oxide composites have been developed recently by Jeon *et al.* to measure body temperature in the range of 35-40 °C[175]. Multiple reports suggest the use of carbon-based materials for temperatures sensing. Shih *et al.* demonstrated a graphite-based

temperature sensor array dispersed in the PDMS matrix with PI films[176]. Polansky *et al.* reported an embroidered temperature sensor for the temperature range from 40 to 120 °C, which would be used as a warning system for the heat stress and thermal imbalance for fire-fighters[177]. This sensor is made up of a hybrid thread, composed of strands containing polyester fibres and stainless steel microwire which are embroidered into the textile (Figure 2.12). Bae *et al.* developed an e-skin based temperature sensor by spray coating rGO on parylene substrate. Though the sensor exhibited linear and fast response against temperature, the e-skin would have to be patched on the skin[178]. Neella *et al*. developed a rGO temperature sensor by vacuum filtration method on cellulose filter[179]. Yang *et al.* demonstrated a temperature sensor using graphene nanowalls with PDMS[165].

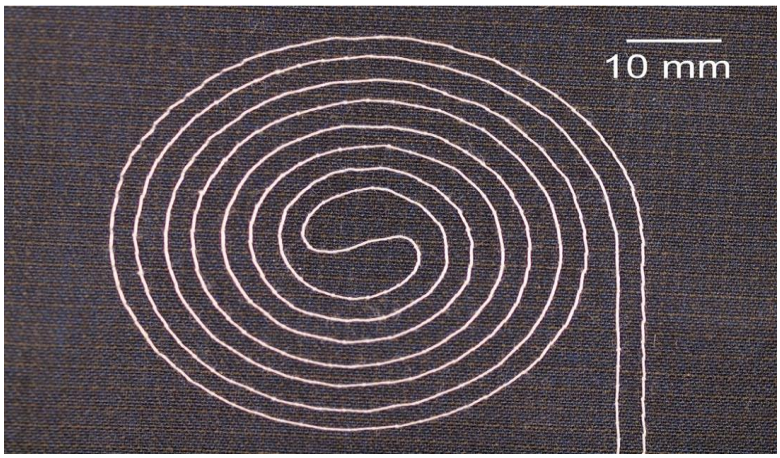

Figure 2.12. Embroidered temperature sensor. Reprinted with permission from Elsevier[177].

Textile-based temperature sensors have been receiving a lot of attention since they can be incorporated in garments to measure body temperature, are suitable for continuous monitoring and can also be used to measure the ambient temperature (e.g., temperature sensing curtains). Hughes-Riley *et al.* fabricated a garment that can sense skin temperature by yarn encapsulation technology[180]. A sensing fabric has been developed by knitting the sensing metal wire along with the textile[181]. Textile thermocouples have also been developed from graphite nonwoven and silver thread,

but the fabricated thermocouples have lower sensitivity and accuracy than the conventional metallic thermocouples[182]. Another textile-based temperature sensor is the development of the conducting cotton fabric with CNTs. The multi-wall CNTs were used to obtain a viscous paste which was then applied on the cotton fabric using knife-over-roll technique[183]. Hilal *et al.* developed a graphene/Ni based textile sensor with high reproducibility, fast response, and recovery times[184]. Luoda *et al.* studied the effect of covering the temperature sensor with a yarn-based protective layer. It was found that the sensitivity of the sensor was reduced up to 14 % as compared to the uncovered sensor[35], which suggests better encapsulation method is required to ensure effective sensing. Table 1 shows the reported flexible temperature sensors, the materials and method used to fabricate them along with the TCR values[235].

Material	Method	Measurement range (°C)	TCR (%/°C)
Graphite- PDMS matrix with polyimide (PI) films	Automatic dispensing	30–110	4.2
PEDOT:PSS-poly(ethylene-phthalate) (PEN)	Dispensing system	25–50	0.77
Graphene nanowalls (GNPs)-PDMS	Polymer-assisted transfer method	25–120	0.214
CuO–Si-adhesive	Drop casting/ doctor blade	25–80	4.0
GO/PEDOT: PSS	Drop casting	25–100	1.09
Graphene- P(VDF-TrFE))	Casting	−20–300	2.5
PEDOT:PSS/rGO-aerogel	Freeze drying	30–50	1.69
rGO	Vacuum filtration	−40–80	0.245
MWCNT/GNP	Vacuum filtration	30–100	0.138
MWCNT/PVDF	Printing/ dip coating	20–120	0.13
Organic silver ink/Kapton	Inkjet printing	20–60	0.223
Silver NP/Paper	Inkjet printing	−20–60	0.11
Graphene-PEDOT: PSS/PU	Inkjet printing	35–45	0.06
rGO/ Aluminum	Spin coating	30–100	0.801
rGO-PEDOT:PSS/ PU	Spin coating	30–80	1.34
rGO/ PET	Air spray coating	30–100	0.6345
rGO/ Parlylene	Spray coating	22–70	0.83
Silver nanowire/ PI	Spray coating	25–60	0.332
PEDOT: PSS-CNT/ Flexible substrate	Mask printing	22–48	0.61
PEDOT:PSS/ FGO–PVDF	Mask printing/ bar coating	10–30	0.395
CNT/ PET	Screen/ gravure printing	−40–100	0.4
FG/CNT/PDMS	Screen printing	40–80	2.8
SWCNT/SEBS	Photolithography	16–55	1.435
Ti-Au/Parylene	Photolithography	30–100	0.481
Graphene-Nickel/ PET	Magnetron sputtering	25–100	0.83
Hybrid thread (PES – Steel microwire)	Embroidery	40–120	0.10

Table 1. Some of the reported flexible temperature sensors: materials, methods, and performances. Reprinted with permission from Elsevier[163].

There are several temperature sensors available commercially. Some of these are TMP35/TMP36/TMP37 sensors made by Analog Devices[251].These devices provide a voltage output that is linearly proportional to the temperature in degree Celsius (°C) and require a supply voltage in the range of 2.7-5.5 V. Another type of commercial sensors includes LM94021 and LM94022 which provide temperature sensors solutions

for low-voltage systems. These are CMOS integrated-circuit temperature sensors that operate at a supply voltage of 1.5 V and as high as 5.5 V[252]. These sensors, though operate at low voltage, are rigid, can't conform to curved surfaces and are not washable or bendable. This thesis aims to develop sensors which can address these issues.

2.5 HUMIDITY SENSORS

Humidity is the amount of water vapour present in a gas (pure or mixture) and commonly measured in the units of relative humidity (RH). Relative humidity is the ratio of the partial pressure of water vapour present in a gas, at a certain temperature, to the saturation vapour pressure of the gas. It is a function of temperature and often expressed as a percentage. Humidity sensors can be categorised into relative humidity sensors or absolute humidity sensors based on the measurement units. Although there are various problems when the RH is high. For example, the occupants of a room with high RH can feel warmer or colder, electronic components in a humid environment get damaged quickly in addition to health issues caused by the mould and mildew growth in a high humid environment. On the other hand, when RH is low occupants of a room can face issues associated with dry and itchy eyes, especially for the users of contact lenses, and spread of pathogens[185]. A low RH can also lead to potential issues such as causing various materials to dry out quickly. Timber, for example, is prone to cracks, deformation and shrinkage when stored in low humidity environment[186]. Therefore, humidity monitoring and corresponding reduction or increase in humidity levels is essential and for the purpose of monitoring, humidity sensors are used widely.

Humidity sensors have gained applications in industrial processing healthcare, environmental control, agriculture, pharmaceuticals, sterilisers, incubators and storage units with cardboard and paper[187]. To manufacture highly intricate electronic devices, it is essential to constantly monitor moisture levels in the air. Most of the humidity sensors are relative sensors and are based on ceramic (e.g. aluminium oxide[188]), semiconductor (e.g. perovskite compounds[189]), polymer (e.g. poly(propargyl benzoate)[190]), and carbon materials (e.g. rGO[191], GO[5], CNTs[192] and graphene[193]).

Rapid developments in flexible humidity sensors have widened the scope of flexible electronics for the applications in multiple sectors and has led to efforts towards the development of a humidity sensor with high sensitivity, selectivity, stability in addition to quick recovery[194]. Most of these reported flexible humidity sensors utilise PET[195,196,197,198], polyimide[199,200], PDMS, cellulose[201], and paper[202] as flexible substrates. Various materials have also been explored to act as a sensing layer for the flexible humidity sensors. Some of these materials are nanostructured ceramics and metal oxides (titanium dioxide nanoparticles, molybdenum trioxide nanosheets[203]), carbon materials (CNTs[204], GO[205], carbon nanocoils[206], graphene[193]); polymers (PEDOT:PSS[195], PTFE[207]), and nanocellulose (cellulose nanofibres/carbon nanotubes)[208].

The humidity sensing materials are susceptible to the adsorption or desorption of water molecules causing changes in their resistance or capacitance[209]. Due to this, humidity sensors have been widely categorised into two categories based on the mechanisms: resistive type or capacitive type[209]. However, a variety of properties such as impedance, mass and surface acoustic wave has also been monitored to detect the humidity. Interestingly, these advancements have been playing a significant role in promoting progress in wearable industry especially e-textiles for healthcare monitoring[209]. In 2019, Torres Alonso *et al.* demonstrated humidity sensors based on graphene suspensions as electrodes and GO as the humidity sensing layer, patterned using lithographic techniques, on silicon wafers and PET sheets (Figure 2.13)[4]. The authors demonstrated carbon contacts as a replacement to the conventional contact metallic materials such as gold and silver. The performance of these sensors was found to be comparable to commercially available humidity sensors.

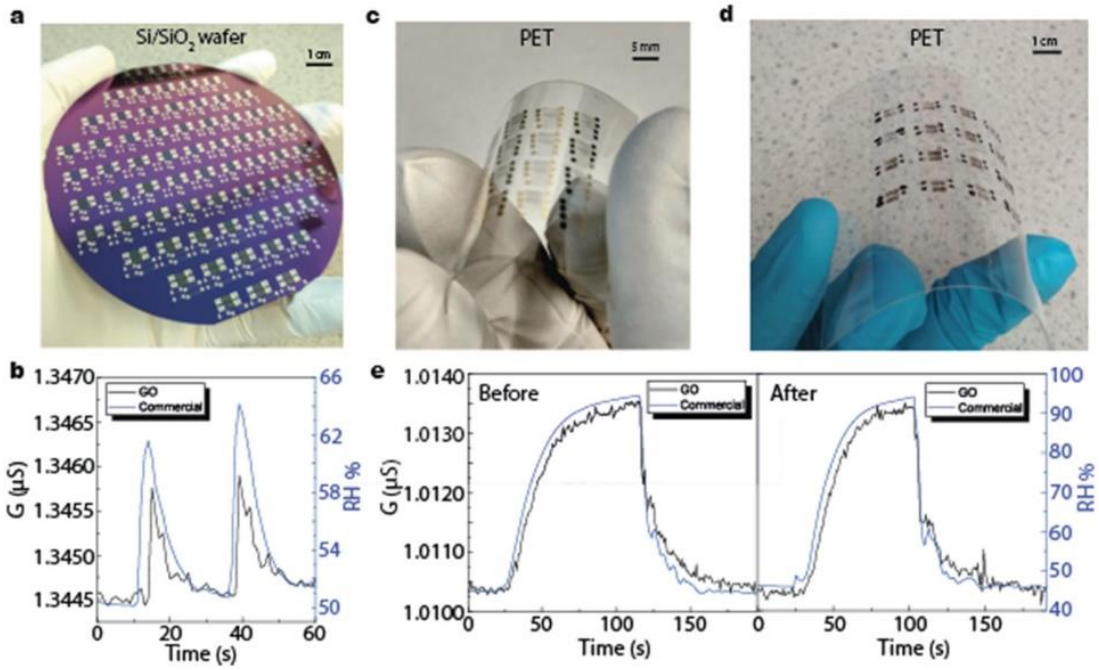

Figure 2.13. a) Photograph of a Si/SiO_2 wafer with multiple graphene/GO-based humidity sensors. b) Humidity response to human blowing. Sensors built on PET substrate: c) with Cr/Au contacts, (d) with carbon paste contacts and (e) Device response before (left), and after (right) 2000 bending cycles [CC BY 4.0][4].

Some of the previously demonstrated textile-based humidity sensors include graphene oxide deposited on aluminium silicate textile[210], multifilament PLA/CNTs yarn[211], thin polyimide sheets integrated into textiles while using cellulose acetate butyrate as sensing material[212]. Several fibres such as rGO, silk, and spider fibres have also been employed to construct wearable humidity devices[213]. Recently, a multi-stimulus sensing device has been demonstrated by layer-by-layer graphene deposition and supercontraction of spidroin fibres[214]. Novel methods have also been adopted such as embroidery of a capacitive interdigitated structure using a conductive yarn on a cotton substrate[52] for moisture sensing and use of inkjet technology to directly print the sensors on textile fabric[215].

Due to their many intrinsic qualities such as low driven power, simple operation, cost-effective fabrication and miniaturisation, resistive humidity sensors remain one of the widely investigated type of humidity sensor[213]. Studies suggest that pristine graphene,

though show high sensitivity suffer from low selectivity and slow recovery[213]. Reduced graphene-oxide based humidity sensors provides an effective way of fabricating resistive sensors but reduces the available functional groups on the surface further decreasing the sensing range and sensitivity. Although some of these issues have been addressed by incorporating different materials such as polymers[216] or metal[217] into GO or rGO film, they may suffer from problems such as irreproducibility and short-term stability.

The commercially available humidity sensors such as the HIH-5030/5031 Series Low Voltage integrated circuit Humidity Sensors which requires a supply voltage of 2.7-5.5 V[253]. HDC302x 1.5% RH Digital Relative Humidity Sensor is an integrated capacitive relative humidity and temperature sensor which provides high accuracy measurements over a supply range of 1.62-5.5 V. The HDC302x measures relative humidity through variations in the capacitance of a polymer dielectric[254]. These sensors, just as the commercial temperature sensors are not flexible or washable and can’t be seamlessly integrated to clothing or to any textile-based applications.

Chapter 3

EXPERIMENTAL METHODOLOGY

3.1 INTRODUCTION

This chapter presents the experimental tools and techniques used in this thesis. This includes the production, transfer, and characterisation of graphene.

3.2 TEXTILE FIBRES

Textile fibres (PP) have been used as flexible substrates in this thesis. PP textile fibres were produced by Centexbel using a monofilament extrusion line, rolled onto a bobbin ready to be cut to the desired length. These monofilament PP fibres are tape-shaped, 0.03 mm thick and 2.4 mm wide (Figure 3.1). The PP fibres were placed in an ultrasonic bath inside a beaker with acetone for 20 minutes and then in isopropanol for another 20 minutes to clean them prior to the usage. The fibres were then stored in a clean and airtight container.

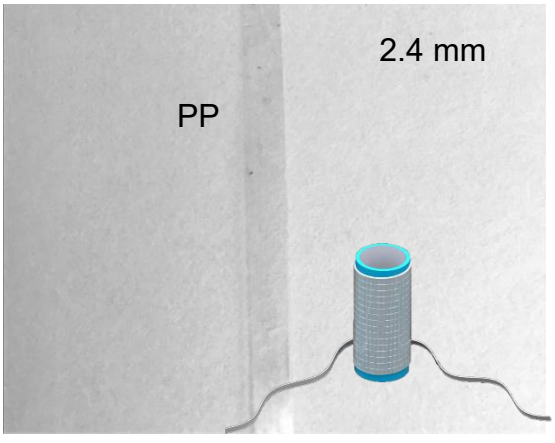

Figure 3.1. Tape-shaped polypropylene (PP) textile fibres. The inset is the sketch of PP rolled in a bobbin (sketch by Hugo Joulie).

3.3 GRAPHENE PRODUCTION

In this thesis, two routes of graphene production have been used. These are chemical vapour deposition (CVD), a bottom-up process, and shear exfoliation of graphite (SEG), a top-down process.

3.3.1 CHEMICAL VAPOUR DEPOSITION

Several types of CVD-graphene have been used in this thesis. Single-layer graphene (SLG) was produced at low-pressure using two different systems, a cold-wall and a hot-wall system. The cold-wall system used was a Moorfield nanoCVD 8G (Figure 3.2), in which the sample is locally heated on a resistive heating stage.

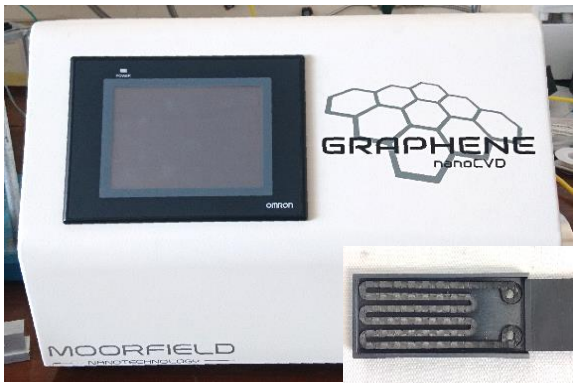

Figure 3.2. Moorfield nanoCVD 8G for growing SLG. The inset shows the coil of the resistive heating stage.

The hot-wall system is based on a quartz tube inside an MTI furnace OTF1200X-III (Figure 3.3d) with three zones which are kept at the same temperature. The sample is placed in the middle of the tube on a quartz substrate holder (Figure 3.3a) to ensure a constant temperature. The gas flows are controlled using mass flow controllers (Figure 3.3b) which are connected to the left-end of the tube. On the right-end, the gas will either flow to a vacuum pump, and then exhausted safely, or diverted through a bubbler (Figure 3.3c) before going to the exhaust system. This allows hot-wall CVD processes at low or atmospheric pressure, respectively.

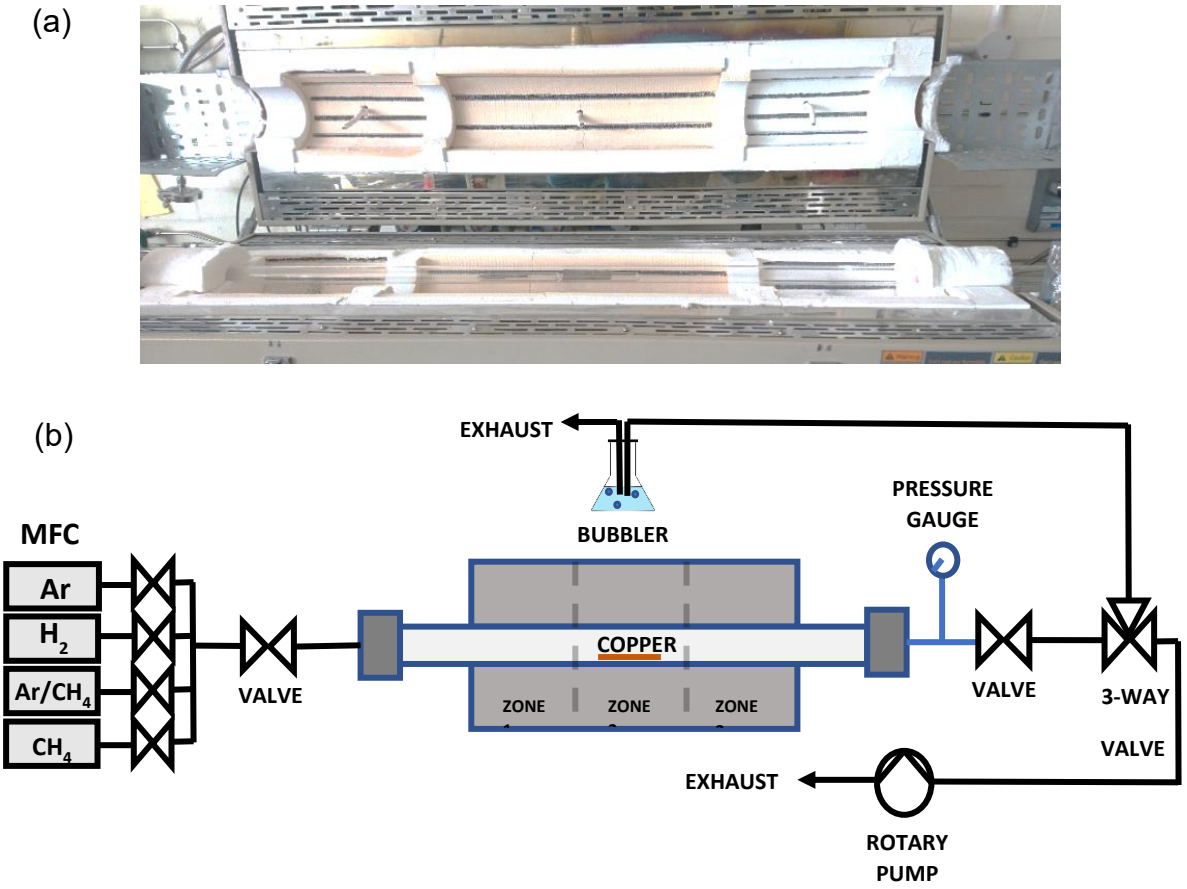

Figure 3.3. (a) Hot-wall CVD (MTI furnace) with the lid open. The Cu foils are placed at the centre of the tube inside quartz boats. (b) Schematics of gas lines the MTI furnace.

The MTI furnace was also used to develop trilayer graphene (TLG) using high-pressure within the growth chamber to force more layers of graphene to be grown on the copper substrate. Another type of commercially available few-layer graphene (FLG) was also used for comparison. As detailed in section 2.2.2, CVD growth of graphene usually comprises of the following steps: (1) *heating*, where the growth temperature is reached at a fixed rate, with or without the presence of H_2; (2) *annealing*, where H_2 cleans the metal from native oxides, also making the surface smoother; (3) *growth*, where the carbon source, CH_4, is introduced; and (iv) *cool down*, with or without CH_4, down to room temperature also at a controlled rate.

Single-Layer Graphene

SLG by cold-wall CVD: As previously reported[2], a 0.025 mm-thick 99.999 % copper foil (1×2cm) by Puratronic®, Alfa Aesar, was annealed at 1035 °C for 10 minutes under H_2 (2 sccm) and CH_4 (35 sccm) for 5 minutes. Then the chamber was rapidly cooled to room temperature which takes about 10 minutes with a large Ar flow (50 sccm).

SLG by hot-wall CVD: A 0.025 mm-thick 99.999 % copper foil (Puratronic®, Alfa Aesar) was horizontally placed on the quartz substrate holder in the central isothermal growth zone of the furnace during the entire process. The system was evacuated and flushed with Ar (300 sccm) to ensure the removal of any residual oxygen and moisture. At low pressure (2×10^{-3} torr) , the temperature was ramped up to 1035 °C (≈ 33 °C/min) under 100 sccm of H_2 and annealed under pure H_2 at that temperature for 30 minutes. Graphene was grown by adding 10 sccm of CH_4 to the mixture for 1 minute, and rapidly cooled down by opening the lid of the furnace.

Trilayer Graphene

TLG was grown using the MTI furnace at atmospheric pressure. The vacuum pump was then switched off and after the evacuation of the system, Ar was introduced at 300 sccm for 6 minutes to increase the pressure and the gas flow was diverted to the bubbler. The temperature was then ramped up to 1000 °C (≈ 33 °C/min) under 230 sccm of Ar and 70 sccm H_2, and the system was kept at that temperature and gas flow for 30 min for annealing. The Ar flow was then replaced by methane (0.1 % CH_4 in Ar) also at 230 sccm for the next 60 minutes. After the growth, the furnace was allowed to cool down to room temperature at a rate of ≈ 16 °C/min, maintaining the CH_4/H_2 flow.

Few-Layer graphene

FLG grown on Ni-sputtered SiO_2/Si (1 × 1 cm) was purchased from Graphene Supermarket with film thickness varying from one to seven layers with an average of four and described as patchwork by the manufacturer, where each patch has a different thickness[218].

3.3.2 SHEAR EXFOLIATION OF GRAPHITE

Liquid-phase exfoliation of graphite can be done using shear forces in a liquid medium, such as water. However, due to the hydrophobic nature of graphite and graphene, a surfactant is required to better disperse the flakes in an aqueous medium and to ensure the graphene does not agglomerate back to graphite flakes. The high-speed rotation of the rotor blades exerts a powerful suction and hence drawing the graphite upwards from the bottom of the vessel into the stator and centrifugal force drives them towards the edge of the rotor blades and the inner wall where they are subjected to fragmentation. Further follows hydraulic shear as the materials are forced out of the perforations in the rotor head into the mixture at high velocity[219].

SEG was produced by dispersing 12 g (15 mg/ml) of graphite flakes (Sigma-Aldrich, +100 mesh) in 800 ml de-ionised water (DIW) with 4 g (5 mg/ml) of sodium cholate as a surfactant. The mixture was stirred using a shear mixer (L5M Silverson Machines Ltd.), with a rotor size of 4.5 cm diameter at 4500 rpm over a period of two hours, as described previously[85]. The suspension was then allowed to rest overnight to allow the unexfoliated graphite to settle at the bottom of the container. The suspension was decanted into centrifuge tubes and the unexfoliated graphite was discarded. The decanted suspension was centrifuged (Thermo Scientific Heraeus Multifuge X1) for 100 minutes at 1500 rpm. The pellet was discarded, and the supernatant was collected. 20 ml of this SEG suspension was added to 60 ml of DIW and vacuum filtered through a polytetrafluoroethylene (PTFE) membrane with a pore size of 200 nm and 47 mm diameter (Millipore) to produce SEG.

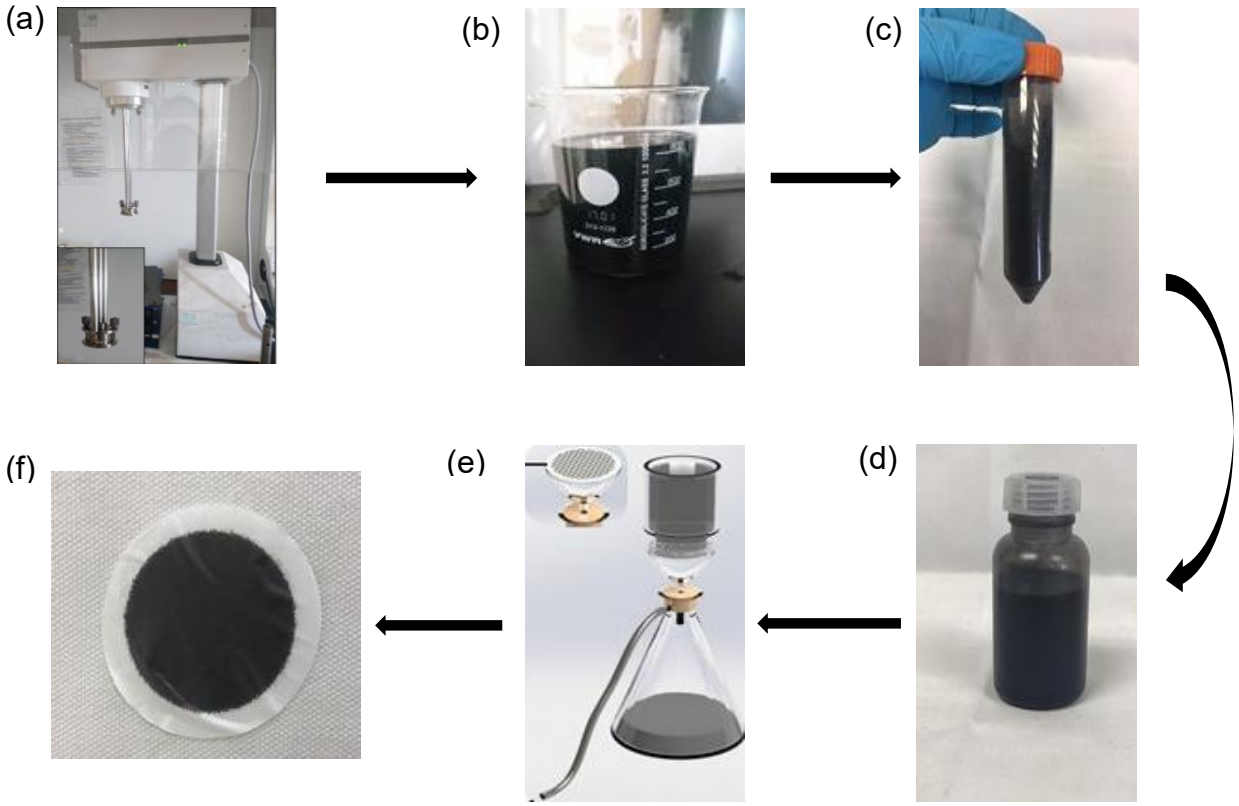

Figure 3.5. (a) L5M Silverson Machines Ltd. shear mixer; (b) exfoliated + unexfoliated graphene suspension; (c) centrifuged suspension; (d) decanted suspension, (e) vacuum filtered using PTFE membrane (sketch by Hugo Joulie); and (f) SEG on the membrane.

3.3.3 GRAPHENE OXIDE (GO)

1 ml of the commercially purchased GO from Graphenea[220], with a concentration of 4 g/L was dispersed in 60 ml of DIW and filtered through the PTFE membrane using the vacuum filtration method described in section 3.3.2.

3.4 GRAPHENE TRANSFER

Depending on the type of graphene, different transfer methods have been employed. PMMA [poly(methyl methacrylate)]-assisted transfer was used to transfer CVD-grown graphene and isopropanol-assisted direct transfer (IDT) to transfer SEG.

3.4.1 CVD GRAPHENE TRANSFER

The CVD graphene samples were spin-coated with A6 950K PMMA (*ca.* 400 nm). This was to support the graphene during the subsequent copper-etching.

Transfer of Single-Layer Graphene and Trilayer Graphene

Since graphene grows on both sides of the copper foil, after PMMA was used to coat the graphene one side, the flip side was subjected to a reactive ion etching process (RIE) to remove any graphene at the surface. The JLS RIE 80 reactive ion etcher uses argon plasma (chamber pressure: 30 mTorr; Ar flow rate: 30 sccm; RF Power: 10 W; gas stabilisation time: 30 s; process time: 50 s, pump out: 20 s) to etch away the graphene while the PMMA protects the graphene on the unexposed side. The samples were then placed at the surface of a 1 M aqueous iron (III) chloride ($FeCl_3$) for an hour, with the PMMA side up. The $FeCl_3$ solution etches the Cu leaving only the PMMA-supported graphene floating on the surface of the solution (Figure 3.6).

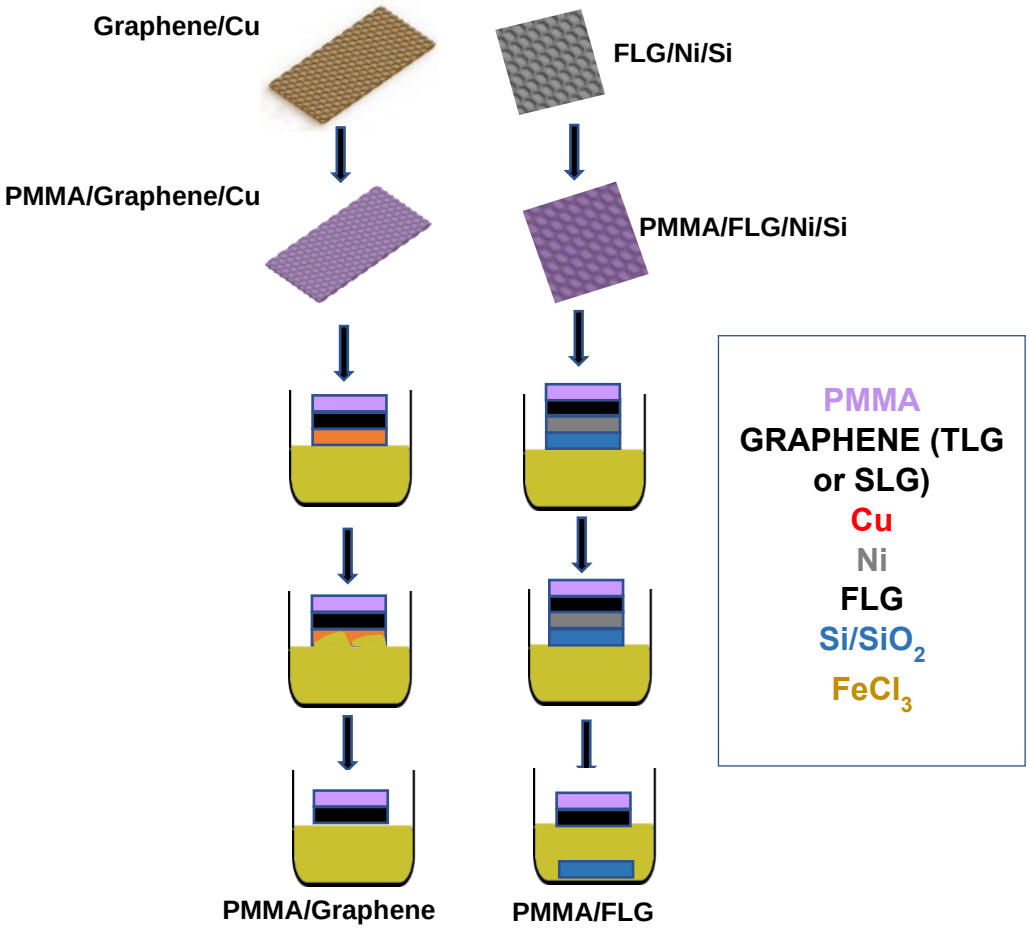

Figure 3.6. Schematic illustration of the chemical etching of the metal substrate for CVD graphene transfer, highlighting the differences between the etching of copper (SLG and TLG, right-hand side) and nickel (FLG, right-hand side) substrates.

A clean glass slide at an angle of *ca.* 120° was used to collect the PMMA-supported graphene samples from the surface and transfer them to clean DIW, repeating this process five times to ensure all $FeCl_3$ residues are eliminated. The PP fibres were immobilised on a glass slide using Kapton tape, and this glass slide was used to collect the floating PMMA-supported graphene. The assembly was first dried in air dried in air until the PMMA layer has completely dried and then placed in a desiccator under vacuum. The PMMA was removed by placing the samples in warm acetone bath (70 ºC) for 30 minutes to dissolve it and allowed to air dry (Figure 3.7).

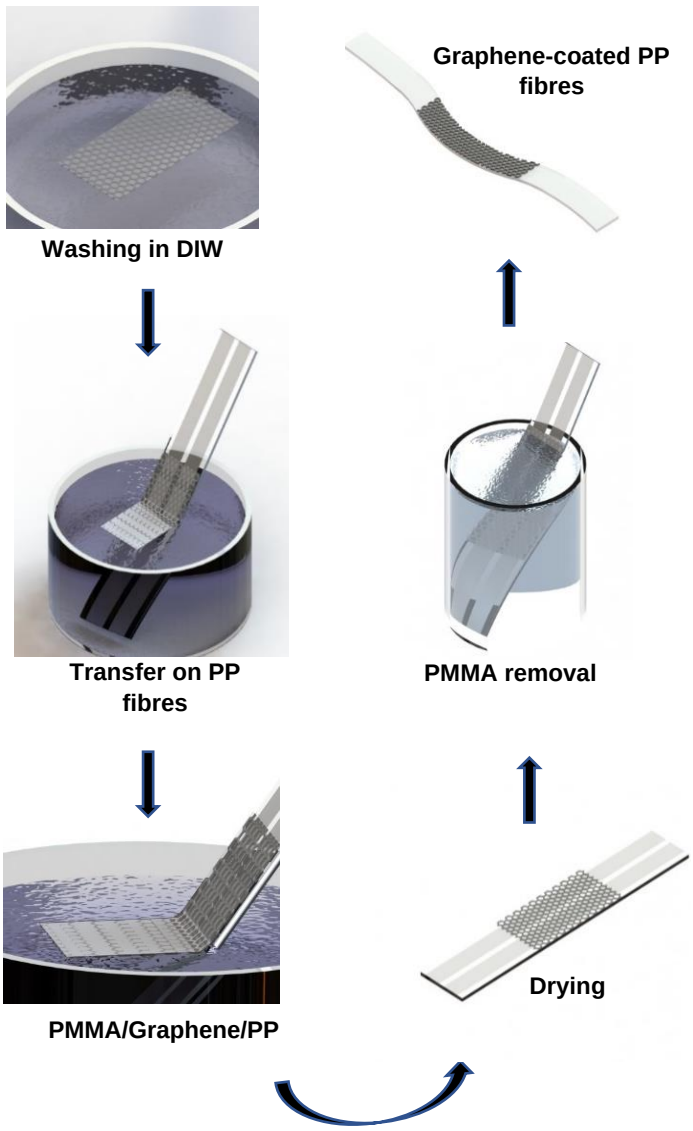

Figure 3.7. Schematic illustration of the washing and PMMA removal steps in CVD graphene transfer.

Transfer of Few-layer Graphene

The method described in 3.3.1 was adapted to the heavier FLG samples because these do not float at the surface of the etchant. For this purpose, a thicker layer of PMMA (800 nm) was spun on the samples, and the corners were carefully scratched with a scalpel, exposing the Ni layer underneath. The samples were then placed in a beaker, to which the $FeCl_3$ etchant solution was added slowly with a dropper until the

edges of the sample are covered with the shallow $FeCl_3$ solution. The samples were left overnight, and as the Ni was being etched, the PMMA-coated graphene was released and floated to the surface of the solution while the Si wafer stayed at the bottom of the glassware (Figure 3.6). It should be noted that in some cases, the graphene was not released completely. To rectify this issue, the graphene was carefully separated from the wafer with the scalpel. Like SLG and TLG, PMMA-coated FLG was then washed, transferred onto the PP fibres and the PMMA was removed.

3.4.2 TRANSFER OF GRAPHENE FROM SHEAR EXFOLIATION OF GRAPHITE

The SEG was transferred onto the bare PP fibres using a solvent-assisted transfer, IDT method, a transfer method developed by Shin *et al*.[85]. This method was previously demonstrated on PET and was modified for the transfer of SEG on PP fibres. In this method, the substrate was coated with 0.5 ml of IPA and the Teflon filter with SEG was placed facing down on the PP fibres such that the SEG is in contact with them. The PP fibres were then heated to 85 ºC. This leads to the evaporation of IPA which causes separation of Teflon filter from the graphene layer and drives the graphene onto the PP fibres. The SEG coated PP fibres were air-dried overnight. The samples were also soaked in water for two hours to remove any surfactant residue from the initial exfoliation and air dried again to obtain the SEG on PP fibres (Figure 3.8). Although this step is not required to obtain conductive SEG, it has been proven to improve the conductivity of the SEG samples by removing any sodium cholate residues from the initial exfoliation[85].

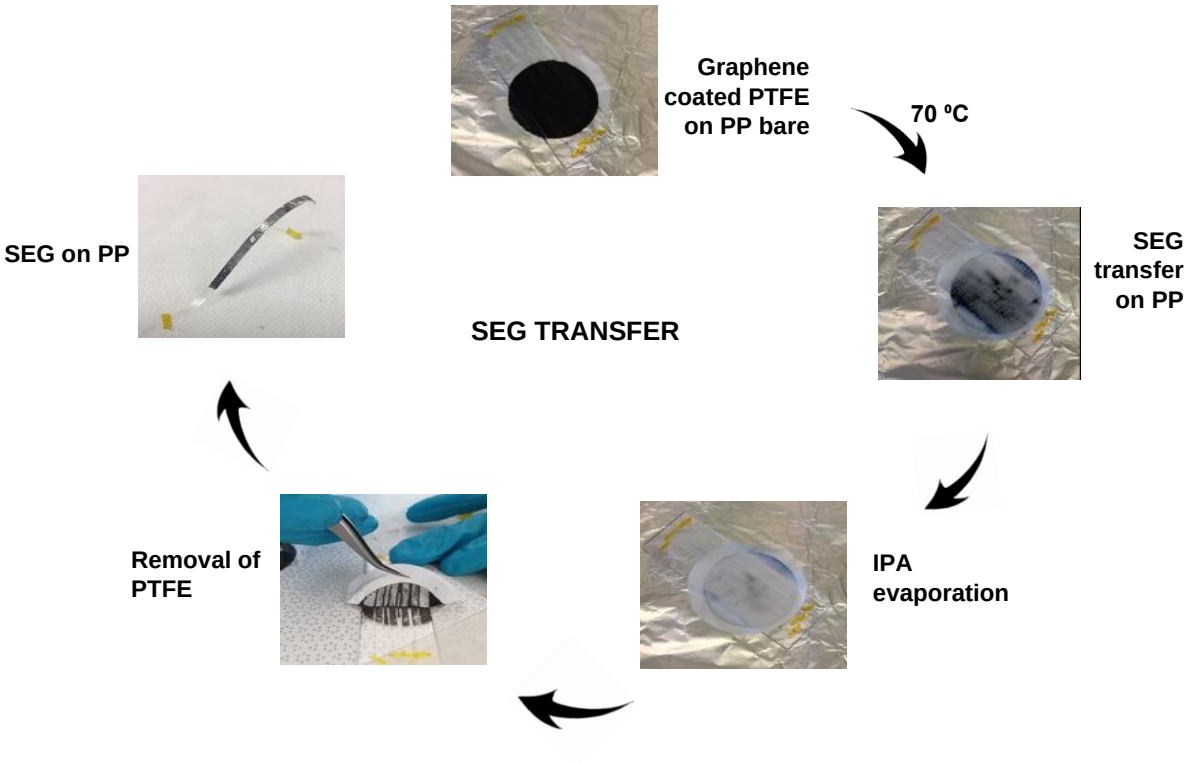

Figure 3.8. IDT transfer method for SEG on PP fibres.

3.4.2 TRANSFER OF GRAPHENE OXIDE

The GO-coated PTFE membrane was placed directly onto the SEG-coated PP fibres and dry-blown on the back of the membrane using a nitrogen-gun, releasing the GO onto the substrate. The samples were then allowed to air dry.

3.5 PATTERNING OF GRAPHENE

The interdigitated electrode geometry is widely accepted for sensors as it enables a large contact area between the electrodes within a limited area, and is therefore often used to improve the sensitivity of a sensor[4]. These structures, previously demonstrated by Torres Alonso *et al.* on PP fibres[3], were attempted in this thesis to produce graphene (SEG) patterns on PP fibres using an optical lithography process (figure 3.9). The PP fibres were first immobilised on a glass slide using double-sided Kapton tape to ensure complete adhesion of fibres to the glass slide, the lack of which can cause some of the materials spun on them to get trapped between the fibres and the glass

slide during the spin-coating process, preventing an efficient patterning. Polymethylglutaramide (PGMI) SF6 from MicroChem Corp, was spin-coated on the PP fibres at 4000 rpm and baked at 180 °C for 6 minutes, achieving a thickness of *ca.* 250 nm, followed by a layer of photoresist (PR) S1813 with a thickness of *ca.* 1.4 µm, spin-coated at 4000 rpm and baked at 120 °C for 1 minute. The samples were then loaded into a laser writer (Durham Magnetoptics Ltd.), exposed to a UV source along a digital input pattern mask to create a pattern and developed in a developer (tetramethylammonium hydroxide). The developer dissolves not only the areas where the PR has been exposed but also the PMGI layer which is underneath the PR. The development process takes about 45 seconds. The PR was then removed by immersing the sample in acetone whereas the patterned PMGI remain. The graphene is then transferred onto the pre-patterned surface using the transfer methods explained in 3.4. Finally, the PMGI is dissolved in *N*-methyl-2-pyrrolidone under mild ultrasonication, leaving the PP fibres with graphene patterns.

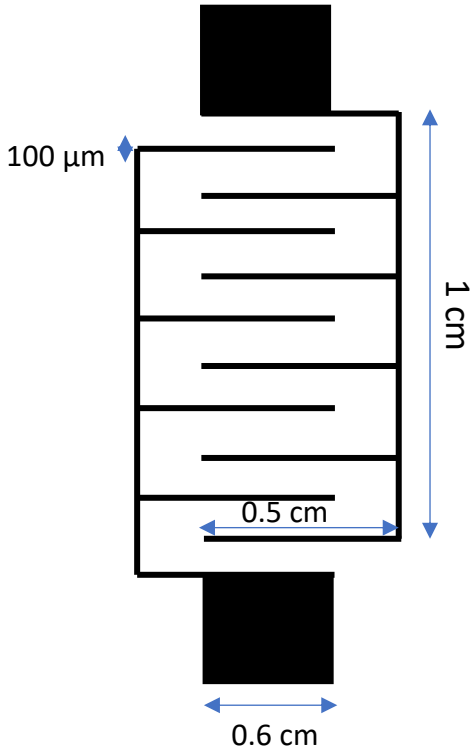

Figure 3.9. Schematics of interdigitated pattern.

3.6 CHARACTERIZATION TECHNIQUES

All the different types of graphene were characterised using various techniques. Table 4.1 summarises all the samples prepared.

Types of Graphene	Number of graphene layers	Production method	Carbon precursor	Substrate for graphene growth	Target substrate	Transfer method
SLG	1	CVD	Methane gas	Copper foil	Si/SiO_2 and PP	PMMA-assisted
TLG	average of 3 layers	CVD	Methane gas	Copper foil	Si/SiO_2 and PP	PMMA-assisted
SEG	average of 4 layers	High shear exfoliation	Graphite flakes	Dispersed in de-ionised water	Si/SiO_2 and PP	IPA-assisted
FLG	average of 4 layers	CVD	Methane gas	Nickel (commercially purchased)	PP	PMMA-assisted
GO	1	Chemical exfoliation	Graphite	Commercially purchased powder	PP	PTFE-assisted

Table 4.1. Summary of all the different types of graphene studied in this thesis

3.6.1 RAMAN SPECTROSCOPY

Raman spectroscopy was used to ascertain the presence of graphene on PP fibres, differentiate graphene based on the number of layers, to assess the quality of the graphene produced, and to study the effect of temperature on the Raman signatures of graphene coated fibres.

Raman measurements were performed with a WITec Alpha 300R (confocal Raman system) spectrometer equipped with a thermoelectrically cooled CCD detector (−60 °C) used with a 532 nm laser excitation source backscattered light collection with a 50× Zeiss objective (EC EPIPLAN NA 0.7) and a spot size of 388 nm. The spectrometer gratings used were 1800 g/mm. WITec Project Plus was used to analyse the data. Different types of graphene were transferred onto several substrates using the transfer methods explained in section 3.4. The spectra were normalised to the Si-peak at 520 nm for an accurate comparison between difference Raman scans. These measurements were performed by Dr. Ellen Green (University of Exeter).

Temperature-dependent Raman measurements were performed to study the effect of temperature on the Raman signatures of the different graphene coated PP fibres at a

heating rate of 5 °C/min, and measurements were taken every 5 °C using the Renishaw Raman system by Dr. Jessica Wade in Prof. Ji-Seon Kim's research lab at Imperial College of London. A long working-distance 50× objective was employed, and 514 nm argon ion laser was set at 10−50 % power in nitrogen to avoid sample damage.

3.6.2 ELECTRICAL CHARACTERISATION

Electrical measurements of graphene-coated PP fibres were performed by using the standard and most used two-probe method. This method employed two metallic probes (tungsten), a source-meter (Keithley 2400) and either carbon paste or silver ink to draw the contacts to facilitate the measurements. Both silver and carbon contact material were purchased from DuPont. A small amount of carbon paste/silver ink was applied on two ends of the graphene section in a way that the contacts are 1 cm apart. They were cured on a hotplate (Thermo Scientific, Super Nuova) at a temperature of 80 °C until the contacts have dried. A probe setup as shown in Figure 3.10 has been custom designed as such that the probes would be 1 cm apart. This setup was built by Dr. Peter Armitage (University of Exeter). This ensured comparable electrical measurements. The body of the setup was constructed with acrylic along with adjustable screws to hold the probes and for simple removal. The measurements were performed at an imposed voltage ranging from 0.5 V to 1 V throughout this thesis. The graphene-coated temperature (chapter 5) and humidity (chapter 6) sensors were also electrically characterised using the same custom-built 2-probe setup. The temperature and humidity sensing responses of the graphene-based sensors were compared with the response of a commercial temperature and humidity sensors against time. The Keithley 2400 source measure unit was used to power the commercial humidity sensor (Honeywell HIH-4000-003) and temperature (Texas Instruments LM35CaZ/NOPB) sensors at 5 V.

The two-probe resistance measurement formula as shown in equation 3.1 includes the resistance value obtained from the source meter using the two probes. This value is R_{2p}. The R_{2p} also includes contact resistance (R_c) which is the resistance contributed to the total resistance of a sample that can be attributed to the contacting interfaces of electrical leads and connections as opposed to the intrinsic graphene resistance (R_G).

Since two probes are used, the contact resistance is doubled. Although for the devices used in this thesis (chapter 4 and 5), only the change in resistance ratio has been used without the need to consider the contact resistance from the probes.

$$R_{2p} = R_G + 2R_C \tag{3.1}$$

where, $R_G = \frac{\rho L}{W}$, L being the channel length, W the channel width, and ρ the graphene resistivity.

The R_c was estimated by a method commonly used for graphene devices, based on measuring the R_{2p} in devices with different contact lengths, L^{Dev1} and L^{Dev2}, while keeping constant channel width ($W^{Dev1} = W^{Dev2}$). In this case, the contact resistance is given by the following relation[231]:

$$R_C = \frac{R_{2p}^{Dev1} - \rho_G\left(\frac{L^{Dev1}}{W^{Dev1}}\right)}{2} \tag{3.2}$$

where:

$$\rho_G = \frac{R_{2p}^{Dev1} - R_{2p}^{Dev2}}{\frac{L^{Dev1}}{W^{Dev1}} - \frac{L^{Dev2}}{W^{Dev2}}} \tag{3.3}$$

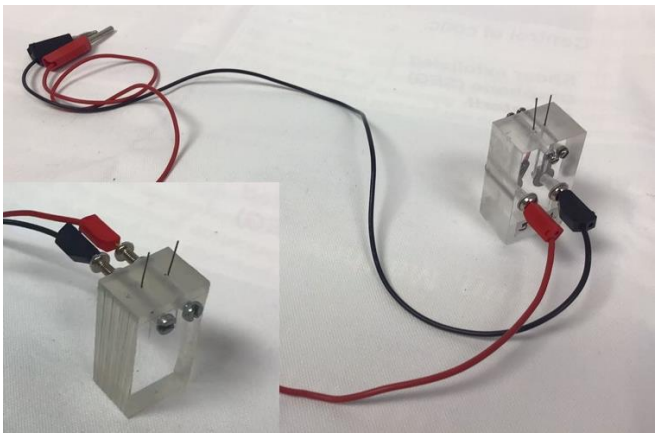

Figure 3.10. Custom-built two-probe setup for electrical measurements. The body of the setup is made up of acrylic and the tungsten probes are placed 1 cm apart.

3.6.3 RESILIENCE TESTS

Washability and the bendability (mechanical resilience) of the graphene-coated fibres were studied by subjecting the conductive fibres through a series of washing tests and bending tests. The change in resistance was monitored by measuring the resistance before and after the bending or washing cycles.

Washing tests

To emulate the washing machine, graphene coated fibres were placed in a glass beaker with a solution consisting of commercially available laundry detergents/fabric softener with tap water and a magnetic stirrer for 60 minutes. Several parameters such as temperature (30, 40 and 50 ºC), spin speed (400, 800, 1000 rpm), and laundry detergents (regular and for sensitive fabrics) were varied.

Bending tests

The bending tests consisted of repeated bending of the graphene coated fibres up to 1000 bending cycles using a cylindrical tube with a fixed bending radius of 5 mm. The fibres were bent and flattened again as shown in figure 3.11a. This was one bending cycle. These cycles are repeated and change in resistance is calculated.

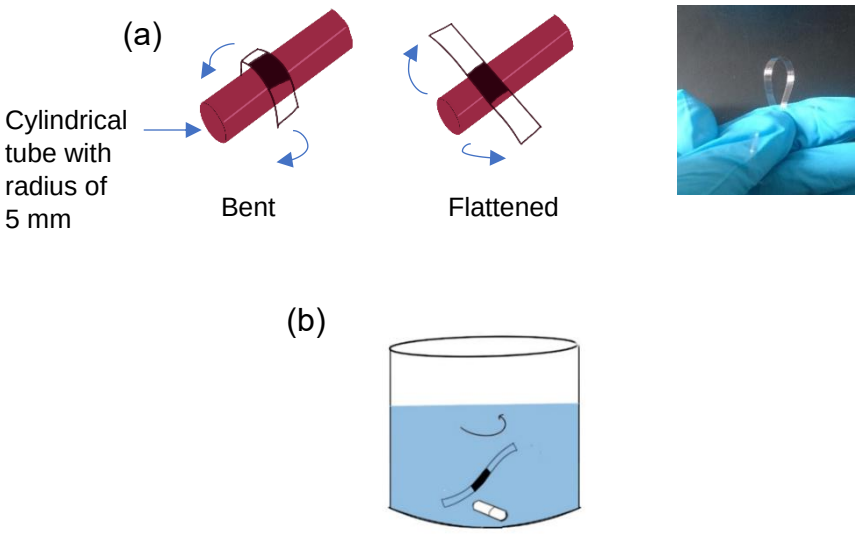

Figure 3.11. Resilience tests: (a) Bending test method (left) and demonstration of bendability of PP fibres (right); (b) washing tests with magnetic stirring.

3.6.4 ATOMIC FORCE MICROSCOPY

AFM is a high-resolution scanning probe microscopy which can be used to study the topology and properties of the surfaces. Here, the different types of graphene-coated fibres were subjected to AFM studies using a Bruker Innova AFM in the tapping mode to study the graphene coverage at the surface. The tapping mode is gentle and will not adhere or stick to the surface of the samples. This mode operates by alternately placing the vertically oscillating sharp tip (attached at the end of a cantilever) in contact with the sample surface where it lightly taps and then lifting the tip off the sample to avoid dragging the tip across the surface. Topography, amplitude, and phase maps were generated for PP coated with the different types of graphene. The graphene-coated PP fibres were fixed on an AFM sample mounting steel disks using double sided Kapton tape since it is crucial to have a flat sample to obtain high quality images. The software used to analyse the AFM data was Gwyddion[221], and WSxM from Nanotec[222] was used to obtain the height profiles. The size of the AFM tip was about 10 µm. The tapping mode parameters were varied during the measurements to obtain better quality images and depended on the sample used. The tapping mode settings used, in general, were as follows: scan rate-0.5 Hz; setpoint-4.00 V; scan size-50 µm; rotation-90°, X and Y-offset- 0.0 µm; samples-256, feedback-4.2 V; and drive-0.83 V.

3.6.5 SCANNING ELECTRON MICROSCOPY (SEM)

To inspect the surface morphology of the conducting samples, SEM can be used to obtain high-resolution images. When a focussed beam of high-energy electrons is scanned in a raster pattern across the surface of the sample, various types of signals are produced at the surface of the sample. A detector collects these signals to reveal information about the texture, crystallinity, and chemical composition of the materials in the sample.

A TESCAN VEGA3 scanning electron microscope was used to perform topological studies of the graphene-coated substrates surface (graphene coverage, tears, cracks, or folds). The samples were cut to an appropriate size (length: 0.5 cm) and mounted securely on circular aluminium sample holders called stubs with the use of carbon tape

(Agar Scientific). The samples were sputtered with a thin film of gold prior to the SEM study.

3.6.6 TRANSMITTANCE STUDIES

Transmittance is defined as the fraction of the incident light of a specific wavelength that passes through the medium without interfering with it[223]. In spectroscopy, transmittance studies are used to characterise the optical or physical properties of different materials. This technique has been used previously to obtain relevant information about the transparency of graphene samples and calculate the number of graphene layers[224]. The measurements were performed by Mr. Conor Murphy (University of Exeter) using a custom-built UV-Vis microspectrometer[225]. The graphene was transferred to a glass slide and inserted in the spectrometer to obtain the transmission spectra.

Transmittance data were also used to ascertain the number of layers in TLG by using a method described by *Zhu et al*.[224] in 2014, with the following non-linear negative exponential function of the form:

$$T = (1 + 1.13\alpha\pi\frac{N}{2})^{-2} \qquad (3.4)$$

where N is the number of graphene layers, 1.13 is the estimation of the correction coefficient, and α is the fine structure constant, defined as:

$$\alpha = e\hbar\frac{2}{c} \approx \frac{1}{137} \qquad (3.5)$$

The relation provides a good description of the transmittance of light through multilayer graphene in the visible range.

3.7 TEXTILE HUMIDITY SENSOR: FABRICATION AND SENSING TESTS

The sensor consists of: (1) PP textile fibre as the flexible substrate; (2) graphene as the humidity-sensing layer; and (3) carbon paste as the contact material. PP fibres were coated with two types of graphene, TLG and SEG using the transfer techniques mentioned in section 3.4.

To study the response of the textile humidity sensors to humidity, two types of tests were performed. The samples were subjected to human blowing tests and continuous measurements. The blowing test includes the gentle human blowing process on the samples at random intervals to study the change in conductance with respect to the humidity as shown in figure 3.10a.

Continuous RH measurements were performed by placing the devices and the two-probe setup in a home-built humidity chamber made of a plastic box with tight lid and a drilled hole for the electrical connections, and with a commercial domestic air humidifier providing increasing humidity levels (figure 3.10b).

For both human blowing and continuous tests, the graphene sensor and commercial sensor were placed next to each other to obtain comparable data. The custom-built two-probe setup was placed on the graphene sensor which was connected to the source meter as explained in section 3.6.2. The supply voltage used was set to 1 V. The Keithley 2400 source measure unit was also used to power the commercial humidity sensor (Honeywell HIH-4000-003) with an operating voltage of 5 V. The conductance was calculated from the resistance data obtained from the measurements.

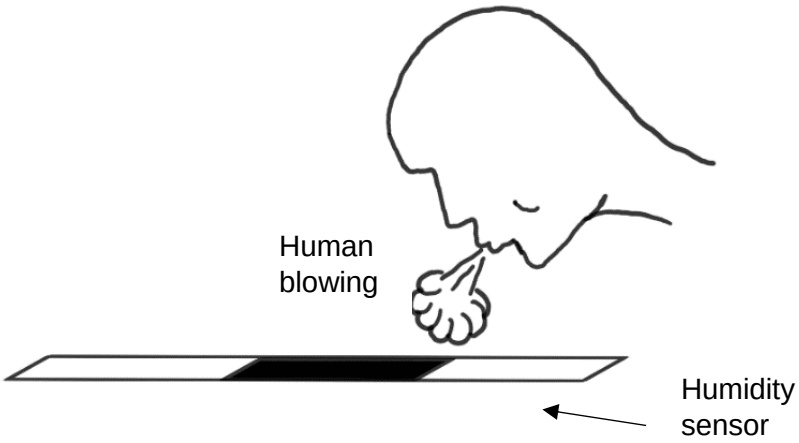

(a)

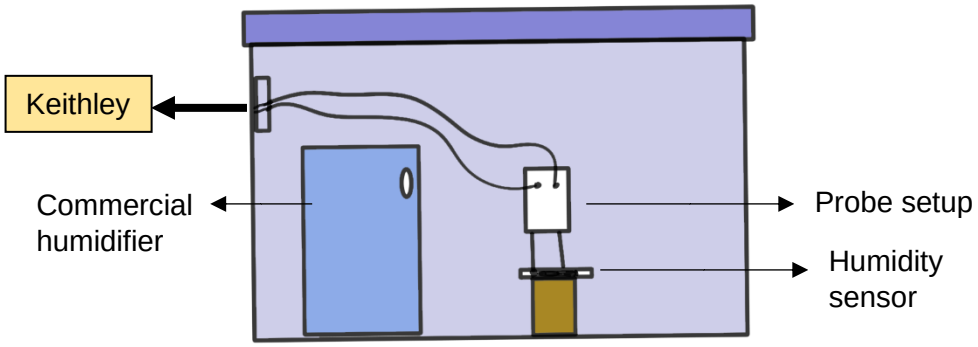

(b)

Figure 3.10 Humidity sensing tests: (a) human blowing tests; (b) continuous measurement inside a home-built humidity chamber consisting of :a plastic box and a lid; a commercial humidifier; probe setup; and humidity sensor.

Chapter 4

CHARACTERISATION OF GRAPHENE-COATED FIBRES

4.1 INTRODUCTION

In this chapter, different types of graphene have been characterised using the different techniques mentioned in section 3.6. The production and transfer of these different types of graphene have been explained in detail in sections 3.3 and 3.4.

4.2 CHARACTERISATION OF GRAPHENE

4.2.1 SINGLE-LAYER GRAPHENE (SLG)

SLG was produced by two different CVD methods: cold-wall CVD (nanoCVD), and hot-wall CVD (MTI furnace), as detailed in section 3.1.1. The SLG production by cold-wall CVD has been shown to be more efficient, have faster heating and cooling rates, shorter growth time and less gas consumption than the hot-wall CVD[226]. Figure 4.1a shows the Raman spectrum of SLG produced in the nanoCVD cold-wall system, showing the characteristic D-peak at 1345 cm^{-1}, G-peak at 1589 cm^{-1} and 2D-peak at 2684 cm^{-1}. The peak positions are comparable to those shown previously for this type SLG when used to coat textile fibres[1,2]. The intensity ratio, I_G/I_{2D}, was found to be *ca.* 0.58, $FWHM_{2D}$ of *ca.* 33.7, and a single Lorentzian fit, suggesting a single layer of graphene according to the graphene characterisation guidelines by NPL[157]. Although the nanoCVD produced high quality SLG, which was also demonstrated by Neves *et al*.[2], due to technical difficulties related with non-uniform temperature in the cold-wall stage, the use of nanoCVD was discontinued and an alternative method of producing SLG had to be developed. The MTI furnace was then used to produce SLG on Cu foils at low pressure. Although this process takes considerably longer than the nano-CVD one, it had the advantage of producing multiple samples in a single run. It has been suggested that low pressure allows fast diffusion and high mass flow rate of precursor gas which prevents the saturation of decomposed carbon atoms leading to the self-limited SLG growth on Cu substrate[227]. Figure 4.1b shows the Raman

spectrum of SLG produced by the MTI furnace showing D-peak at 1347 cm^{-1}, G-peak at 1588 cm^{-1} and 2D-peak at 2680 cm^{-1} which are like the peak positions obtained for SLG produced by nanoCVD along with the single Lorentzian fit. The intensity ratio, I_G/I_{2D} was found to be *ca.* 0.59 and $FWHM_{2D}$ of *ca.* 26.4, suggesting a single layer of graphene. It should be noted that the SLG produced by MTI has a larger D-peak than expected for a high quality SLG. Further optimisation of the growth processes would lower the defect peak.. The presence of a large D-peak could be due to the of large number of defects such as carboxyl and hydroxyl groups that have been associated with the use of PMMA to transfer the graphene. The Raman spectroscopy can be used to characterise the edges and the grain boundaries of graphene. The presence of a strong D-peak could mean there are armchair edges present in this type of graphene since only they are capable of elastically scattering charge carriers which can give rise to the D-peak. An increased D-peak could also represent the nucleation centre in graphene as well as the grain boundaries which are formed where two separate seed points grow together[267].

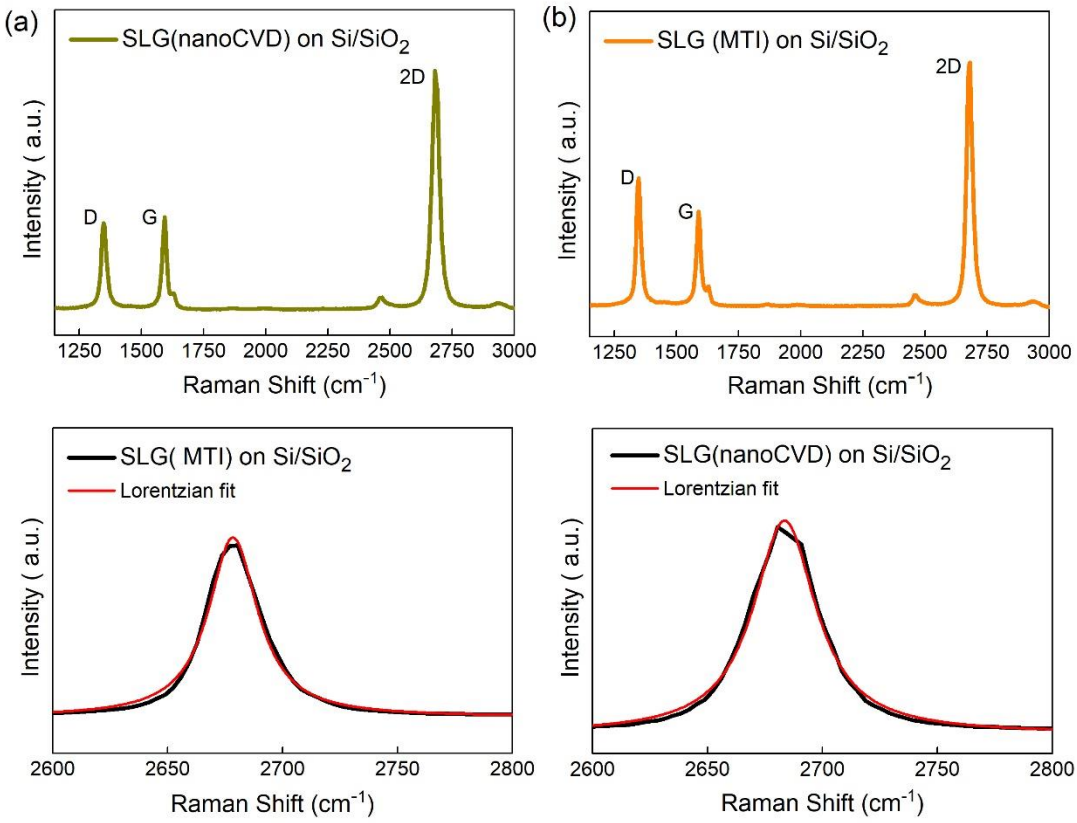

Figure 4.1. Raman spectra of: (a) SLG on Si/SiO₂ produced using nanoCVD (top) and 2D-peak with the Lorentzian fitting (bottom), (b) SLG produced using MTI-furnace (top) and 2D-peak with the Lorentzian fitting (bottom).

4.2.2 TRILAYER GRAPHENE (TLG)

TLG is a purposely developed CVD-graphene which has an average of three layers of graphene. The methodology to produce TLG has been mentioned in section 3.3.1. Figure 4.2a shows the representative Raman spectrum of TLG on Si/SiO_2 with the Si peak at 520.7 cm^{-1}, the graphene D peak at 1351 cm^{-1}, G peak at 1592 cm^{-1} and 2D-peak at 2680 cm^{-1}. By the guidelines published by the National Physical Laboratory (NPL), UK, Raman spectroscopy can only be used to indicate the number of layers in CVD graphene. The indicators of SLG are a $FWHM_{2D}$ < 35 cm^{-1} along with I_G/I_{2D} < 1[157]. In principle, this ratio can provide a discrete estimate of the number of layers. However, it has been found that the 2D-peak depends strongly not only on the number of layers

but on the carrier density, which depends on the impurities present in the graphene sample[157].

The NPL guide further suggests that the above-mentioned indicators can also be affected by strain and doping in the graphene. Therefore, on its own, the relative intensity ratio is not a reliable metric for the estimation of graphene layers. A more convenient approach was developed by Koh *et al.*, also based on Raman spectroscopy, which involves estimation of the number of layers of graphene by comparing the intensity of G peak of the graphene on Si/SiO_2 and the distinct Si-peak (I_G/I_{Si})[228]. Following this method, the average number of graphene layers in TLG samples was found to be three, corresponding to an I_G/I_{Si} ratio of *ca.* 0.28. The same method was also employed to an area of 30 × 30 μm^2 to produce a Raman map of the TLG (Figure 4.2b), which shows the distribution in terms of the number of graphene layers, ranging from one to four layers by using the WITec Project Plus software. In a Raman map, every pixel consists of a Raman spectrum which are produced by obtaining Raman spectrum at various consecutive positions on a sample. To visualise this in a single image, values are generated that represent the chemical information of each measurement point. These values were then plotted in a Raman map using a MATLAB program.

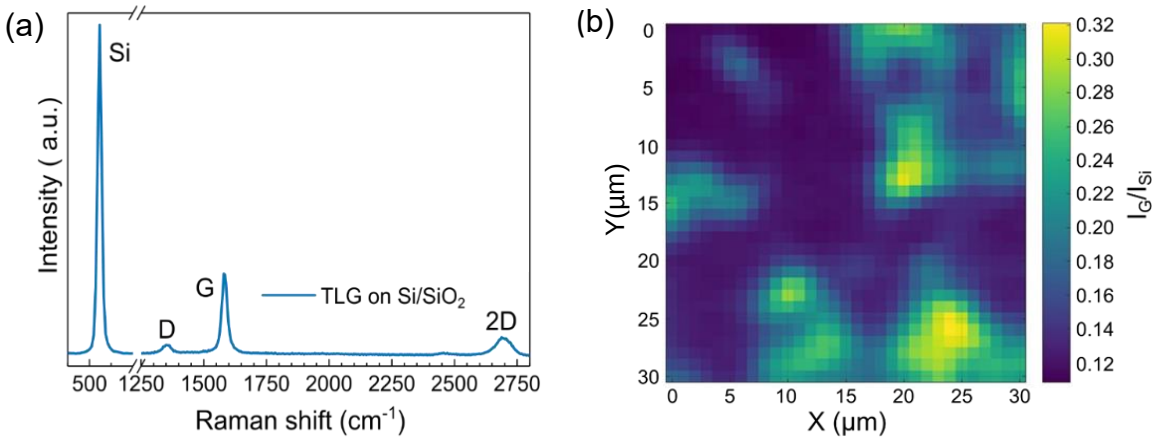

Figure 4.2. Raman spectroscopy for TLG on Si/SiO_2: (a) single spectrum highlighting the characteristic graphene Raman signatures, (b) Raman map with an area of 30 × 30 μm^2 showing the distribution of graphene layers. Reproduced with permission from ACS publications[229]. Reproduced with permission from ACS publications.

Three different TLG samples were subjected to the optical transmittance study by transferring them to glass. Figure 4.3 shows the experimental data (transmittance vs wavelength). The number of layers was extracted at 550 nm since the transmittance is free of stacking sequence at that wavelength[230]. As mentioned in section 2.2.1, a single layer of graphene absorbs about 2.3% of visible light at 550 nm and the addition of another layer leads to increase in the absorption by approximately the same percentage. This agrees with the percentage of transmittance (89.1-93.3%) and the average of the calculated number of layers of graphene (*ca.* 3) in TLG at 550 nm, as shown in Figure 4.3 inset table, which is why the developed graphene was named as TLG.

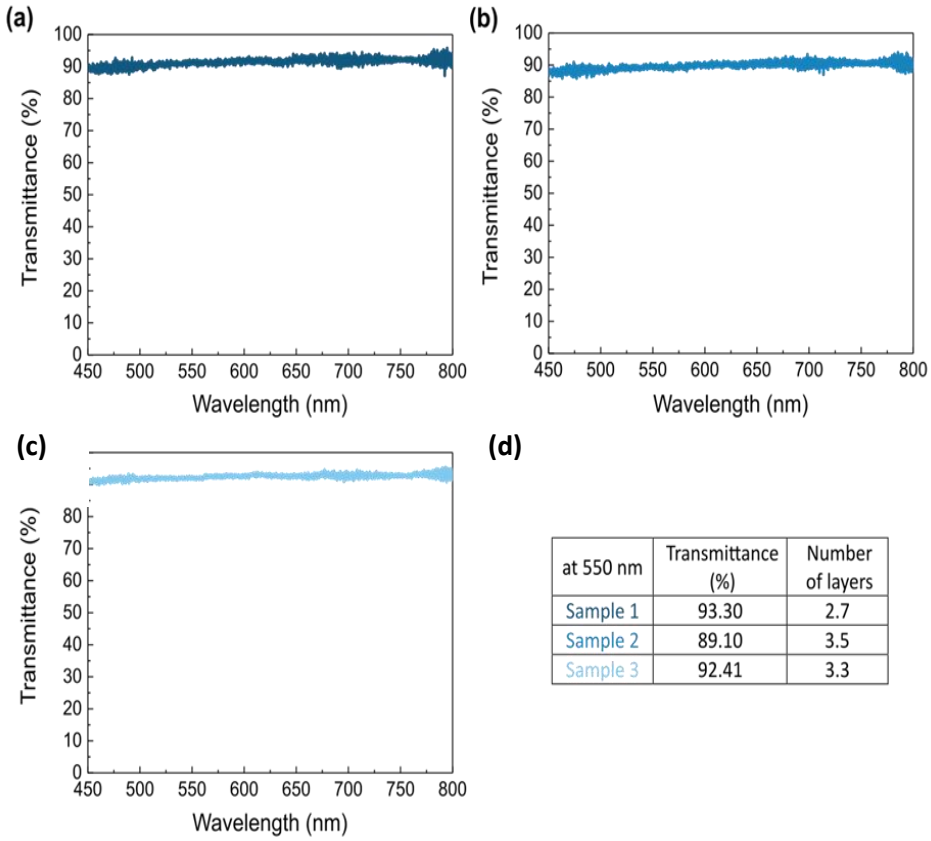

at 550 nm	Transmittance (%)	Number of layers
Sample 1	93.30	2.7
Sample 2	89.10	3.5
Sample 3	92.41	3.3

Figure 4.3. Transmittance of TLG on glass in: (a) sample 1; (b) sample 2; (c) sample 3. (d) Table with the number of layers calculated at the transmittance taken at 550 nm. Reproduced with permission from ACS publications[229]. Reproduced with permission from ACS publications

This type of graphene was developed to be more conductive than SLG. The number of layers was expected to be more than one layer but fewer than the commercially available FLG, grown on Ni, that has an average of 4 layers, but a wider range from 1 to 7 layers. Several mechanisms have been suggested in the literature for the formation of more than one layer of graphene on Cu substrates which could have contributed to the growth of TLG. As described in section 2.2.2, the graphene growth on Cu substrate is usually self-limiting which leads a growth of a single layer of graphene at low-pressure. However, at atmospheric pressure, in the CVD-reactor tube, where the mass flow rate is slower than in the low-pressure CVD, saturation of carbon atoms occurs which leads to formation of multiple domains and deposition of decomposed carbon atoms to form thicker layers over the monolayer[103]. In 2012, Kalbac *et al.* suggested that the grain boundaries in the single-layer graphene provide nucleation sites to decomposed carbon atoms to form another layer of graphene[105]. Another possible mechanism was suggested by Jun Li *et al.* in 2016, which suggests that during the catalytic decomposition, some of the carbon atoms get trapped between the first layer and the substrate to form adlayers which leads to be formation of multiple layers of graphene[87].

In the Raman spectrum of TLG, the D-peak is smaller than the SLG which suggests a low-defect graphene. Like SLG, the presence of D-peak could be due to PMMA processing which leaves behind residues. With the increase in the number of layers in graphene, stacking is also considered which could have gaps, adding to the defects. The other types of defects could be a carbon atom missing in some hexagonal lattice site, forming a vacancy at this site or extra atoms might also be left between layers of the TLG. These carbon atoms can form interlayer bonds with the atoms in the two sandwiching layers[267]. It should be noted that the growth temperature of TLG is lower than the SLG. This is because the formation of bilayer or few-layer graphene is highly preferred at relatively low temperatures (900-1000 °C). Xing *et al.* did a kinetic study of graphene growth where the effect of temperature on growth rate and film thickness was studied. The low temperature phenomenon can be explained as follows: The decomposition of methane leads to supersaturation of active carbon species at the Cu surface, which then reaches a critical point and graphene nucleation (C_{nuc}) occurs followed by a drop in the growth level(C_{growth}). The difference (dC) between the C_{nuc} and C_{growth} is the amount of carbon consumed during the nucleation. At low

temperatures, both C_{nuc} and C_{growth} drop, but the difference dC increases compared to that of high temperatures. This contributes to multi-layer nucleation[250].

4.2.3 FEW-LAYER GRAPHENE (FLG)

As mentioned in section 3.3.1, FLG is the graphene grown on Ni-sputtered SiO_2/Si and has a distribution of one to seven layers with an average of four layers of graphene and was purchased from Graphene Supermarket[218]. The manufacturers of the FLG suggest that Raman spectra of FLG would dramatically change depending upon the spot of study since with Ni as a catalyst, it is difficult to produce graphene with uniform layering and thickness[218].

Figure 4.4 shows the Raman spectrum (at a random spot) of FLG on Si/SiO_2 which has an intensity ratio of I_G/I_{2D} of *ca*. 4, suggesting a multilayer graphene. The positions of the characteristic Raman peaks are as follow: D at 1357 cm^{-1}, G at 1580 cm^{-1} and 2D at 2697 cm^{-1}.

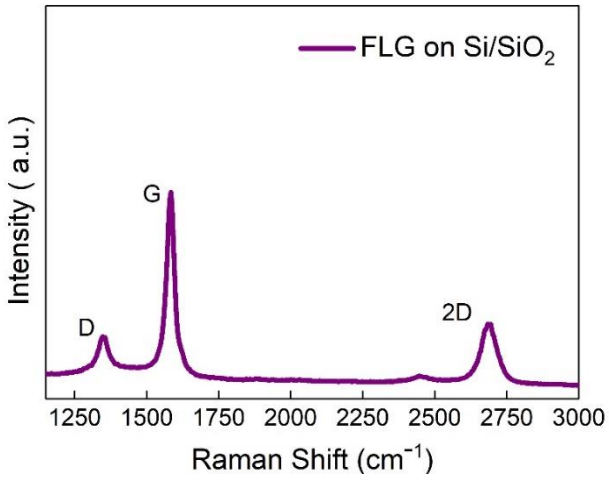

Figure 4.4. Raman spectrum of FLG on Si/SiO_2.

4.2.4 GRAPHENE FROM SHEAR-EXFOILATION OF GRAPHITE (SEG)

SEG was produced using graphite flakes as carbon source by high-shear exfoliation process, as mentioned in section 3.3.2, and was transferred on to Si/SiO_2 and PP fibres

using IDT method explained in 3.4.2. The only modification to the previously reported transfer process was that the temperature used for the evaporation of IPA was 85 °C instead of 90 °C as suggested by Shin *et al.*[85]. Figure 4.5 shows the SEG-coated PP fibres transferred using the IDT method at 90 °C and 85 °C. Although at 90 °C the graphene was still transferred, there were gaps and holes in the transferred graphene. This was not the case at 85 °C which could be due to the slightly lower temperature preventing the rapid evaporation of IPA leading to a relatively better graphene transfer.

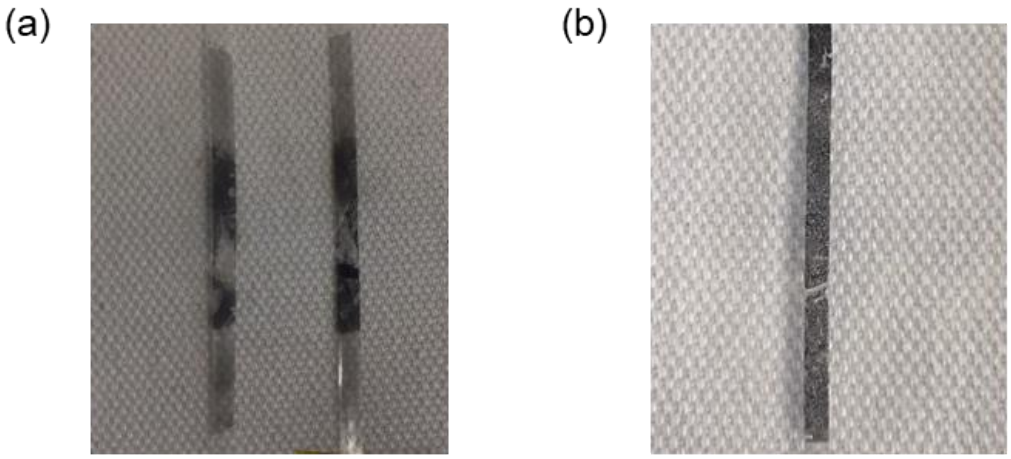

Figure 4.5. (a) Optical image of SEG on PP transferred at (a) 90 °C showing partial graphene transfer with gap in the graphene, (b) 85 °C showing SEG with no gaps.

Figure 4.6 shows the Raman spectrum of SEG on Si/SiO_2. The positions of the characteristic Raman peaks for SEG were found to be D at 1343 cm^{-1}; G-peak at 1588 cm^{-1}; and 2D-peak at 2682 cm^{-1}. The obtained SEG sheets have the average lateral size of *ca.*110 nm and an average of four layers with more than ≈50 % containing one, two and three layers with a transparency between 45 to 70 % with an I_G/I_{2D} intensity ratio of *ca*. 4, suggesting a multilayer graphene[85]. The spectrum also shows a large defect peak as compared to the graphene produced by CVD, which was expected since SEG films comprise separate graphene flakes that overlap during the filtration process, increasing the presence of edges. The concentration of the obtained SEG suspensions were found to vary with the shear exfoliation time and was ≈16.45 µg/ml. This concentration was found in line with the previously reported concentration at shear exfoliation time of 60 minutes[85]. This concentration is lower than

the graphene yield obtained when organic solvents are used as a solvent instead of water. However, using water as a solvent adds to the simplicity, eco-friendliness, and cost-effectiveness of the process, especially during the mass production of SEG.

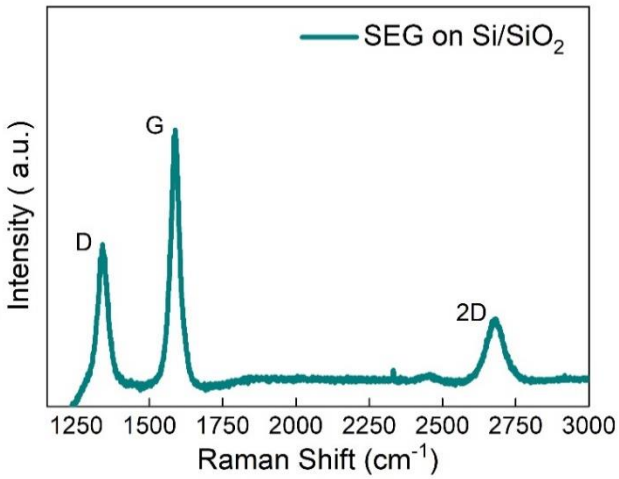

Figure 4.6. Raman spectrum of SEG on Si/SiO_2,

4.3 GRAPHENE- COATED PP FIBRES

The different types of graphene mentioned in the previous subsections were transferred to clean PP fibres with the transfer methods described in section 3.4. Raman spectroscopy was used to confirm the presence of different types of graphene in the graphene-coated PP fibres. Figure 4.7 shows PP coated (left to right) with SLG, TLG, FLG and SEG with decrease in transparency. Figure 4.9 shows the Raman spectra of bare PP fibre, SLG-coated PP, TLG-coated PP, FLG-coated PP and SEG-coated PP fibre. The dashed lines indicate the expected positions for D, G, and 2D peaks. As can be seen in Figure 4.8a, the D peak (*ca.* 1350 cm^{-1} for SLG), is close to one of the PP peaks, is very small in the case of SLG and not distinguishable from the PP peak. The 2D peak in the case of all graphene-coated PP fibres is almost indistinguishable from the peaks of the PP fibres nearby because of the partial overlap with the PP peaks.

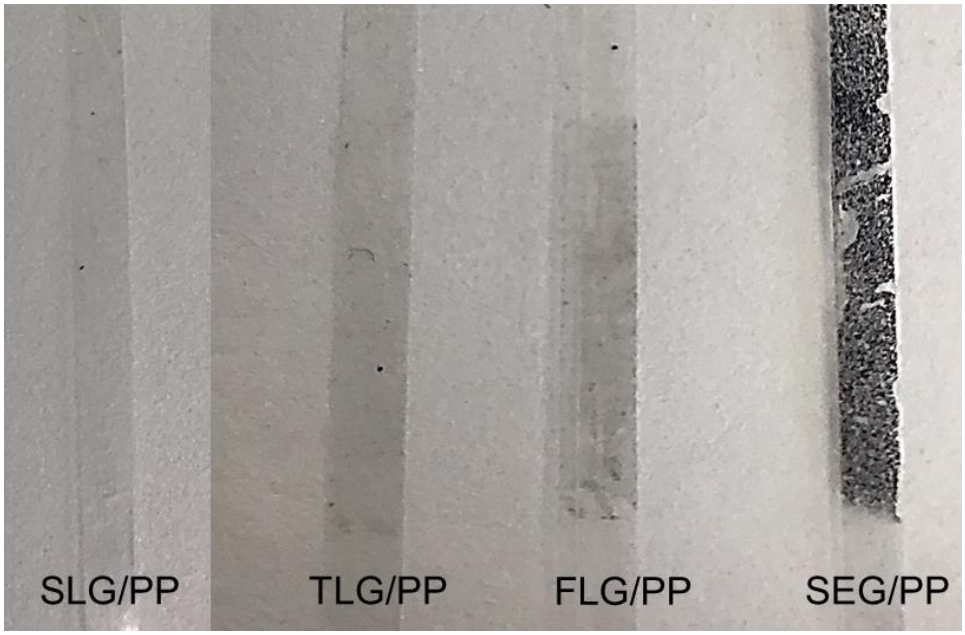

Figure 4.7. Optical image of PP coated (left to right) with SLG, TLG, FLG and SEG.

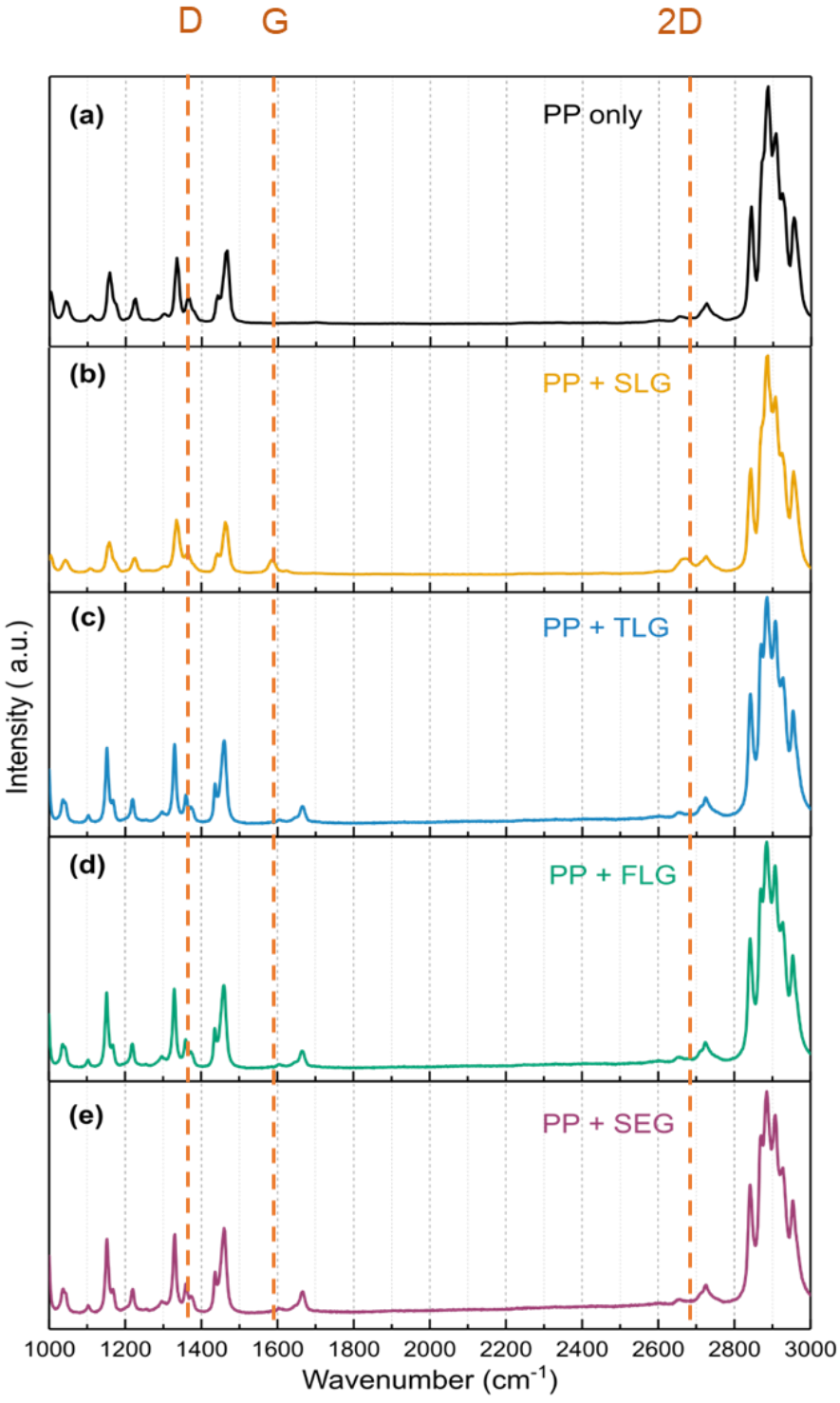

Figure 4.8. Raman spectra of: (a) PP bare fibre; (b) PP + SLG; (c) PP + TLG; (d) PP + FLG; and (e) PP + SEG. The dashed lines show the expected position of the D, G, and 2D-peaks in SLG. Reproduced with permission from ACS publications[229]. Reproduced with permission from ACS publications

4.4 ATOMIC FORCE MICROSCOPY (AFM)

The nanoscale graphene coverage at the surface of the PP fibre with SLG (MTI), TLG and SEG was evaluated with topography, amplitude, and phase AFM maps of 5 x 5 µm. Figure 4.9 shows the AFM maps of uncoated PP fibres with the extrusion lines.

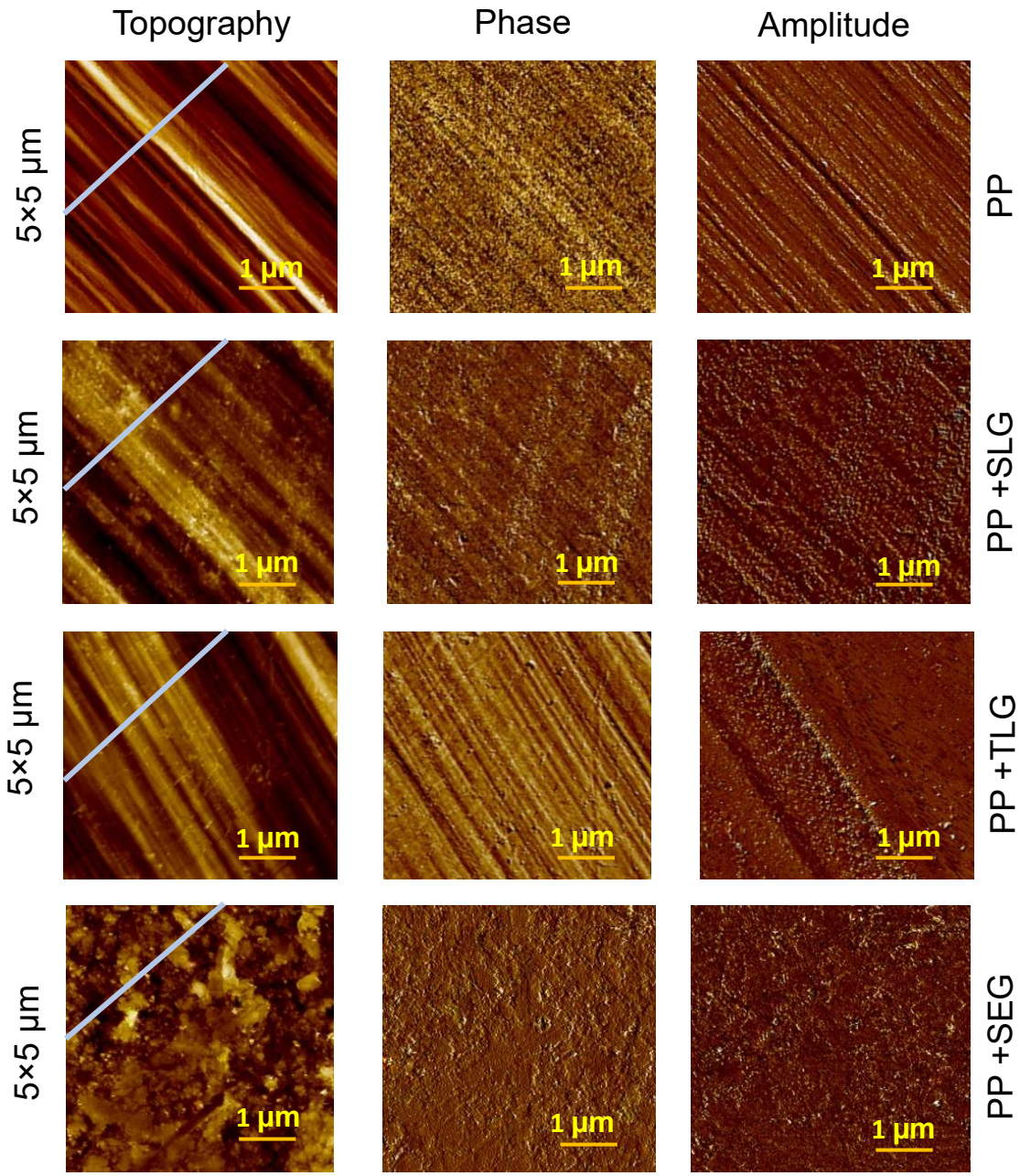

Figure 4.9. Tapping mode AFM of graphene-coated PP with Topography (left), Phase (middle) & Amplitude (right) maps of (top to bottom), PP bare fibres, SLG(MTI)-coated PP, TLG-coated PP, and SEG-coated PP.

The height profiles of the different types of graphene were obtained perpendicular to the fibre length and the extrusion axis as shown by the blue lines in the topography maps in Figure 4.9, to make sure the height profiles are comparable (Figure 4.10).

The surface of PP have been studied in detail by Torres Alonso *et al.* who assessed the micro-roughness of the PP fibre using profilometry along the direction of the extrusion of the fibre in the manufacturing line[3] and Neves *et al*. in 2017. The height profile of PP fibres (Figure 4.10a) shows well-pronounced extrusion lines as expected. However, it should be noted that even though the extrusion lines along the fibre length are always present, how well-pronounced they are is dependent on the spot of investigation or the sample. The transverse lines used at different spots would yield different height profiles. The topography maps of PP coated with SLG and TLG (Figure 4.10) shows visible extrusion lines, suggesting conformation of the graphene to the extrusion lines on surface of the PP fibres and good adhesion of graphene on PP. This has been previously reported for SLG-coated PP by Neves *et al.* using AFM studies and surface maps obtained through an optical non-contact method[1,227]. Figure 4.10b and c shows the height profile of SLG and TLG, respectively, suggesting these types of graphene are relatively thin and homogenous when compared with SEG where the extrusion lines are masked by the graphene that is not only thicker, but also inhomogeneous which could explain the pronounced change in height as can be seen in Figure 4.10d.

It should be noted that the data presented in this section has been obtained from a single sample and spot. Further investigation needs to be undertaken with several samples to make sure the data is representative.

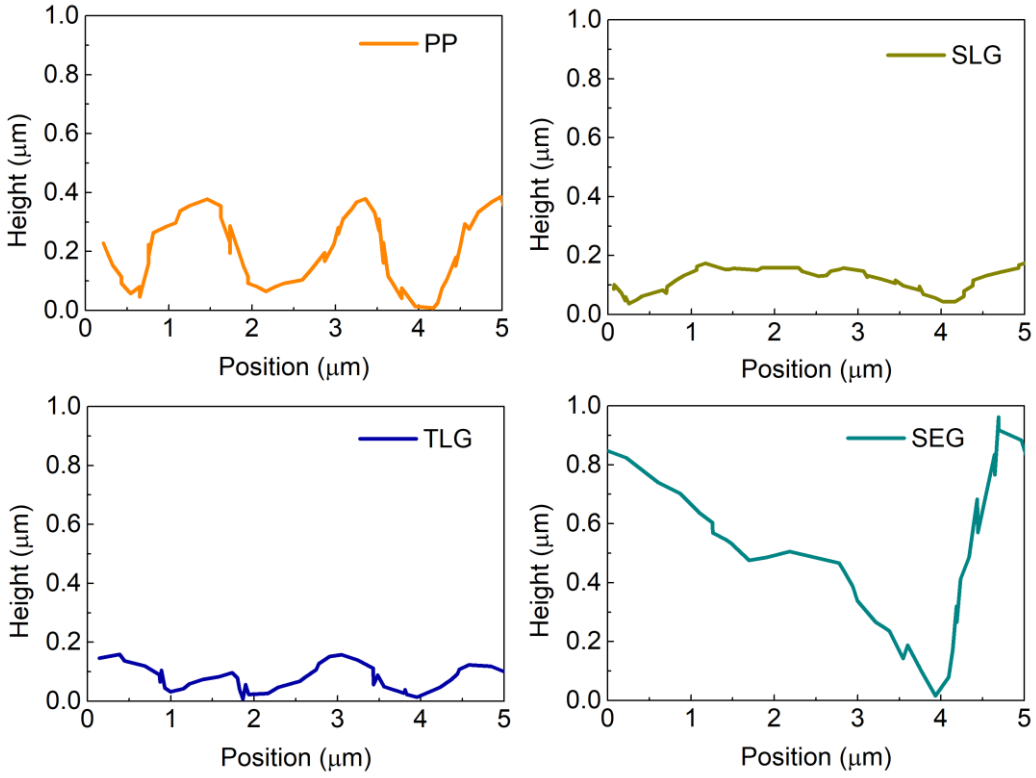

Figure 4.10. AFM height profiles of (a) PP (b) SLG, (c) TLG, and (d) SEG

The AFM phase maps are capable of sensing stiffness variations and can be used to distinguish between the parts of the fibre surface which are covered and not covered with graphene. The graphene is stiffer than the PP fibre suggesting the stiffer areas are covered with graphene and the rest are not covered, which is distinctly visible in the phase image. The lack of such visible difference in rigidity suggested a uniform coverage of graphene and no discontinuities without any holes or tears can be seen in Figure 4.10 for SLG and TLG-coated PP fibres. The PMMA residues from the transfer process can also be seen as elevated drops on all the AFM maps as shown previously[1]. Although, TLG has a distribution of one to four layers of graphene, the extrusion lines are still visible unlike in SEG which consists of thick and overlapping graphene flakes with the top surface covered with loose flakes as shown in figure 4.9. It is possible that the some of the layers conform to the extrusion lines of the PP well and what is visible on the AFM maps are just loose flakes on the top.

4.5 ELECTRICAL CHARACTERISATION

The sensing devices presented in chapters 4 and 5 require the measurement of the resistance of the graphene-coated PP fibres upon different stimuli. Since the width of the fibres is constant, maintaining a constant length would ensure that each resistance measurement is directly comparable and therefore it will not be necessary to normalise and calculate the sheet resistance for each measurement in each sample. Several techniques were tested to ensure the aspect ratio of sample area is the same for each measurement. One of the techniques involved inserting the two probes into a cork, 1 cm apart, as shown in Figure 4.11c. However, due to the porous and soft nature of the cork, the position of the probes changed easily rendering the results unreliable since it was difficult to maintain the necessary gap between the probes. To solve this, a two-probe setup with an acrylic body where the probes could be inserted and removed easily while being apart at a fixed distance of 1 cm with screws to keep the probes in place and for easy removal was built (Figure 4.11d). It was found that contact materials, such as carbon paste and silver inks, protected the graphene from the damage (scratches) caused by the probes during repeated use on the same sample in addition to maintaining good electrical contact during the electrical measurements.

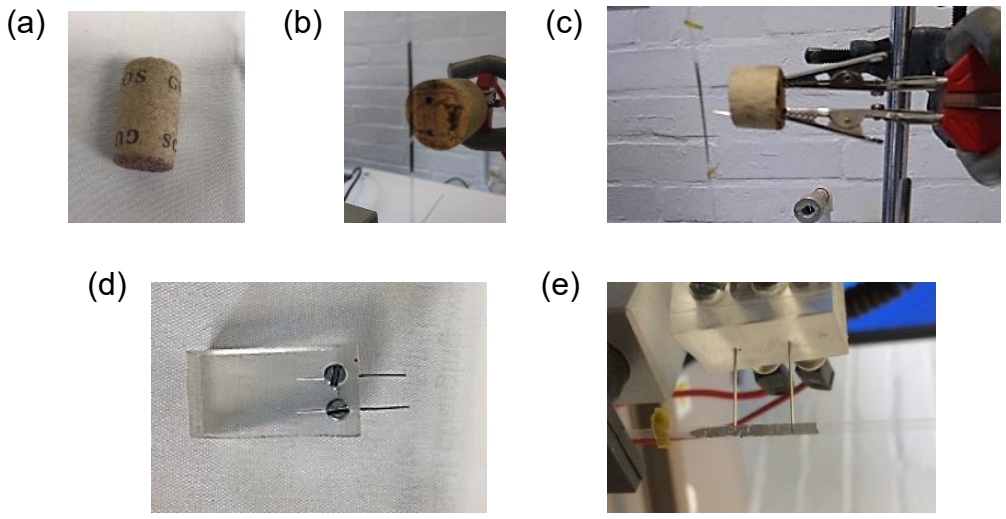

4.11. Photographs of the preliminary two-probe setup: (a) cork as the body of the setup; (b) front-view of the two-probe setup; (c) side-view of the setup with the graphene-coated fibres. Photographs of the custom-built two-probe setup: (d) setup with acrylic body with tungsten probes; (e) setup being used with the graphene-coated fibres.

The R_c for TLG-coated PP with no contact material, silver and carbon contacts was found to be 1204.72, 1356.26 and 1808.48 Ω, respectively. Therefore, the calculated sheet resistance for TLG-coated PP was 1101.7, 1028.5 and 811.8 Ω/sq for no contact material, silver, and carbon contacts, respectively. Using the same methodology, the calculated sheet resistance for SLG-coated PP was found to be 1096 Ω/sq and for FLG-coated PP is 580 Ω/sq which is in agreement with the previously reported results of 600 Ω/sq for FLG on PP and 1000 Ω/sq for SLG on PP[1]. These values are higher than those reported in the literature of the order of a few hundreds of Ω/sq and those of the same type of FLG transferred on glass, 200 -300 Ω/sq[249]. The sheet resistance of SEG was found to be higher at 3120 Ω/sq. This could be since the SEG is different than the graphene produced by CVD process, with overlapping flakes and percolating network in addition to the sodium cholate residues (an insulting material) from the shear exfoliation production process which causes the increase in the sheet resistance of the SEG. As suggested previously, the sheet resistance of SEG can be lowered by the water treatment[85].

4.6 RESILIENCE TESTS

The commercialisation of e-textiles requires them to be washable and durable, as mentioned in section 2.1.1. For this, the resilience of graphene-coated PP fibres was tested by subjecting them to a series of washing and bending tests, as described in section 3.6.3. The values of resistance were normalised to the initial resistance (before the washing and bending tests) at room temperature (RT) to better understand how it changed afterwards. The two types of graphene tested were TLG and SEG to compare the effect of resilience tests on graphene produced by different methods. A similar study has already been published where SLG produced by the nanoCVD (cold-wall) was subjected to bending tests and were found to be resilient to bending cycles.

It was observed that TLG samples performed better than SEG samples in the washing (Figure 4.12) and bending tests (Figure 4.13).

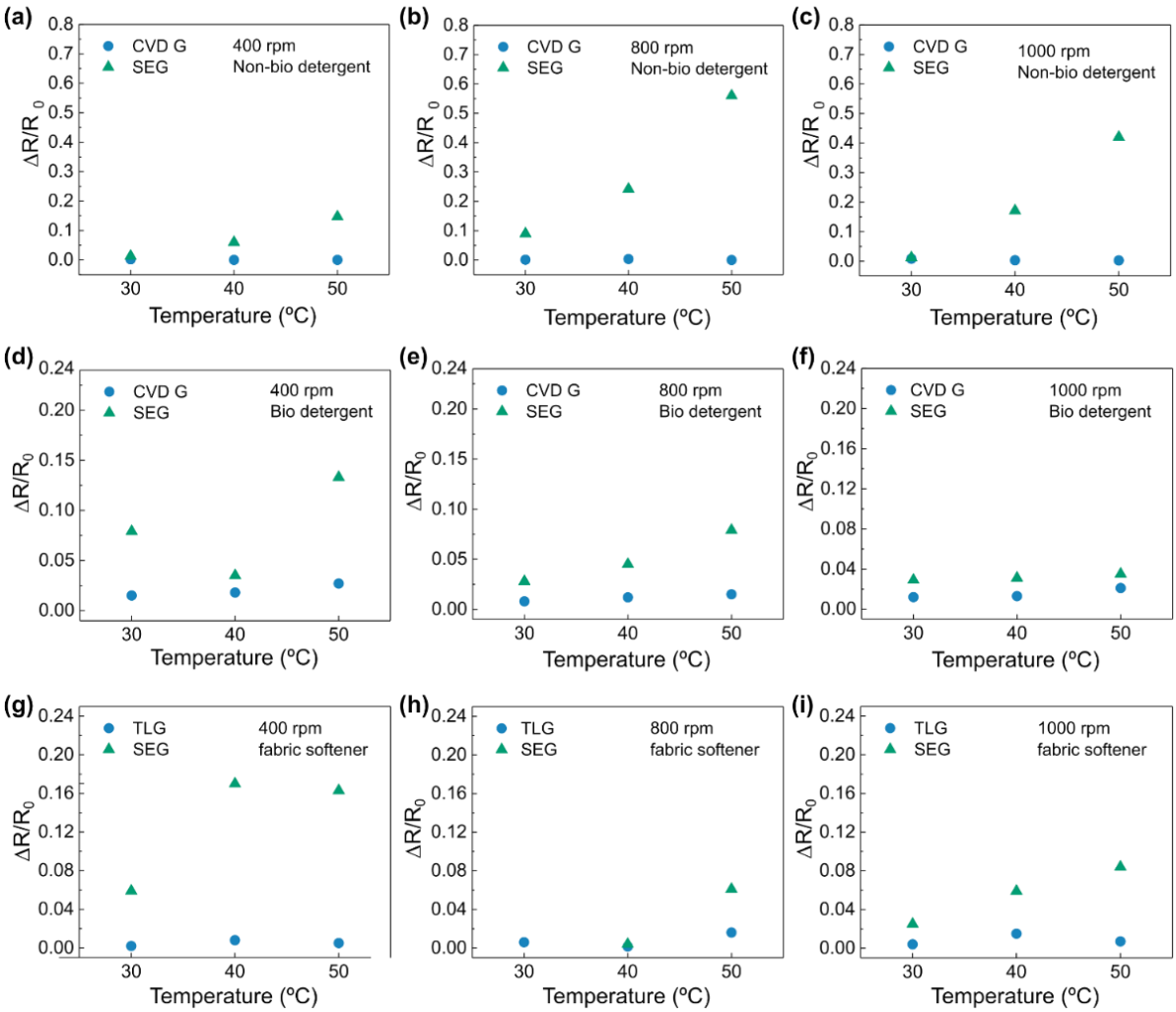

Figure 4.12. Change in resistance of TLG- and SEG - coated PP fibres against washing temperature with varying stirring speeds and different detergents: non-bio at (a) 400, (b) 800 and (c) 1000 rpm; bio detergent at (d) 400, (e) 800 and (f) 1000 rpm; and fabric softener at (g) 400, (h) 700, and (i) 1000 rpm. Reproduced with permission from ACS publications[229].

In the washing tests, the TLG samples did not show significant change in resistance when the stirring speeds, type of detergents, washing temperatures were varied. Subjecting them to 1000 bending cycles did not result in a significant change in resistance, either. SEG samples, on the other hand, exhibited an increase in resistance in most of the washing tests. This could be since SEG is made up of overlapping graphene flakes which do not adhere well as to the PP substrate or among themselves,

as the CVD graphene layers do, which causes the top flakes to get washed off easily. This was not the case with CVD-graphene where the layers are more continuous, uniform and have a very good adhesion to the PP substrate, which probably is responsible for their robustness.

It was observed that, although, the SEG is resistant to bending stress initially, the SEG-coated fibres are affected by it after several bending cycles. This might be because of the possible detachment or displacement of graphene flakes from the PP fibre surface during rigorous bending. It should be noted that new CVD/SEG samples were used to perform the experiments for each of the studied stirring speeds and detergents/fabric softener in the washing tests. Depending on the application of these graphene-coated textile fibres, an encapsulating polymer could be applied to protect the active part of the device from abrasion, prevent direct contact of graphene with the skin and the environment, and to ensure the mechanical properties do not change significantly while not interfering with the function of the device itself. The observed changes with bending can be minimised by locating these graphene-coated fibres in appropriate areas where their movement is minimal.

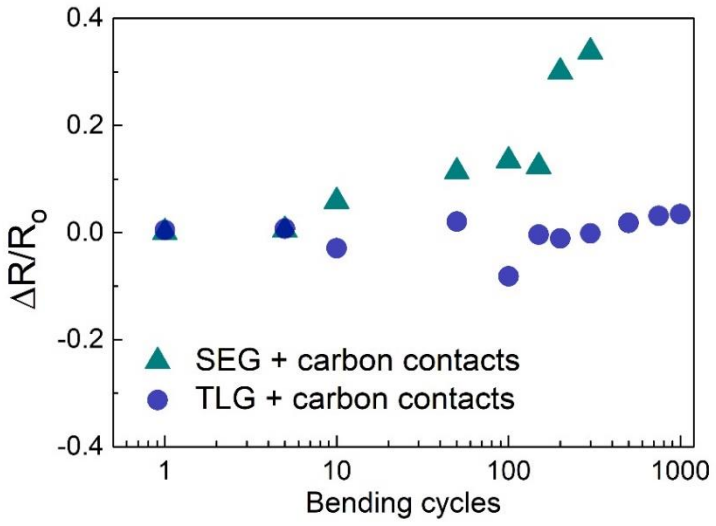

Figure 4.13. Sensitivity of an SEG- and TLG-coated PP fibres as a function of the number of bending cycles.

4.7 SUMMARY

This chapter focussed on the characterisation of different graphene, especially, the purposely developed TLG using transmittances and Raman spectroscopic analysis to estimate the number of graphene layers in TLG. Raman characterisation of the different types of graphene was done by transferring them to Si/SiO_2 and PP fibres with the Raman signatures found at the expected positions. Although AFM provides information about the coverage and continuity of graphene, it was not a suitable characterisation method for soft materials like PP fibres. The evolution of a custom-built 2-probe setup has been mentioned which was used to perform electrical characterisation of the samples at a fixed channel length of 1 cm to have the measurements comparable. The sheet resistance of all types of graphene produced by CVD was calculated and found to be in the order of 1 kΩ/sq for SLG as previously reported, 585 Ω/sq for FLG which is comparable to the reported values on PP, 811.8 Ω/sq for TLG when carbon paste which is lower than the sheet resistance of TLG when silver ink (in the order of 1 kΩ/sq) is used as a contact material, evidencing that carbon paste provides a better electrical contact than silver ink. Resilience tests were performed to study the washability and bendability of TLG and SEG-coated PP fibres. It was found that CVD-graphene is more robust and washable than SEG because of the graphene uniformity and continuity as opposed to the SEG which has overlapping and loose graphene flakes as the top layers which gets displaced and detached from the PP fibre during the resilience tests.

Chapter 5

BODY WEARABLE TEMPERATURE SENSORS

5.1 INTRODUCTION

This chapter provides a detailed study of textile temperature sensors, using graphene as the sensing layer. The motivation behind this work was to fabricate textile-based temperature sensors which can be easily integrated in clothing to sense human body temperature. The stable body temperature usually ranges between 35-37 °C. A low core body temperature in humans, below 35 °C leads to hypothermia and a high core temperature leads to hyperthermia[159]. Therefore, body temperature monitoring has always been essential in the healthcare sector. Conventionally, the body temperature can be measured by temperature detectors either by direct contact with the skin, such as in the case of commercial digital thermometers and adhesive liquid crystal thermometers[232], or indirectly by using infrared temperature sensors. Some of the recent developments in the measurement of body temperature include pacifier thermometers for infants[233] and tympanic (ear-based) thermometers[234]. These temperature sensors measure a range of temperatures with varying accuracy and sensitivity. However, most of them, especially the direct contact sensors, which are preferred for high-precision sensing, need to be positioned in an enclosed environment such as prosthetic areas or inside the clothing while being in direct contact with the skin, which could be uncomfortable and not ideal for children[235].

Although flexible temperature sensors provide great deal of flexibility due to their ability to conform to uneven surfaces, establishing comfort for prolonged usage is provided better by the textile platform for sensing temperature in a seamless manner without causing any issues like a skin irritation. In addition to the other drawbacks, conventional temperature sensors cannot always be used for continuous temperature monitoring. Integration of textile-based temperature sensors in the clothing enables the patients to monitor their body temperature continuously either on their own (data being sent wirelessly to their mobile phones) or remotely by their health providers without the need

to leave the comfort of their residence. Hence, there is a need to fabricate textile-based temperature sensors which are lightweight, biocompatible, flexible, can be fully integrated in the garment or linen and offers continuous temperature monitoring.

In this chapter, different types of graphene are presented for their use as temperature sensors with polypropylene fibres as the substrate, and their sensing behaviours have been compared. The results discussed herein have been published in ACS Applied Materials and Interfaces[229].

5.2 FABRICATION AND MEASUREMENT METHOLODY

The general architecture for the textile temperature sensor consists of: (1) PP textile fibre as the flexible substrate; (2) graphene as the temperature-sensing layer; and (3) carbon paste or silver ink as the contact material (Figure 5.1). Different types of graphene (SLG, TLG, FLG and SEG) were employed as the temperature sensing layer. The fabrication and transfer of these different types of graphene on PP fibres is described in sections 3.3 and 3.4, respectively. Multiple devices consisting of different types of graphene were subjected to temperature-dependent electrical resistance measurements by the two-probe method (section 3.6.2) using a hot plate at 1 V and an incremental step of 1 °C from 30 to 70 °C. As mentioned in section 3.6.2, the probes were placed at a set channel length of 1 cm to have the measurements at different temperatures comparable.

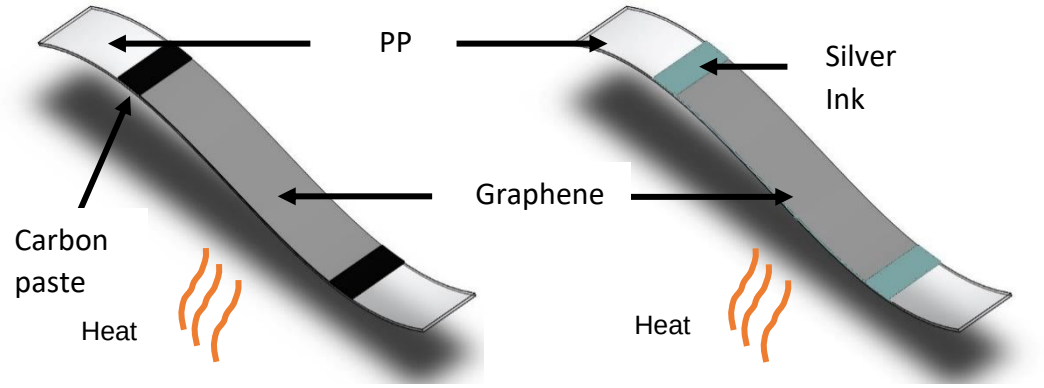

Figure 5.1. Schematic depiction of graphene-coated PP fibres with carbon paste (left) and silver ink (right) as contact materials.

5.3 RESULTS AND DISCUSSION

PP has a melting point from 161-167 °C[236] and begins to appreciably soften at 90 °C[237]. It was observed that exposing the graphene-coated PP fibres to temperatures higher than 100 °C led to mechanical deformation in the fibres, especially when they were subjected to temperature-dependent resistance measurements and complete damage above 130 °C (Figure 5.2). Although temperature sensing at temperatures higher than 70 °C was probed, due to the tendency of PP fibres to get damaged at such temperatures, the temperature sensing measurements was limited from room to 70 °C.

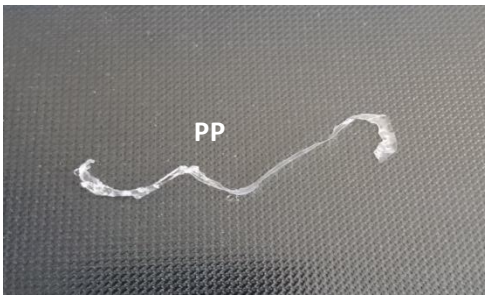

Figure 5.2. PP fibre damaged when exposed to temperatures higher than 130 °C.

There was no trend in the change of resistance with temperature in the FLG-coated PP sensors, as shown in Figure 5.3a and b, for silver and carbon contacts, suggesting that this type of graphene is not suitable to be applied as temperature sensor. This could be due to the large number of layers in FLG, which are distributed in patches. As this type of graphene is grown on a Ni substrate, the multilayer patches grown on top of each other as the dissolved carbon precipitates from nickel with as the temperature of the growth decreases[97,238]. SEG-coated PP sensors exhibited some sensitivity towards the change in temperature for both types of contacts, carbon, and silver, as shown in Figures 5.3c and 5.3d. These measurements, however, are not reproducible after a single temperature run (Figures 5.3e and 5.3f). Although, the sensing seems better when carbon paste is used, it is still not enough for temperature sensing applications. This suggests that, in this device architecture and material combination, SEG is not a good candidate for temperature sensing either, due to the

lack of repeatability. Previous work suggested that SEG samples prepared using the IDT method have residual sodium cholate used as a surfactant to disperse the graphene flakes as they are being exfoliated in water[85]. The large and electrically insulating surfactant molecules can act as spacers and prevent graphene flakes from overlapping, which would hamper conduction. Furthermore, these flakes can have poor adhesion and thus, detach from the PP substrate, particularly the ones near the surface, which could have led to poor and inaccurate temperature sensing.

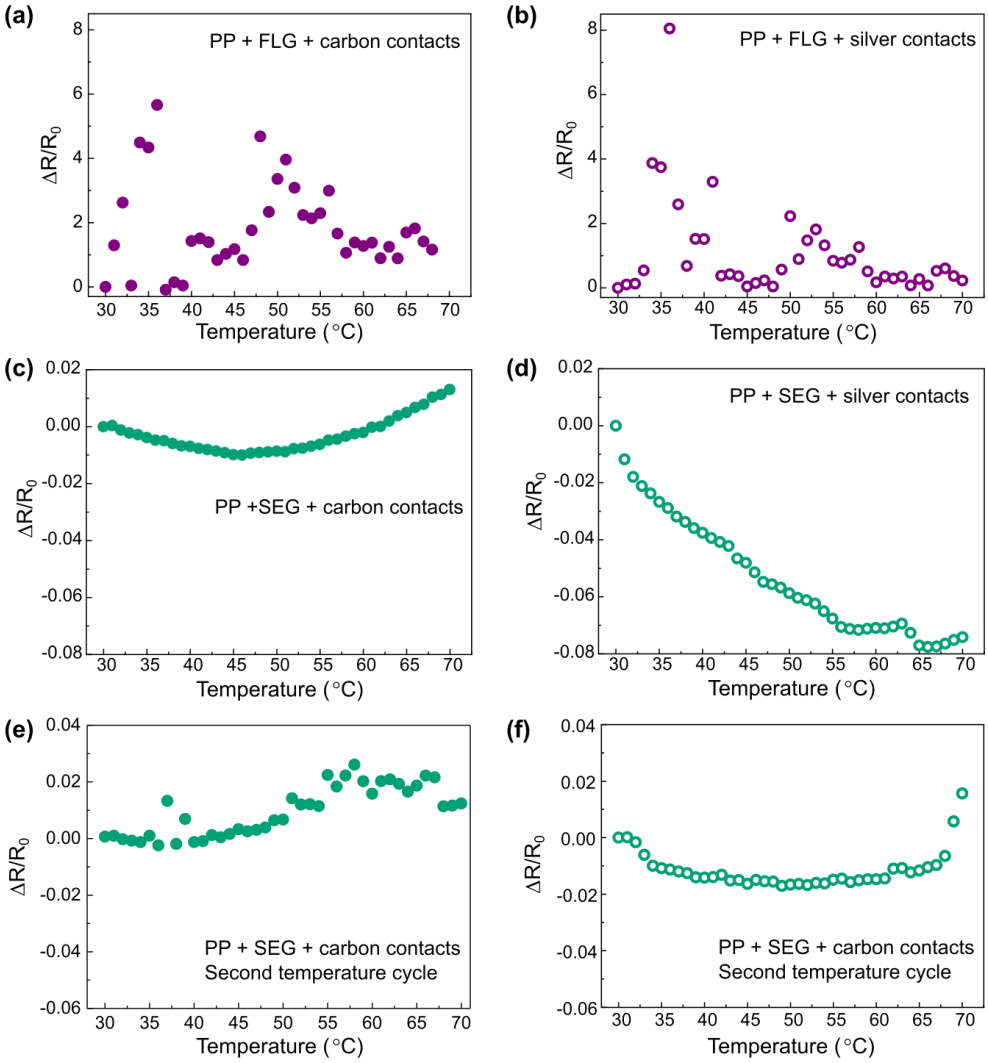

Figure 5.3. Sensitivity (change in resistance ratio) as a function of temperature for PP-coated with: (a) FLG with carbon contacts; (b) FLG with silver contacts; (c) SEG with carbon contacts; (d) SEG with silver contacts; second temperature cycle for PP coated with SEG with (e) silver contacts, and (f) silver contacts. Reproduced with permission from ACS Publications[229].

The observed trend for SLG, TLG and SEG-based temperature sensors was the decrease in resistance with the increase in the temperature. This is the expected behaviour for graphene where being a semi-metal[76], quenching of electrical resistance takes place when the temperature exceeds room temperature[239]. This negative thermal coefficient of resistance behaviour has been reported multi-wall CNTs[240] and printed graphene electrodes on PET[241]. SLG-coated PP sensors initially indicated a linear response to increasing temperature as shown in Figures 5.4a and 5.4b. Although, these cycles were only from 30 to 45 °C to include the human body temperature range, the devices showed no sensing ability after four cycles. This was the case with both silver and carbon contacts suggesting SLG is somehow damaged by the temperature cycles and does not offer any redundancy unlike the other types of graphene. Comprising only one layer of graphene, this type of graphene coating is the most fragile of those studied, which can justify the lack of robustness in the SLG-based temperature sensors.

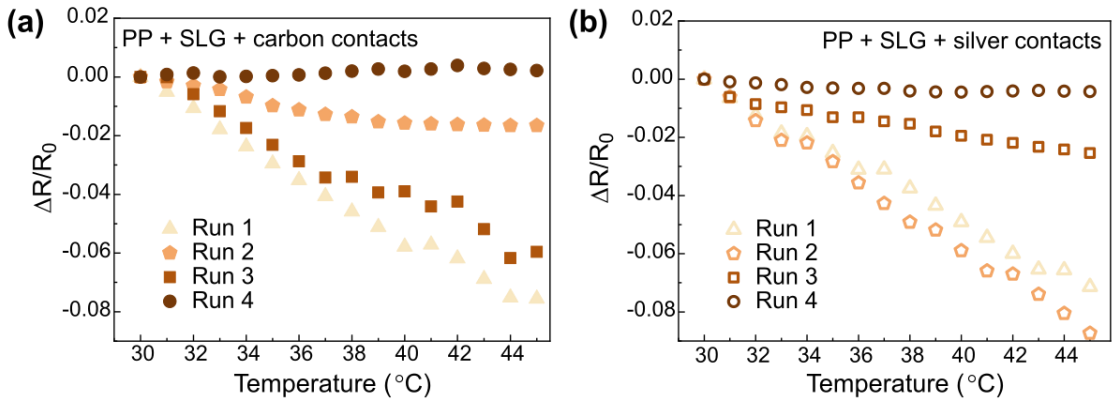

Figure 5.4. Sensitivity as a function of temperature for PP-coated with SLG with carbon contacts (a) and silver contacts (b), showing lack of reproducibility over multiple temperature runs. Reproduced with permission from ACS Publications[229].

Figure 5.5 shows that, in the case of TLG sensors, a linear response is observed between 30 to 45 °C. As mentioned in section 2.4, a high TCR is associated with high sensitivity. The TCR for TLG sensors with carbon paste as contact material was calculated as *ca*. - 0.001792 $°C^{-1}$ for the temperature range studied, which is slightly

higher than the other reported TCR of graphene on flexible substrates[242] which is about 1.11% increase in TCR.

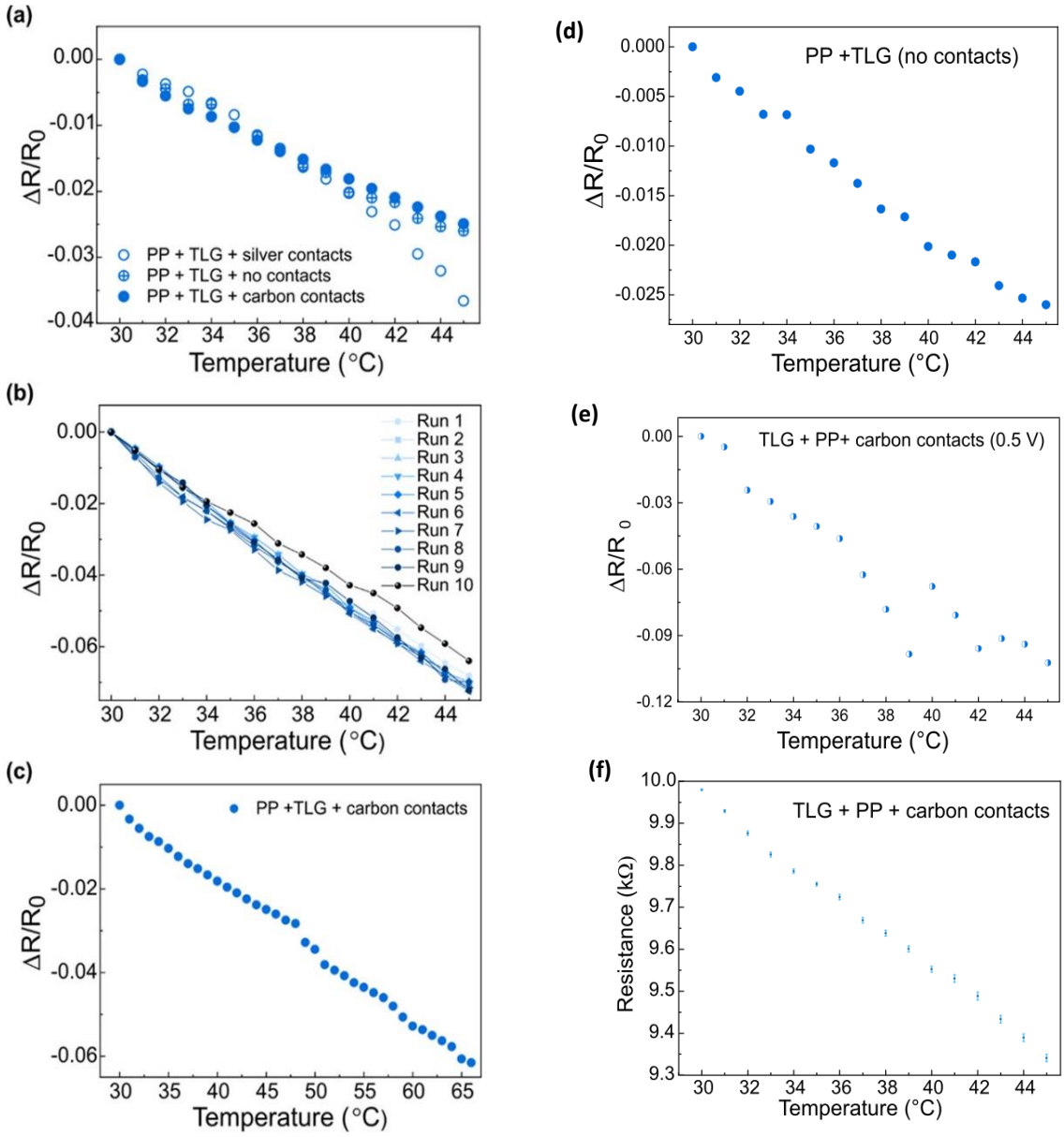

Figure 5.5. Sensitivity as a function of temperature for a TLG sensor with carbon contacts in contact mode: (a) in the human body temperature range with different types of contacts; (b) for multiple body temperature runs; (c) for temperature range of 30−70 °C; (d) for TLG without additional contacts. (e) Temperature sensing at 0.5 V for a TLG sensor. (f) Absolute resistance of a TLG sensor with error bars in the body temperature range. Reproduced with permission from ACS Publications[229] *.*

To study the robustness of the TLG sensors with carbon paste, one device was subjected to 10 temperature cycles (Figure 5.5b) and linearity was found to be consistent with a low standard error and significant variation between the measurement results (Figure 5.5f). It was also found that linear behaviour is observed in TLG sensors when the measuring probes are directly used on the graphene layer without using any contact material (Figure 5.5b). When silver ink was used as a contact material, it was observed that unlike carbon paste, TLG sensors with silver contacts often displayed different responses (Figure 5.6a), and the ones that seemed to be sensitive to temperature in the first run were unable to withstand multiple runs (Figure 5.6b). This could be due lack of flexibility in the silver ink which can easily detach from the graphene coating with any mechanical stress caused by experimentation process, leading to poor electrical contact with the graphene. Therefore, silver ink is not a good candidate for drawing metallic contact in textile fibres and therefore unsuitable for the purpose of textile-based devices.

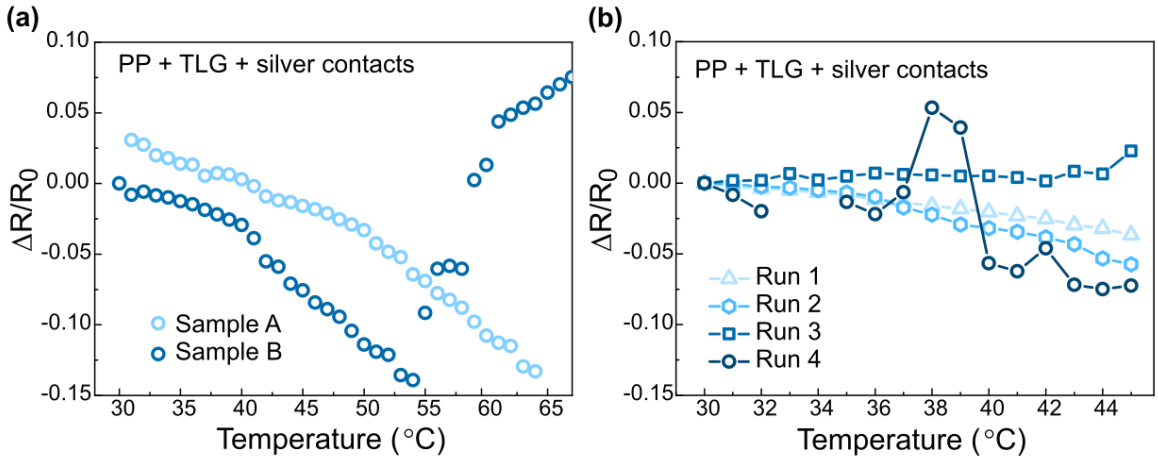

Figure 5.6. Sensitivity as a function of temperature for PP coated with TLG and silver contacts for: (a) two samples that shows irreproducibility; (b) for multiple runs in a sample, showing that the device is not robust. Reproduced with permission from ACS Publications[229].

It should be noted that the supply voltage for all the devices reported here was 1 V, which suggests low operating voltage applications as well as wearable technological applications where exposing the user to higher voltages is a concern. The TLG sensor

was also tested at 0.5 V with carbon contacts to demonstrate the potential for a low-voltage sensing application. As shown in Figure 5.5e, although the temperature sensing response is not as good as that at 1 V, still the operating voltages of these sensors could further be brought down upon suitable optimisation.

To assess the performance of TLG sensors for a non-contact temperature measurement, a heat gun was used instead of a hot plate over a short period. A commercial temperature sensor was used as a reference sensor to obtain accurate temperature measurements (Figure 5.7). As evidenced, the graphene sensor follows similar trend i.e., increase in conductivity when the temperature in increased constantly. The TLG sensor has a quicker response to the change in temperature than the commercial sensor when the heat gun is turned on at point A. At point B, the heat gun was turned off (*ca*. 360 s), the TLG sensor seems to recover quicker whereas the commercial sensor displays a temperature which is higher than the ambient temperature. This shows that the TLG temperature sensor has a faster response and recovery time than the commercially available sensor.

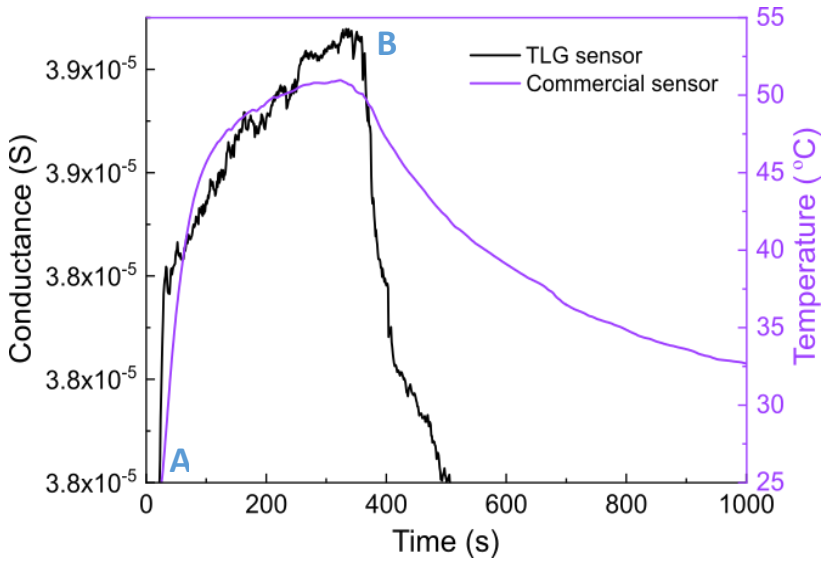

Figure 5.7. Ambient continuous temperature measurement over time. Sensing performance of TLG-based sensor and a commercial sensor have been compared. Point A is when the heat gun is turned on and point B is when it is turned off. Reproduced with permission from ACS Publications[229] .

The graphene-coated PP fibres were subjected to temperature-dependent Raman studies to check how the increasing temperature affect the graphene as well as the PP fibre. To study this, the bare PP fibre was subjected to temperature range (RT to 85 °C) with a temperature increment of 5 °C while recording the Raman spectra. Five distinct peaks (peak A at 841 cm^{-1}, peak B at 998 cm^{-1}, peak C at 1151 cm^{-1}, peak D at 1328 cm^{-1}, and peak E at 1460 cm^{-1}) were chosen in the Raman spectra of PP, as shown in Figure 5.8a. It can be seen in Figure 5.8b that there is no significant change in the Raman spectra in the temperature range of 25-85 °C. The graphene-coated PP fibres were then subjected to the same study in the temperature range of 25-85 °C.

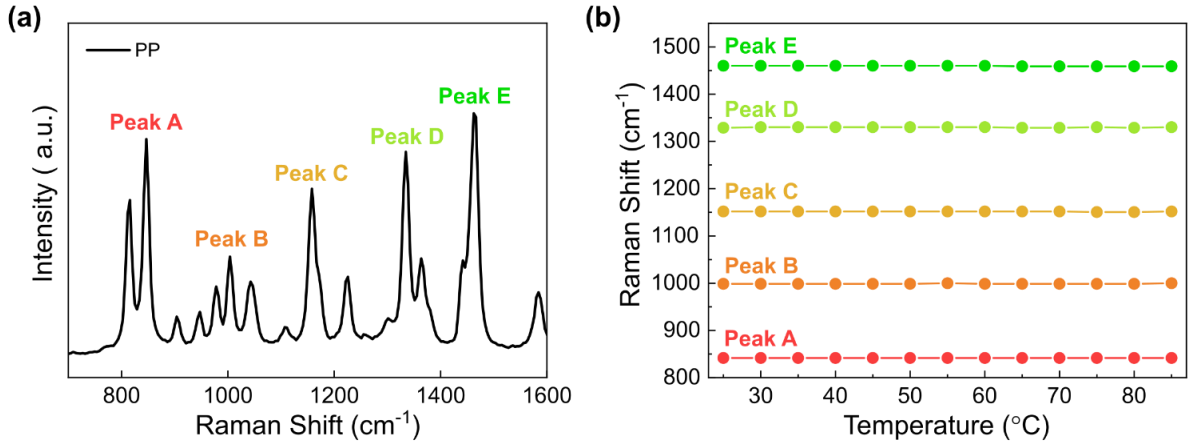

Figure 5.8. *(a) Raman spectrum of PP highlighting five distinct peaks. (b) Raman shift as a function of temperature for the same peaks. Reproduced with permission from ACS Publications*[229] .

Following a temperature-dependent Raman study done by Calizo *et al. for* graphene[243], who observed a non-linear decrease in the graphene G-peak position when the temperature is increased, the G-peak positions were extracted, and slopes were calculated for each type of graphene by linear fitting (Figure 5.9a - d). It was observed that all the types of graphene studied had a negative slope of -0.0683 cm^{-1}/ °C (SLG), -0.0127 cm^{-1}/ °C (TLG), -0.0183 cm^{-1}/ °C (FLG) and -0.0997 cm^{-1}/ °C (SEG), suggesting a G-peak decrease with the increase in temperature as expected.

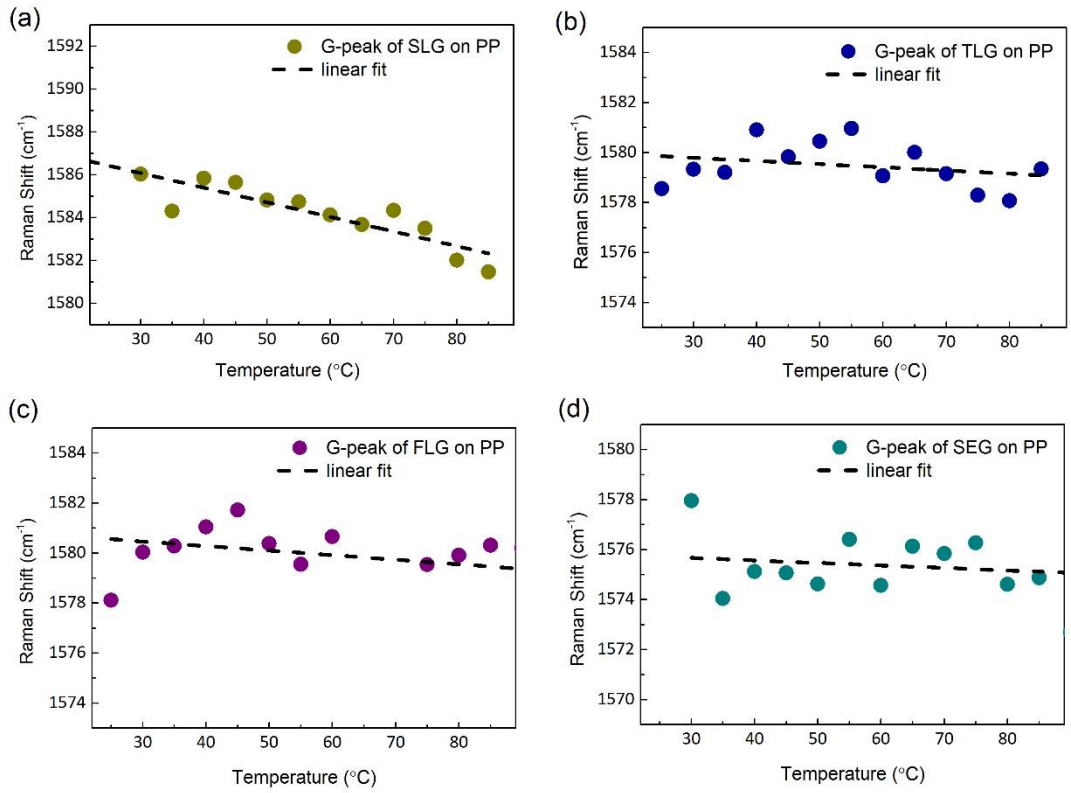

Figure 5.9*. Raman shift of the G peak of TLG on PP as a function of temperature for (a) SLG, (b) TLG, (c) FLG, and (d) SEG.*

The TLG-sensors were subjected to washing and bending tests, as explained in section 3.6.3, and then temperature. It was found that TLG-sensors performed well in the temperature 30-45 °C, even after rigorous washing and bending cycles, as shown in Figure 5.10.

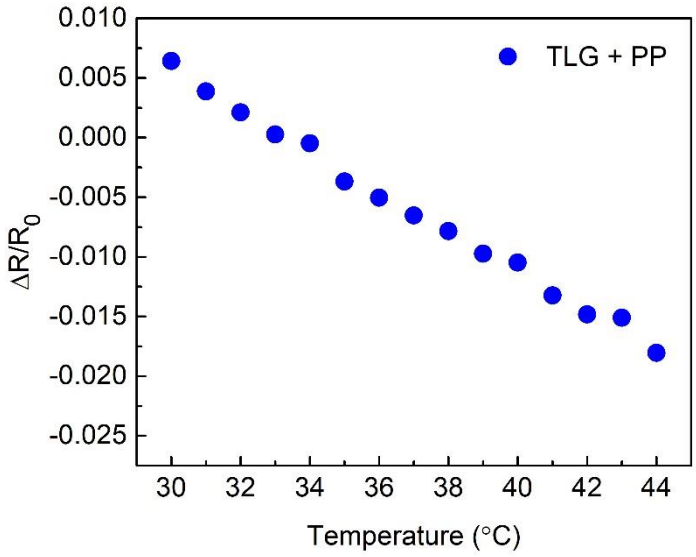

Figure 5.10*. Sensitivity as a function of temperature for PP coated with TLG after washing and bending tests.*

The different graphene coated fibres were subjected to SEM investigation to study the possible damages at the morphological level and to obtain information about the surface topology before and after being exposed to the temperature. The temperature range studied for this purpose was from room temperature to 70 °C. An uncoated PP fibre with no graphene was also subjected to the same temperature treatment as a reference. There are no visible differences in the topography of the PP fibres (coated and uncoated with graphene) with the change in temperature. Figure 5.11a shows PP extrusion lines from its production. The white spots visible could be the PMMA residues from the transfer of TLG on PP. Even though the extrusion lines of the PP fibres are visible since the CVD films (Figure 5.11b-c) are thin, it can be seen they are slightly blurred in the case of FLG as compared to TLG. This could be due to the increased number of layers and the graphene patches in FLG, making the extrusion lines of PP less pronounced. The CVD coatings also have some PMMA residues which is the inherent feature of the PMMA-assisted CVD transfer process. SEG films comprises of overlapping graphene flakes which are considerably thick in some places (Figure 5.11d). However, in the case of SEG films (Figure 5.11e), the samples displayed cracks in the coating prior to any mechanical or thermal stress since, unlike CVD films

where the film is reasonably continuous, SEG films comprise of overlapping graphene flakes which are considerably thick in some places. Figure 5.11d shows the SEM image of SEG on PP fibres with inhomogeneous and thick graphene. The loose graphene flakes on the top of the conformed graphene makes SEG thick enough to entirely mask the PP fibres as such that the extrusion lines are not visible.

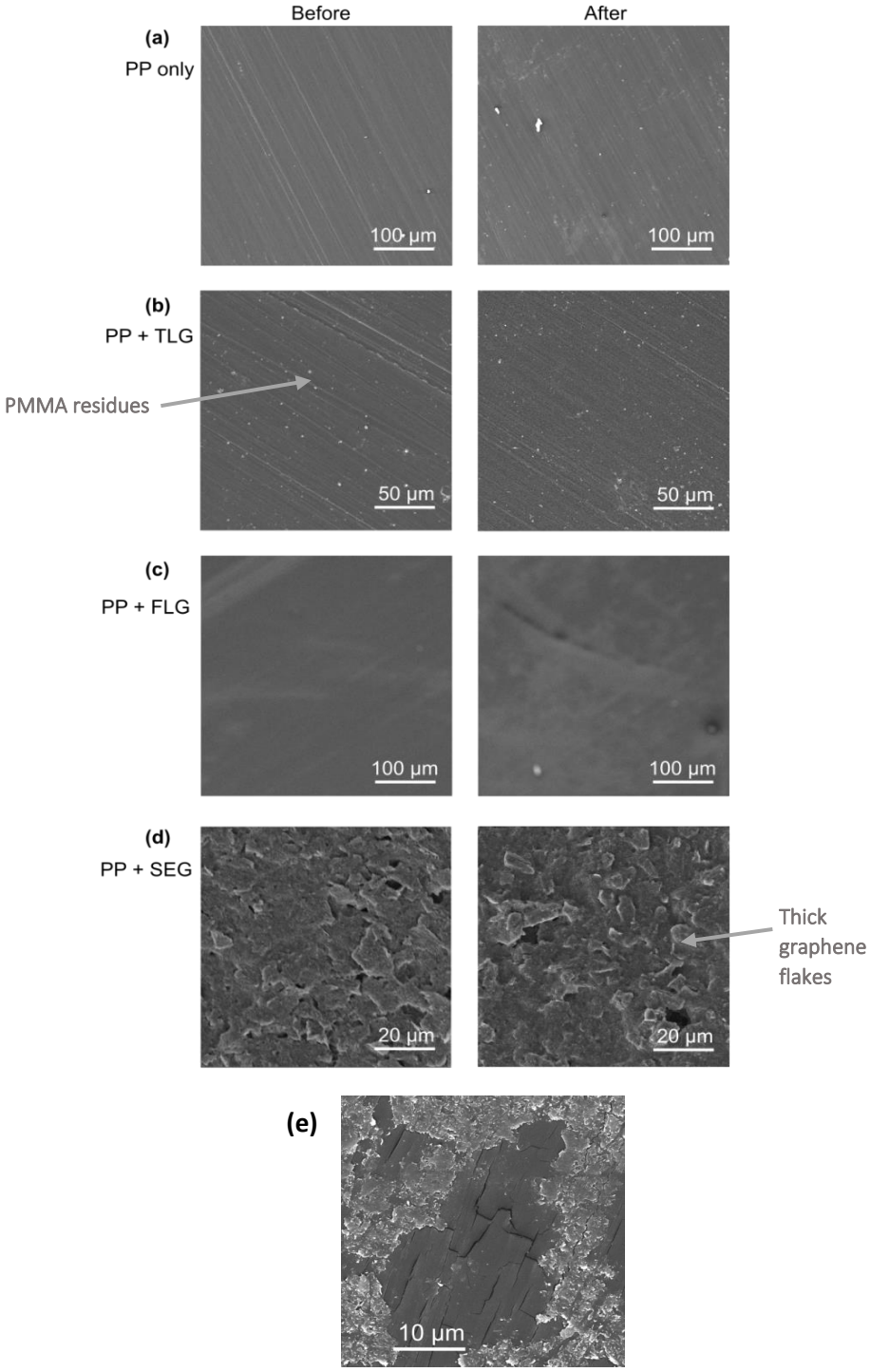

Figure 5.11. SEM images of: (a) PP fibre; PP fibres coated with: (b) TLG; (c) FLG; and (d) SEG. Images on the left and right columns were taken before and after a temperature cycle (room temperature to 70 °C), respectively. Reproduced with permission from ACS Publications[229] *.*

5.4 SUMMARY

This chapter provides a detailed report demonstrating the application of graphene as an excellent candidate for sensing temperature in e-textiles. Various types of graphene were studied as temperature sensors. It was found that the TLG with carbon paste generated consistent temperature sensing in the temperature range of 30-45 °C unlike the other types of graphene studied. The TLG-sensors studied in this chapter required input voltages as low as 0.5 V, making these sensors suitable for low power e-textile technology. The TCR of the TLG-based temperature sensor was found to be slightly higher than the reported TCR for flexible substrates. It can also be concluded that graphene grown by CVD process is more suitable to temperature sensing applications than SEG despite the scalability of graphene inks. Nevertheless, the roll-to-roll processability for CVD graphene does not preclude large-scale fabrication. The effect of temperature on Raman peak characteristics of the TLG sensor was also studied which suggested that there is no significant change in the peak characteristics of the PP substrate while an expected decrease was observed in the G-peak of graphene in the examined temperature range. Statistical analysis of the change in the G-peak position due to temperature shows that in the case of all the graphene studied, at least 70% of the variation in the G-peak position is caused by the change in temperature. This is in line with the imaging done on the surface of the devices before and after a temperature cycle, with no visible changes. The TLG temperature sensors were demonstrated to having potential healthcare application for the continuous temperature measurement of the human body temperature in addition to their potential to be easily integrated in clothing, linen, or upholstery.

Chapter 6

TEXTILE FIBRE-BASED HUMIDITY SENSORS

6.1 INTRODUCTION

Humidity control is essential for maintaining a healthy indoor air quality, prevent condensation on cold surfaces which could lead to corrosion, control mould growth, prevent slip hazards, protect the integrity of materials in storage and especially in healthcare for respiration monitoring[244]. As mentioned in section 2.5, relative humidity (RH) is the common measure of the humidity levels. Most of the commercially available humidity sensors are rigid, cannot conform to the curved surfaces and often require multiple layers to fabricate them which increases the complexity and commercial cost of the sensors. Textile-based humidity sensors can overcome most of the drawbacks of the conventional humidity sensors.

The motivation behind this chapter was to fabricate textile-based humidity sensors which can easily be incorporated in clothing, household items such as curtains, wallpapers, bathroom rugs, in areas where moisture monitoring is essential. These sensors are washable, flexible, resistant to microbes and can withstand a humid atmosphere. This chapter provides a detailed description of the study of textile-based humidity sensors, using graphene as the humidity sensing layer. Two types of graphene have been presented for their use as humidity sensing layers in textile-based humidity sensors with polypropylene as textile substrates and their humidity sensing behaviours have been compared. PP fibres are a poor bacterial host, and it is damp, and mildew resistant due to the fast moisture transport through them which makes the PP fibres ideal for applications where the environment is damp and humid[70,68].

It is important to mention that this work followed the demonstration of flexible graphene-based humidity sensors by Torres Alonso *et al.* in our group[4]. In this work, GO, the humidity sensing layer, was coated on to an interdigitated patterned created on a solution-processed graphene, which acts as the electrode, using a PET sheet as the substrate.

6.2 FABRICATION AND MEASUREMENT METHODOLOGY

Following the work by Torres Alonso *et al.,* the initial device architectures included GO as the active layer and SEG as the sensing electrode[4]. To see if the complex patterning process could be avoided, the first device architecture tested consisted in PP fibres, first coated with SEG, and then coated with GO, with carbon paste as the contact material (Fig. 6.1a). Since GO itself is an insulating material, a conducting material, like graphene, is required to assist with the conduction process[5]. Carbon paste has been shown to be a better contact material for PP fibres than silver ink, as detailed in Chapter 5 (section 5.3). Therefore, it was used to draw the contacts on these devices to facilitate the measurements. The response of graphene-sensors to humidity was compared with a commercial humidity sensor (section 3.6.2). It should be noted that the commercial sensor was placed next to the graphene sensor to obtain comparable data. The conductance of the samples was measured at an imposed voltage of 1 V as a function of time.

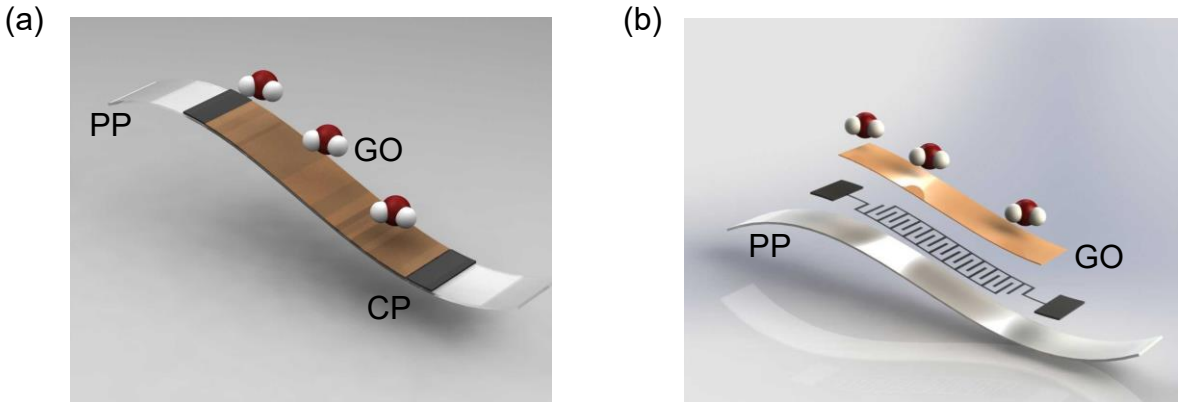

Figure 6.1. (a) Initial textile humidity sensing device architecture, with GO coating SEG (both continuous) on PP fibres, and CP, exposed to ambient humidity, (b) Second device architecture, with a patterned SEG electrode covered in a GO coating on PP fibres, also with carbon contacts.

The GO-SEG devices showed a very poor response to blowing humidity tests (in green in Figure 6.2a), compared to the response of a commercial humidity sensor exposed to the same blowing (in purple). The lack of trend in the conductance can be explained

by poor adhesion and subsequent easy peeling-off of the GO, as can be seen in the SEM image on Figure 6.2b, showing the exposed SEG underneath where the GO film peeled off.

(a)

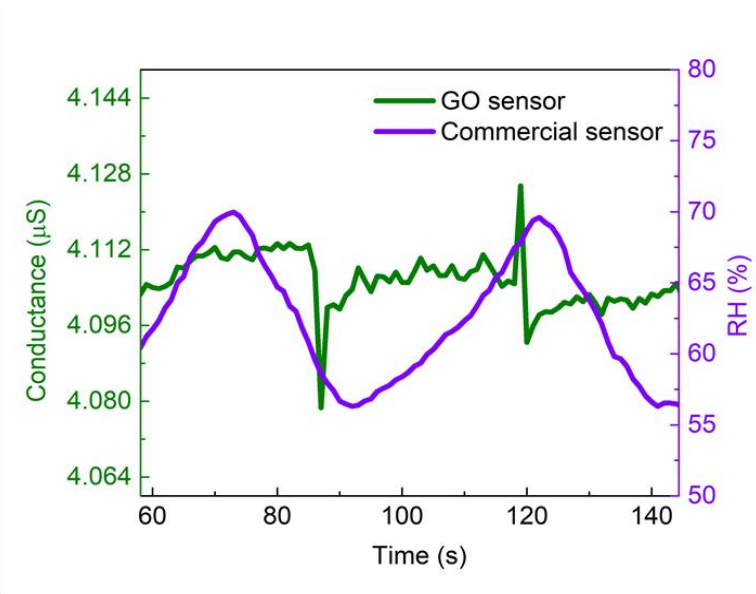

(b)

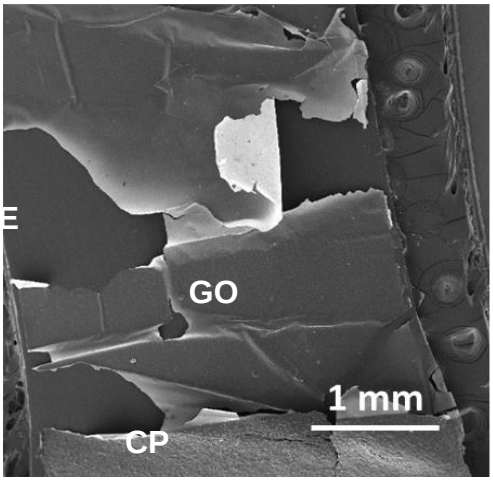

Figure 6.2. (a) Conductance of SEG and RH as a function of time. (b) SEM image of a GO/SEG/PP with carbon paste (CP).

An interdigitated graphene electrode structure was also considered to improve the sensitivity as suggested by Torres Alonso *et al.*[4], as shown in Fig. 6.1b. In that work, the PET substrate was patterned using the optical lithography and SEG was transferred first using a transfer method, which depends on the type of graphene being

transferred, and then GO was transferred over the pattern again using a second set of lithographic steps. Following this work, the PP fibres were patterned using the steps using laser writing system. Once the PP fibres were patterned as shown in Figure 6.3, the graphene was to be transferred on to the patterned fibre.

Figure 6.3. Interdigitated structure on PP fibre using optical lithography.

As discussed in section 5.3, although the coating of PP fibres with SEG is continuous, some loose flakes are often observed. The SEG-based humidity sensors in the work of Torres Alonso *et al.* consist in multiple SEG films stacked via multiple transfers of graphene-coated PTFE membranes, since graphene transferred from a single membrane would not produce patterns with enough conductivity to allow sensing[4]. This would have added to the problem of loose flakes, resulting in poor adhesion of subsequent layers. Furthermore, the SEG-coated PP fibres are not washable and durable, as shown in section 4.2.9. With these potential issues with SEG, TLG was considered for the textile-humidity sensors, as it can also be lithographically patterned while on PP[3]. However, it was observed that the transfer of TLG to pre-patterned PP was quite challenging since the graphene failed to conform well to the pattern on the fibres and was damaged during the process. Therefore, the transferring the graphene at a later stage was not suitable to produce interdigitated graphene structures.

Another approach was considered where the TLG would be transferred first on the PP fibre, followed by optical lithography to create an inverted interdigitated pattern (the

pattern features that were required were preserved and undesired sections were exposed) and then removal of graphene using reactive ion etching process. However, despite promising initial patterning attempts, the patterning process was discontinued because the transfer process to PP fibres to produce graphene electrodes would have taken several steps further increasing the cost of fabrication.As compared to GO, graphene has a higher electrical conductivity and lower cost of production which is the reason graphene, particularly in the form of rGO has been considered as an alternative humidity sensing layer to GO[245]. Several previously demonstrated rGO-based humidity sensors have been mentioned in section 2.5. Here, we investigate the humidity sensing potential of graphene produced by CVD (TLG) and SEG methods. The final device architecture for the graphene-based textile humidity sensor is shown in Figure 6.4.

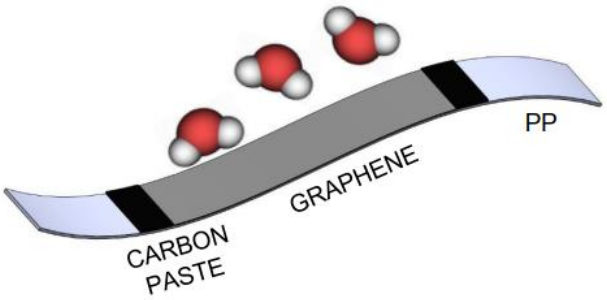

Figure 6.4. Final textile-based humidity device architecture, with graphene-coated PP and carbon contacts, exposed to ambient humidity.

6.3 RESULTS AND DISCUSSION

The TLG and SEG sensors respond differently to human blowing. For TLG-based sensors, an increase in conductance was observed (Figure 6.5a), whereas for the TLG-based sensor, (Figure 6.5b) it decreased with the increase in RH.

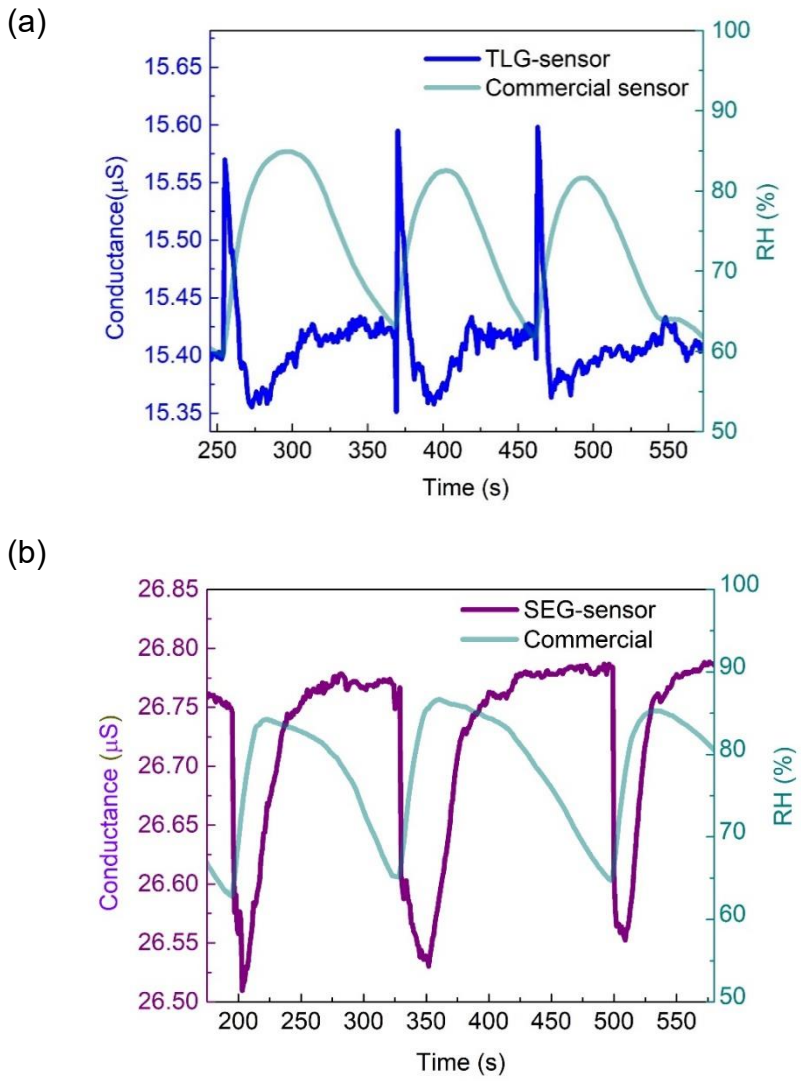

Figure 6.5. Response to human blowing. Conductance vs. time at 1 V for: (a) a TLG-based sensor; (b) a SEG-based sensor.

There could be several mechanisms responsible for the behaviour of TLG-sensors. The adsorption of water molecules on the surface of the exposed surface is usually the mechanism by which the conductance increases in resistive or capacitive humidity

sensors. Among the carbon materials for humidity sensors, GO has been one of the most investigated materials and often used as a humidity sensing layer for its hydrophilicity. However, this has been observed in bilayer CVD graphene on glass, with ionic transfer being proposed as the main conduction method[246]. The presence of defects in the graphene layer has also been attributed to its humidity sensing tendency. Physical and chemical defects in the graphene film are known to have an impact on the electrical properties of graphene. The PMMA residues from the TLG transfer onto the fibre could act as chemical defects and enhance the water adsorption[247] as well as the grain boundaries and edge defects[193]. The issue of power consumption in textile-sensors have been raised frequently, which is very important for the successful future of textile electronics. To address this, the sensors were imposed at a further low voltage of 0.5 V. Both TLG and SEG-sensors show a good response to humidity blowing tests at 0.5 V, evidencing the low operating voltage requirement (Figure 6.6a and b).

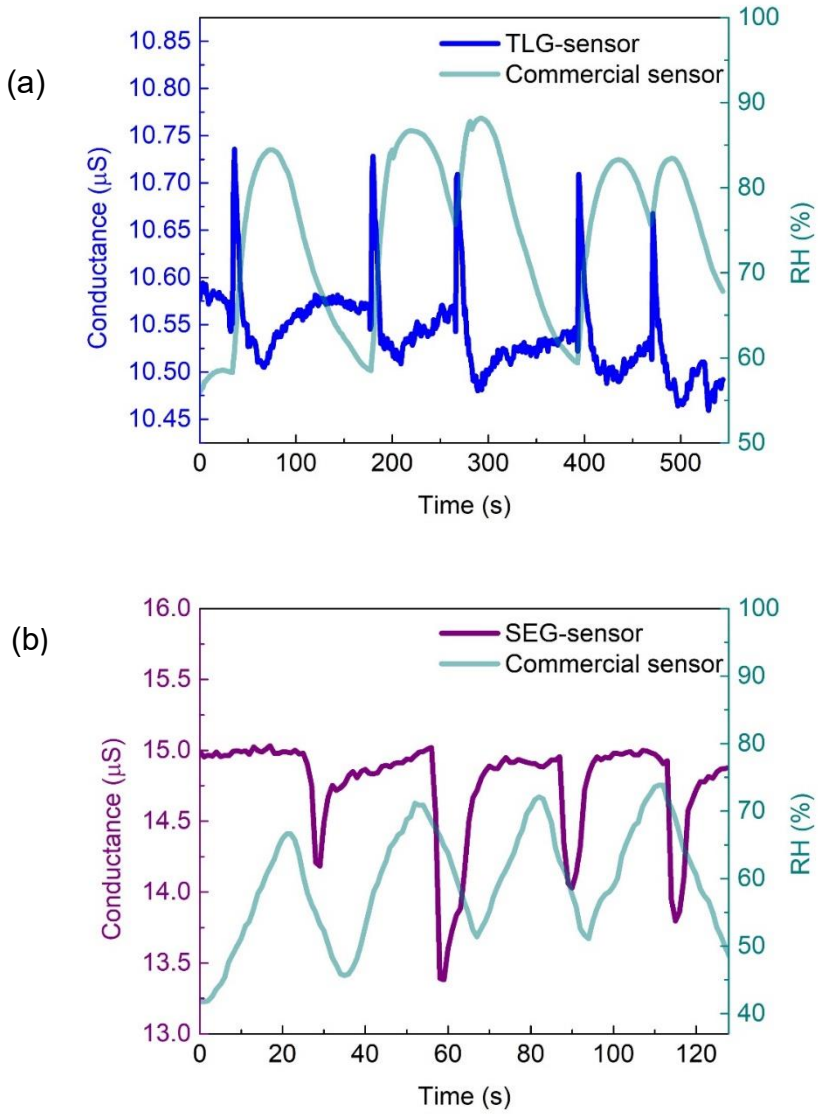

Figure 6.6. Response to human blowing. Conductance vs. time at 0.5 V for: (a) a TLG-based sensor; (b) a SEG-based sensor.

The devices were also subjected to continuous measurements from 25-100% RH to confirm the sensing behaviour of the sensors. It can be seen in Figure 6.7a and b that the conductance increases and decreases with increase in RH in the case of TLG and SEG, respectively, as suggested by the human blowing tests.

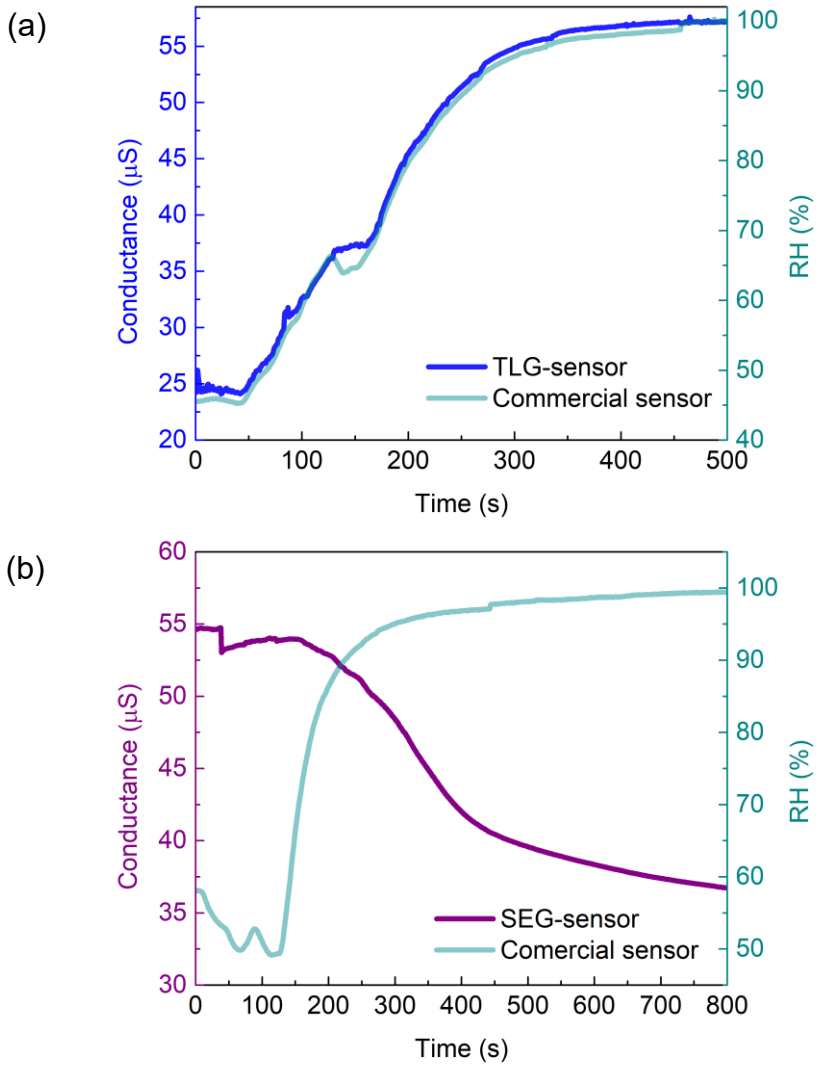

Figure 6.7. Response to continuous humidity measurements. Conductance vs. time at 1 V for: (a) a TLG sensor; (d) a SEG sensor.

The sensors were subjected to humidity sensing tests after washing and bending tests (section 3.5.3) to check their durability. The TLG-sensor showed better performance after repeated washing and bending (Figure 6.8a). However, the SEG sensor failed to

sense humidity after the washing and bending tests, which agrees with the resilience study on SEG-coated PP fibres, indicating that the percolating network of overlapping graphene flakes are easily disrupted by the mechanical stress as opposed to the continuous TLG. It was found that in addition to being resilient, the TLG-sensors also have an excellent response time of *ca.* 1 s and quick recovery in the broad humidity range of 50-100 %. This can be seen in all the human blowing data plots presented in this chapter for TLG where commercial sensor with the same response time of *ca.* 1 s as the TLG sensor, senses humidity but recovers slower than TLG. There is no time difference in the responses of the graphene and the commercial sensors when subjected to humidity. However, the graphene sensors have a sharper recovery than the commercial sensors, with a time difference of *ca.* 50-100s.

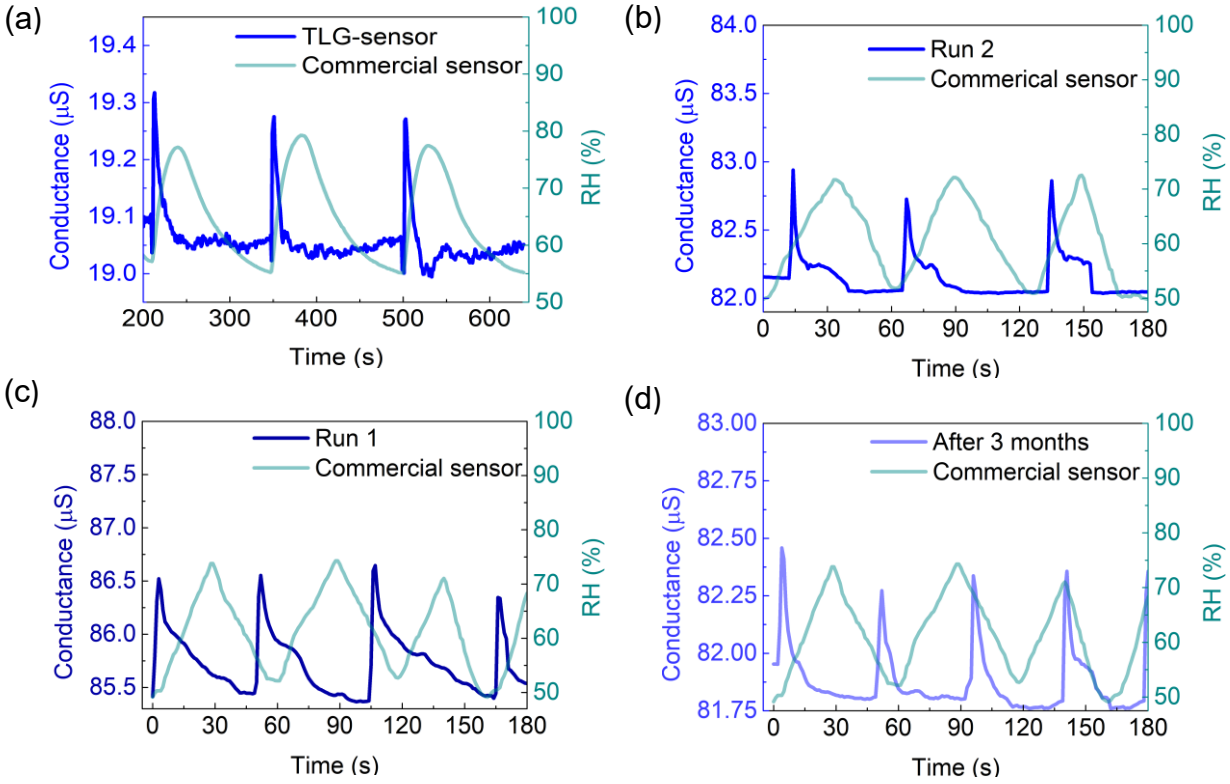

Figure 6.8. Durability of TLG-sensor with resilience tests and multiple runs. Conductance vs. time at 1 V: (a) after washing and bending tests; (b) human blowing - run 1; (c) human blowing - run 2; and (d) human blowing-measurement after 3 months.

It was observed that when the SEG-sensors were subjected to 1 V, the response time of the sensor was found to be *ca.* 1-2s. The devices were faster response to relative humidity than the commercial sensor in some devices and slower in some. This could be due to the non-uniform percolating network of graphene flakes because of the SEG transfer process, which makes it difficult to SEG-sensors with similar response times. It was observed that at a low voltage of 0.5 V, the response to RH was slower than the commercial sensor.

Although the SEG-sensors lack the durability, they are more cost- and area-effective and could still find applications as disposable short-term humidity sensors. Figure 5.8b and c shows two subsequent runs of a TLG-sensor's response to human blowing. It can be seen in Figure 6.8d that even after three months, the same TLG-sensor still shows good humidity sensing which suggests long term stability and reliability, suggesting these sensors could be used multiple times.

6.4 SUMMARY

Two types of textile-based humidity sensors have been studied in this chapter with TLG and SEG as humidity sensing layers and PP as the flexible textile substrate. It was found that the humidity sensing behaviours of TLG and SEG was opposite to each other with the increase (TLG) and decrease (SEG) in conductance with increasing RH (human blowing). This was confirmed with continuous measurement, using a commercial humidifier in a closed environment. Although the TLG-sensors showed better durability suggesting multiple uses than the SEG-sensors when they were subjected to resilience (washing and bending) and repeatability tests, the SEG-sensors can still find applications as disposable humidity sensors. The response and recovery of these sensors were compared with that of a commercial humidity sensor. It was found that the TLG-sensor has a similar response time (*ca.* 1s) as the commercial sensor and recovers quicker than the commercial sensor. The SEG-sensor, on the other hand, had a slightly varied response time difference to the commercial sensor, but recovered quicker than the commercial sensor. The recovery time difference between the commercial and graphene sensors was in the range of *ca.* 50-100s. The devices were imposed with two voltages, 1 V and 0.5 V, and the results with TLG and

SEG show low operating voltage requirement that we can achieve good humidity sensing with a simpler device architecture that does not require any lithographic steps or strict clean room environments, potentially reducing the costs in view of commercialisation. The textile-humidity sensors can be integrated in clothing and employed in environments such as the bathroom (curtains, rugs), storage houses (wallpapers), where humidity monitoring and control is essential.

Chapter 7

CONCLUSIONS AND OUTLOOK

In this thesis, the potential of graphene in textile-based temperature and humidity sensors has been investigated. The work began with a purposely developed type of graphene, produced by CVD on Cu foil, with an average of three layers i.e., TLG, at atmospheric pressure, making it more conductive than a single layer of graphene. The number of layers in TLG were confirmed with transmittance studies and Raman spectroscopic analysis and were found to agree with the previously reported results. Monofilament and taped-shaped PP textile fibres were used as the textile-based substrate because of the non-toxic, cost-effective, bacterial, and mould-resistant properties of the PP fibres. The other types of graphene studied were SLG (CVD-grown), FLG, commercially sourced, and grown on Ni sputtered Si/SiO_2, and SEG, produced from the shear exfoliation of graphite.

The graphene-coated PP fibres were subjected to several characterisation techniques to assess their properties. It was found, through a series of washing and bending tests, that the TLG graphene performed better than SEG since TLG is more continuous domains making them robust. On the other hand, SEG has overlapping flakes which are easily displaced or detached from the surface of the PP substrate during the rigorous washing and bending cycles. SEM images and AFM maps (tapping mode topographic, phase, and amplitude), were used to study the surface topology of the graphene-coated PP fibres, suggesting continuous and uniform surface coverage with no visible tears or cracks in the graphene coating for CVD-grown. Furthermore, the height profile suggests that CVD graphene can adopt the conformation of the PP fibres underneath. In contrast to the CVD-graphene, the SEM images and AFM maps of SEG showed the overlapping graphene flakes which completely covered the PP surface and made it difficult to see the PP fibre underneath. However, they also revealed thick and loose stacks of flakes that can easily detach from the film.

To ensure the electrical measurements were repeatable and the values were comparable to each other, a 2-probe setup was designed with fixed channel length of 1 cm. The sheet resistance of each type of graphene was calculated and was found to be in the order of 1 kΩ/sq for CVD-grown graphene which agrees with the previously reported sheet resistance values. The sheet resistance of SEG was found to be in the order of 3 kΩ/sq which could be higher due to the presence of overlapping flakes and sodium cholate residues, used during the SEG production. Two contact materials, carbon paste and silver ink, were used to prevent the damage to the fibres by the repeated exposure to the measuring probes. Carbon paste was found to offer more flexibility, have a better adhesion to the fibres and better electrical contact than silver ink.

All the types of graphene studied were used to fabricate graphene-based textile temperature sensors and their sensing behaviours were compared in the temperature range of 30-45 °C. The device architecture consisted of graphene-coated PP fibres with carbon paste contacts 1 cm apart. For these sensors, the change of graphene resistance in response to the change in temperature was considered as the sensing parameter. TLG-coated sensors were found to provide consistent temperature sensing results, with extremely low error, even after 10 subsequent runs, suggesting durability and reliability. The TLG-temperature sensors were compared with a commercially available temperature sensor and were found to have a quicker response and recovery time. The TCR of the TLG-based temperature sensor was found to be slightly higher (1.11 %) than the reported TCR for flexible substrates. These textile-based temperature sensors can easily be integrated into clothing, linen, or upholstery for continuously measuring the temperature without any human interference.

The humidity sensors fabricated have a much simpler device architecture as compared to the previously reported textile-based humidity sensors, also consisting of graphene-coated PP fibres with carbon paste contacts. The humidity sensing behaviour of TLG and SEG-sensors were compared with a commercially available humidity sensor with a series of human blowing and continuous ambient humidity tests. It was found that the behaviours of TLG and SEG were opposite to each other, i.e., the TLG-sensor and SEG-sensor exhibited an increase and decrease in

conductivity, respectively, with an increase in relative humidity. It was found that both humidity and temperature sensors can operate at operating voltage as low as 0.5 V leading to low-power wearable applications. The studied sensors have a simple architecture which would add to the cost-effectiveness of the sensors in terms of commercialisation. They do not require the use of any toxic chemicals, often used to produce or any other material incorporated in e-textiles, in addition to getting completely integrated in clothing with no rigid, heavy or fragile components.

These textile-based sensors, in the future, can be connected to a wireless system which would help minimising the patient visits to the hospital, allow doctors to practice while sitting at home, and increasing the patient autonomy. This would also increase the data collected at regular intervals without any human interference and with a greater degree of accuracy. The textile-based humidity sensors can also be easily employed in humid environments such as bathroom rugs where humidity monitoring is essential or quality and health safety purposes as well as in close contact to humans for respiration monitoring, for example. They can be used not only in healthcare for continuous humidity and temperature monitoring as well as in greenhouses or storage places where high or low relative humidity can lead to spoilage or damage of the occupant products. The sensors mentioned in this thesis are compatible with roll-to-roll processing which can be used to mass-produce these sensors.

An option to investigate would be to combine the sensors with triboelectric nanogenerators, producing a self-powering sensing device which can harvest power from the act of walking or the bending motion of the arms. Another option would be to pattern the PP fibres with different types of deformable structures with either optical lithography or nano-beam lithography such as interdigitated, serpentine, fractal, island-bridge and compare their temperature and humidity sensing behaviours. For integrating textile-temperature sensors in the clothing, appropriate choice of encapsulation material would prevent their abrasion. These sensors can be combined with the light-emitting technology and can have light-emitting temperature sensor every time the temperature falls outside a certain range. In terms of foundation studies, investigation of the stacking order and defect densities would provide more information about the produced TLG. Attempts could be made to further optimise the growth process to ensure uniform distribution of three or more layers of graphene on Cu foil.

A different approach to remove the sodium cholate residues from SEG would ensure improvement in the conductivity and sensing abilities in SEG-sensors.

BIBLIOGRAPHY

(1) Neves, A. I. S.; Rodrigues, D. P.; De Sanctis, A.; Alonso, E. T.; Pereira, S.; Amaral, V. S.; Melo, L. V.; Russo, S.; de Schrijver, I.; Alves, H & Craciun, M. F., Towards conductive textiles: coating polymeric fibres with graphene, 2017, *Sci. Rep.* 7, 4250. https://doi.org/10.1038/s41598-017-04453-7.

(2) Neves, A. I. S.; Bointon, T., Melo, L.; Russo, S.; de Schrijver, I.; Craciun, M. F & Alves, H., Transparent conductive graphene textile fibres, 2015, *Sci. Rep.* 5, 9866. https://doi.org/10.1038/srep09866.

(3) Alonso, E. T.; Rodrigues, D. P.; Khetani, M.; Shin, D.; De Sanctis, A.; Joulie, H.; de Schrijver, I.; Baldycheva, A.; Neves, A. I. S; Russo, S. & Craciun, M. F., Graphene electronic fibres with touch-sensing and light-emitting functionalities for smart textiles*,* 2018 *npj Flex. Electron.* 2, 25. https://doi.org/10.1038/s41528-018-0040-2.

(4) Alonso, E. T.; Shin, D.; Rajan, G.; Neves, A. I. S.; Russo, S. & Craciun, M. F., Water-based solution processing and wafer-scale integration of all-graphene humidity sensors, 2019, *Adv. Sci.* 6 (15), 1802318. https://doi.org/10.1002/advs.201802318.

(5) Borini, S.; White, R.; Wei, D.; Astley, M.; Haque, S.; Spigone, E.; Harris, N.; Kivioja, J. & Ryhänen, T., Ultrafast graphene oxide humidity sensors, 2013, *ACS Nano* 7, 11166-11173. https://doi.org/10.1021/nn404889b.

(6) Khurana, G., Sahoo, S., Barik, S., Kumar, N., Sharma, G. L.; Scott, J. F. & Katiyar, R. S., Reduced graphene oxide as an excellent temperature sensor, 2018, *J. Nanosci. Nanotechnol. Appl.* 2, 101. http://article.scholarena.co/Reduced-Graphene-Oxide-as-an-Excellent-Temperature-Sensor.pdf.

(7) Zhang, M.; Saeed, R.; Saeed, S.; Stankovski, S. & Zhang, X., Wearable technology, and applications: a systematic review, 2020, *J. Mechatron. Autom. Identif. Technol.* 5, 5-16. http://dx.doi.org/10.1136/bmjinnov-2016-000133

(8) Gao, F.; Wang, L. & Lin, T., Intelligent wearable rehabilitation robot control system based on mobile communication network, 2020, *Comput. Commun.* 153, 286-293. https://doi.org/10.1016/j.comcom.2020.01.054.

(9) Pierleoni, P.; Belli, A.; Palma, L.; Pellegrini, M.; Pernini, L.& Valenti, S., A high reliability wearable device for elderly fall detection, 2015, *IEEE Sens. J.* 15 (8), 4544-4553. https://doi.org/10.1109/JSEN.2015.2423562.

(10) Wang, Y.; Cang, S. & Yu, H. A survey on wearable sensor modality centred human activity recognition in health care, 2019, *Expert Syst. Appl.* 137, 167-190. https://doi.org/10.1016/j.eswa.2019.04.057.

(11) Saleem, K.; Shahzad, B.; Orgun, M. A.; Al-Muhtadi, J.; Rodrigues, J. J.& Zakariah, M, Design, and deployment challenges in immersive and wearable technologies, 2017, *Behav. Inf. Technol.* 36 (7), 687-698. http://dx.doi.org/10.1080/0144929X.2016.1275808

(12) Grand View Research, June 2020, Wearable technology market size, share & trends analysis report by product (wrist-wear, eye-wear & head-wear, foot-wear, neck-wear, body-wear), by application, by region, and segment forecasts, 2020-2027, Report ID: 978-1-68038-165-8. https://www.grandviewresearch.com/industry-analysis/wearable-technology-market.

(13) https://www.Samsung.Com/Uk/Wearables/Gear-S2/Features (accessed on 23rd February 2021).

(14) https://www.Fitbit.Com/in/Sense (accessed on 23rd February 2021).

(15) https://www.Wahoofitness.Com/Instructions/Tickrx (accessed on 23rd February 2021).

(16) https://www.Google.Com/Glass/Start (accessed on 23rd February 2021).

(17) https://Lechal.Com/#More-than-Just-Tech (accessed on 23rd February 2021).

(18) Liang, J.; Li, L.; Niu, X.; Yu, Z. & Pei, Q., Elastomeric polymer light-emitting devices and displays, 2013, *Nat. Photon.* 7 (10), 817-824. https://doi.org/10.1038/nphoton.2013.242.

(19) Kim, Y.-H.; Lee, E. Y.; Lee, H. H. & Seo, T. S. Characteristics of reduced graphene oxide quantum dots for a flexible memory thin film transistor, 2017, *ACS Appl. Mater. Interfaces* 9 (19), 16375-16380. https://doi.org/10.1021/acsami.7b00714.

(20) Zhu, H.; Wang, X.; Liang, J.; Lv, H.; Tong, H.; Ma, L.; Hu, Y.; Zhu, G.; Zhang, T.; Tie, Z.; Liu, Z., Li, Q.; Chen, L.; Liu, J. & Jin, Z., Versatile electronic skins for motion detection of joints enabled by aligned few-walled carbon nanotubes in flexible polymer composites, 2017, *Adv. Funct. Mater* 27 (21), 1606604. https://doi.org/10.1002/adfm.201606604.

(21) Yamada, T.; Hayamizu, Y.; Yamamoto, Y.; Yomogida, Y.; Izadi-Najafabadi, A.; Futaba, D. N. & Hata, K., A stretchable carbon nanotube strain sensor for human-motion detection, 2011, *Nat. Nanotechnol.* 6 (5), 296-301. https://doi.org/10.1038/nnano.2011.36.

(22) Nagaraju, G.; Raju, G. S. R.; Ko, Y. H. & Yu, J. S., Hierarchical Ni–Co layered double hydroxide nanosheets entrapped on conductive textile fibres: a cost-effective and flexible electrode for high-performance pseudocapacitors, 2016, *Nanoscale* 8 (2), 812-825. https://doi.org/10.1039/C5NR05643H.

(23) Jung, M.; Kim, J.; Noh, J.; Lim, N.; Lim, C.; Lee, G.; Kim, J.; Kang, H.; Jung, K.; Leonard, A. D. & Tour, J. M., All-printed and roll-to-roll-printable 13.56-MHz-operated 1-bit RF tag on plastic foils, 2010, *IEEE Trans. Electron. Devices*, 57 (3), 571-580. https://doi.org/10.1109/TED.2009.2039541.

(24) Oh, J. Y.; Kim, S.; Baik, H. & Jeong, U., Conducting polymer dough for deformable electronics, 2016, *Adv. Mater.* 28 (22), 4455-4461. https://doi.org/10.1002/adma.201502947.

(25) Xia, M.; Cheng, Z.; Han, J. & Zhang, S., Extremely stretchable all-carbon-nanotube transistor on flexible and transparent substrates, 2014, *Appl. Phys. Lett.* 105 (14), 143504. https://doi.org/10.1063/1.4897528.

(26) Yang, Y.; Yang, X.; Zou, X.; Wu, S.; Wan, D.; Cao, A.; Liao, L.; Yuan, Q. & Duan, X., Ultrafine graphene nanomesh with large on/off ratio for high-performance flexible biosensors, 2017, *Adv. Funct. Mater.* 27 (19), 1604096. https://doi.org/10.1002/adfm.201604096.

(27) Khang, D.; Rogers, J. A. & Lee, H. H., Mechanical buckling: mechanics, metrology, and stretchable electronics*, 2009, Adv. Funct. Mater.* 19 (10), 1526-1536. https://doi.org/10.1002/adfm.200801065.

(28) Fan, J. A.; Yeo, W.-H.; Su, Y.; Hattori, Y.; Lee, W.; Jung, S.-Y.; Zhang, Y.; Liu, Z.; Cheng, H.; Falgout, L.; Bajema, M; Coleman, T; Gregoire, D; Larsen, R; Huang, Y & Rogers, J. A., Fractal design concepts for stretchable electronics, 2014, *Nat. Commun.* 5 (1), 3266. https://doi.org/10.1038/ncomms4266.

(29) Xu, S.; Zhang, Y.; Cho, J.; Lee, J.; Huang, X.; Jia, L.; Fan, J.A.; Su, Y.; Su, J.; Zhang, H.; Cheng, H.; Lu, B.; Yu, C.; Chuang, C.; Kim, T.-l.; Song, T.; Shigeta, K.; Kang, S.; Dagdeviren, C.; Petrov, I.; Braun, P.V.; Huang, Y.; Paik, U. & Rodgers, J.A., Stretchable batteries with self-similar serpentine interconnects, and integrated wireless recharging systems, 2013, *Nat. Commun.* 4,1543. https://doi.org/10.1038/ncomms2553.

(30) Mondal, K. Recent advances in soft e-textiles. 2018, *Inventions* 3 (2), 23. https://doi.org/10.3390/inventions3020023.

(31) https://www.Astm.Org/Search/Fullsite-Search.Html?Query=textile%20fibre& (accessed on 19th February 2021).

(32) Alagirusamy, R. ; Das, A. & Fangueiro, R. Yarns: Production, Processability and Properties, 2011, *In Woodhead publishing series in textiles, fibrous and composite materials for civil engineering applications, Woodhead publishing*,

ISBN 9781845695583, 29-61. https://doi.org/10.1533/9780857095583.1.29

(33) Needles, H. L., Textile fibres, dyes, finishes and processes: a concise guide, 1986. *Noyes,* 1st ed., ISBN: 9780815510765, 343.

(34) Park, M.; Im, J.; Shin, M.; Min, Y.; Park, J.; Cho, H.; Park, S.; Shim, M.-B.; Jeon, S.; Chung, D.-Y.; Bae, J.; Park, J; Jeong, U & Kim, K., Highly stretchable electric circuits from a composite material of silver nanoparticles and elastomeric fibres, 2012, *Nat. Nanotechnol.* 7, 803-809. https://doi.org/10.1038/nnano.2012.206.

(35) Lugoda, P.; Costa, J. C.; Oliveira, C.; Garcia-Garcia, L. A.; Wickramasinghe, S. D.; Pouryazdan, A.; Roggen, D.; Dias, T. & Münzenrieder, N., Flexible temperature sensor integration into e-textiles using different industrial yarn fabrication processes, 2020, *Sensors* 20 (1), 73. https://doi.org/10.3390/s20010073.

(36) Zhou, G.; Byun, J.-H.; Oh, Y.; Jung, B.-M.; Cha, H.-J.; Seong, D.-G.; Um, M.-K.; Hyun, S. & Chou, T.-W., Highly sensitive wearable textile-based humidity sensor made of high-strength, single-walled carbon nanotube/poly(vinyl alcohol) filaments, 2017, *ACS Appl. Mater. Interfaces* 9 (5), 4788-4797. https://doi.org/10.1021/acsami.6b12448.

(37) Luo, C.; Tian, B.; Liu, Q.; Feng, Y. & Wu, W., One-step-printed, highly sensitive, textile-based, tunable performance strain sensors for human motion detection, 2020, *Adv. Mater. Technol.* 5 (2), 1900925. https://doi.org/10.1002/admt.201900925.

(38) Lilja, J.; Salonen, P.; Kaija, T. & de Maagt, P., Design, and manufacturing of robust textile antennas for harsh environments, 2012, *IEEE Trans. Antennas Propag.,* 60 (9), 4130-4140. http://dx.doi.org/10.1109/TAP.2012.2207035.

(39) Zhang, X.; Pan, N. & Sun, G., Antistatic and conductive textiles, 2011, *Functional textiles for improved performance, protection, and health*, 1st ed., Woodhead Publishing Series in Textiles, 27-44, ISBN: 9781845697235, https://doi.org/10.1533/9780857092878.27.

(40) Asghar, A.; Ahmad, M.; Yahya, M.; Ali, M.; Ab Aziz, A.; Abd Rahman, N.; Hassan, S. Z. U. & Kashif, M., An alternative approach to design conductive hybrid cover yarns for efficient electromagnetic shielding fabrics, 2018, *J. Ind. Text.* 48 (1), 38-57. https://doi.org/10.1177%2F1528083717721922.

(41) Yun, M. J.; Cha, S. I.; Seo, S. H. & Lee, D. Y., Highly flexible dye-sensitized solar cells produced by sewing textile electrodes on cloth, 2014, *Sci. Rep.* 4, 5322. https://doi.org/10.1038/srep05322.

(42) Wu, R.; Ma, L.; Patil, A., Meng, Z.; Liu, S.; Hou, C.; Zhang, Y.; Yu, W.; Guo, W. & Liu, X. Y., Graphene decorated carbonized cellulose fabric for physiological

signal monitoring and energy harvesting, 2020, *J. Mater. Chem. A* 8, 12665-12673. https://doi.org/10.1039/D0TA02221G.

(43) Zeng, W.; Shu, L.; Li, Q.; Chen, S.; Wang, F. & Tao, X., Fibre-based wearable electronics: a review of materials, fabrication, devices, and applications, 2014, *Adv. Mater.* 26, 5310-5336. https://doi.org/10.1002/adma.201400633.

(44) Ahmed, A.; Jalil, M. A.; Hossain, M. M.; Moniruzzaman, M.; Adak, B.; Islam, M. T.; Parvez, M. S. & Mukhopadhyay, S. A., PEDOT: PSS and graphene-clad smart textile-based wearable electronic joule heater with high thermal stability, 2020, *J. Mater. Chem. C* 8 (45), 16204-16215. https://doi.org/10.1039/D0TC03368E.

(45) Bali, C.; Brandlmaier, A.; Ganster, A.; Raab, O.; Zapf, J. & Hübler, A., Fully inkjet-printed flexible temperature sensors based on carbon and PEDOT:PSS, 2016, *Mater. Today Proc.* 3 (3), 739-745. https://doi.org/10.1016/j.matpr.2016.02.005.

(46) Wang, C.; Xia, K.; Wang, H.; Liang, X.; Yin, Z. & Zhang, Y., Advanced carbon for flexible and wearable electronics, 2019, *Adv. Mater.* 31, 1-37. https://doi.org/10.1002/adma.201801072.

(47) Fatema, U. K. & Gotoh, Y., Iodine-aided palladium-free catalysation process for durable electroless nickel plating on Kevlar® fibre, 2012, *Surf. Coat. Technol.* 206 (16), 3472-3478. https://doi.org/10.1016/j.surfcoat.2012.02.014.

(48) Little, B. K.; Li, Y.; Cammarata, V.; Broughton, R. & Mills, G., Metallization of Kevlar® fibres with gold, 2011, *ACS Appl. Mater. Interfaces* 3 (6), 1965-1973. https://doi.org/10.1021/am200193c.

(49) Kalanyan, B.; Oldham, C. J.; Sweet III, W. J. & Parsons, G. N., Highly conductive and flexible nylon-6 nonwoven fibre mats formed using tungsten atomic layer deposition, 2013, *ACS Appl. Mater. Interfaces* 5 (11), 5253-5259. https://doi.org/10.1021/am401095r.

(50) Zeng, W.; Tao, X.-M.; Chen, S.; Shang, S.; Chan, H. L. W. & Choy, S. H., Highly durable all-fibre nanogenerator for mechanical energy harvesting. 2013, *Energy Environ. Sci.* 6 (9), 2631-2638. https://doi.org/10.1039/C3EE41063C.

(51) Fobelets, K.; Thielemans, K.; Mathivanan, A. & Papavassiliou, C., Characterization of knitted coils for e-textiles, 2019, *IEEE Sens. J.* 19 (18), 7835-7840. https://doi.org/10.1109/JSEN.2019.2917542.

(52) Martinez-Estrada, M.; Moradi, B.; Fernández-Garcia, R. & Gil, I., Embroidery textile moisture sensor, 2018, *Proceedings* 2, 1057. https://doi.org/10.3390/proceedings2131057.

(53) Lee, J. B. & Subramanian, V., Weave patterned organic transistors on fibre for e-textiles, 2005, *IEEE Trans. Electron. Devices* 52 (2), 269-275. http://dx.doi.org/10.1109/TED.2004.841331.

(54) Tajitsu, Y., Development of e-textile sewn together with embroidered fabric having motion-sensing function using piezoelectric braided cord for embroidery, 2020, *IEEE Trans. Dielectr. Electr. Insul.* 27 (5), 1644-1649. https://doi.org/10.1109/TDEI.2020.008448.

(55) Wu, Y.; Mechael, S. S.; Lerma, C.; Carmichael, R. S. & Carmichael, T. B., Stretchable ultrasheer fabrics as semitransparent electrodes for wearable light-emitting e-textiles with changeable display patterns, 2020, *Matter* 2 (4), 882-895. https://doi.org/10.1016/j.matt.2020.01.017.

(56) Gao, C.; He, S.; Qiu, L.; Wang, M.; Gao, J. & Gao, Q., Continuous dry–wet spinning of white, stretchable, and conductive fibres of poly (3-hydroxybutyrate-co-4-hydroxybutyrate) and ATO@ TiO_2 nanoparticles for wearable e-textiles, 2020, *J. Mater. Chem. C* 8 (25), 8362-8367. https://doi.org/10.1039/D0TC01310B.

(57) Cao, R.; Pu, X.; Du, X.; Yang, W.; Wang, J.; Guo, H.; Zhao, S.; Yuan, Z.; Zhang, C. & Li, C., Screen-printed washable electronic textiles as self-powered touch/gesture tribo-sensors for intelligent human–machine interaction, 2018, *ACS Nano*, 12 (6), 5190-5196. https://doi.org/10.1021/acsnano.8b02477.

(58) Hong, H.; Jiyong, H.; Moon, K.-S.; Yan, X. & Wong, C. Rheological properties, and screen printability of UV curable conductive ink for flexible and washable e-textiles, 2021, *J. Mater. Sci. Technol.* 67, 145-55. https://doi.org/10.1016/j.jmst.2020.06.033.

(59) Locher, I. & Tröster, G. Enabling technologies for electrical circuits on a woven monofilament hybrid fabric, 2008, *Text. Res. J*., 78 (7), 583-594. https://doi.org/10.1177%2F0040517507081314.

(60) Tang, G.; Qiao, Y.; Yu, L.; Li, C. M. & Lu, Z., Re-stickable all-solid-state supercapacitor supported by cohesive thermoplastic for textile electronics, 2020, *ACS Appl. Mater. Interfaces* 12 (40), 45322-45331. https://doi.org/10.1021/acsami.0c13687.

(61) Kim, Y.; Kim, H. & Yoo, H.-J., Electrical characterization of screen-printed circuits on the fabric, 2009, *IEEE Trans. Adv. Packag.* 33 (1), 196-205. https://doi.org/10.1109/TADVP.2009.2034536.

(62) Tao, X.; Koncar, V.; Huang, T.; Shen, C. & Ko, Y., How to make reliable, washable, and wearable, 2017, *Sensors* 17(4), 673. https://doi.org/10.3390/s17040673.

(63) Stoppa, M. & Chiolerio, A., Wearable electronics, and smart textiles: a critical review, 2014, *Sensors* 14 (7), 11957-11992. https://doi.org/10.3390/s140711957.

(64) Phillips, K. & Ghosh, T. K., The technology of polypropylene tape yarns: processing and applications. 2003, *Text. Prog.* 33 (1), 1-53. https://doi.org/10.1080/00405160308688957.

(65) Vargha, V.; Chetty, A.; Sulyok, Z.; Mihály, J.; Keresztes, Z.; Tóth, A.; Sajó, I.; Korecz, L.; Anandjiwala, R. & Boguslavsky, L., Functionalisation of polypropylene non-woven fabrics (NWFs) functionalisation by oxyfluorination as a first step for graft polymerisation, 2012*, J. Therm. Anal. Calorim.* 109 (2), 1019-1032. https://doi.org/10.1007/s10973-011-1940-8.

(66) Rawal, A. & Sayeed, M.M.A., Mechanical properties and damage analysis of jute/polypropylene hybrid nonwoven geotextiles, 2013, *Geotext. Geomembr.* 37, 54-60. https://doi.org/10.1016/j.geotexmem.2013.02.003.

(67) Karger-Kocsis, J., Polypropylene structure, blends, and composites: Volume 3 Composites, 2012, *Springer Science & Business Media*. ISBN: 9789401105231. https://doi.org/10.1007/978-94-011-0523-1.

(68) Terry, B. & Slater, K., Comparative analysis of synthetic fibres for marine rope, 1998, *J. Consum. Stud. Home Econ.* 22 (1), 19-24. https://doi.org/10.1111/j.1470-6431.1998.tb00712.x.

(69) Hirte, R., Polypropylene fibres – science and technology,1982, *Textile Science and Technology* 5 . Von M. AHMED. Amsterdam/Oxford/New York: Elsevier Scientific Publishing Company XIV, 766. https://doi.org/10.1002/actp.1983.010340911.

(70) The Merck Index, 1976, 9th ed. Rahway, New Jersey: Merck & Co., Inc., 985.

(71) Kellie, G. Developments in nonwovens as agrotextiles. In: *Advances in Technical Nonwovens*, 2016, 1st ed., Woodhead Publishing, 365-384, ISBN: 9780081005750. https://doi.org/10.1016/B978-0-08-100575-0.00013-9.

(72) Bajwa, G. S., Singari, R. M., & Mishra, R. S., The natural fibre and nano talc-based hybrid composite of polypropylene: Thermal performance, 2021, *Indian J Eng Mater S* 27 (4), 866-871. http://dx.doi.org/10.5958/0974-1283.2018.00093.2.

(73) Heijenrath, R., & Peijs, T., Natural-fibre-mat-reinforced thermoplastic composites based on flax fibres and polypropylene, 1996, *Adv. Compos. Lett.* 5 (3), 096369359600500303. https://doi.org/10.1177%2F096369359600500303.

(74) Soldano, C.; Mahmood, A. & Dujardin, E., Production, properties, and potential of graphene, 2010, *Carbon* 48 (8), 2127-2150. https://doi.org/10.1016/j.carbon.2010.01.058.

(75) Novoselov, K. S.; Geim, A. K.; Morozov, S. V.; Jiang, D.; Katsnelson, M. I.; Grigorieva, Iv.; Dubonos, Sv. & Firsov, A., Two-dimensional gas of massless dirac fermions in graphene, 2005, *Nature* 438 (7065), 197-200. https://doi.org/10.1038/nature04233.

(76) Geim, A. K. & Novoselov, K. S., The rise of graphene, 2007, *Nature Mater.* 6, 183-191. https://doi.org/10.1038/nmat1849.

(77) Lee, C.; Wei, X.; Kysar, J. W. & Hone, J., Measurement of the elastic properties and intrinsic strength of monolayer graphene, 2008, *Science* 321 (5887), 385-388. https://doi.org/10.1126/science.1157996.

(78) ISO 2017 ISO/TS 80004-13. Nanotechnologies-Vocabulary-Part 13: Graphene and Related Two-Dimensional (2D) Materials.

(79) Brownson, D. A.; Kampouris, D. K. & Banks, C. E., Graphene electrochemistry: fundamental concepts through to prominent applications, 2012, *Chem. Soc. Rev.* 41, 6944-6976. https://doi.org/10.1039/C2CS35105F.

(80) Nair, R. R.; Blake, P.; Grigorenko, A. N.; Novoselov, K. S.; Booth, T. J.; Stauber, T.; Peres, N. M. & Geim, A. K., Fine structure constant defines visual transparency of graphene, 2008, *Science* 320 (5881), 1308-1308. https://doi.org/10.1126/science.1156965.

(81) Davaji, B.; Cho, H. D.; Malakoutian, M.; Lee, J.-K.; Panin, G.; Kang, T. W.; Lee, C. H., A patterned single layer graphene resistance temperature sensor, 2017, *Sci. Rep.* 7 (1). https://doi.org/10.1038/s41598-017-08967-y.

(82) Yoon, H. J.; Yang, J. H.; Zhou, Z.; Yang, S. S. & Cheng, M. M.-C., Carbon dioxide gas sensor using a graphene sheet, 2011*, Sens. Actuators B Chem.* 157 (1), 310-313. http://dx.doi.org/10.1016/j.snb.2011.03.035.

(83) Shen, D; Xiao, M; Xiao,Y; Zou,G; Hu, L; Zhao, B; Liu, L; Duley, W.W & Zhou.Y.Y., Self-Powered, Rapid-Response, and Highly Flexible Humidity Sensors Based on Moisture-Dependent Voltage Generation, 2019, *ACS Appl. Mater. Interfaces* 11 (15), 14249-14255. https://doi.org/10.1021/acsami.9b01523.

(84) Wang, H.; Sun, K.; Tao, F.; Stacchiola, D. J. & Hu, Y. H., 3D honeycomb-like structured graphene and its high efficiency as a counter-electrode catalyst for dye-sensitized solar cells, 2013, *Angew. Chem. Int. Ed.* 52 (35), 9210–9214. https://doi.org/10.1002/anie.201303497.

(85) Shin, D. W.; Barnes, M. D.; Walsh, K.; Dimov, D.; Tian, P.; Neves, A. I. S.; Wright, C. D.; Yu, S. M.; Yoo, J. B.; Russo, S. & Craciun, M. F., A new facile route to flexible and semi-transparent electrodes based on water exfoliated graphene and their single-electrode triboelectric nanogenerator, 2018, *Adv. Mater.* 30 (39), 1802953. https://doi.org/10.1002/adma.201802953.

(86) Dimov, D.; Amit, I.; Gorrie, O.; Barnes, M. D.; Townsend, N. J.; Neves, A. I. S.; Withers, F.; Russo, S. & Craciun, M. F., Ultrahigh performance nanoengineered graphene-concrete composites for multifunctional applications, 2018, *Adv. Funct. Mater.* 28, 1705183. https://doi.org/10.1002/adfm.201705183.

(87) Li, J.; Zhuang, J.; Shen, C.; Tian, Y.; Que, Y.; Ma, R.; Pan, J.; Zhang, Y.; Wang, Y.; Du, S.; Ding, F. & Gao, H. J., Impurity-induced formation of bilayered graphene on copper by chemical vapor deposition, 2016, *Nano Res*, 9, 2803-2810. https://doi.org/10.1007/s12274-016-1169-8.

(88) Yang, G.; Li, L.; Lee, W. B. & Ng, M. C., Structure of graphene and its disorders: a review, 2018, *Sci. Technol. Adv. Mater.* 19 (1), 613–648. https://doi.org/10.1080/14686996.2018.1494493.

(89) Huang, P. Y.; Ruiz-Vargas, C. S.; Van Der Zande, A. M.; Whitney, W. S.; Levendorf, M. P.; Kevek, J. W.; Garg, S.; Alden, J. S.; Hustedt, C. J. & Zhu, Y., Grains, and grain boundaries in single-layer graphene atomic patchwork quilts. 2011, *Nature* 469 (7330), 389-392. https://doi.org/10.1038/nature09718.

(90) Zhang, Y.; Gao, T.; Gao, Y.; Xie, S.; Ji, Q.; Yan, K.; Peng, H. & Liu, Z., Defect-like structures of graphene on copper foils for strain relief investigated by high-resolution scanning tunneling microscopy, 2011, *ACS Nano* 5 (5), 4014-4022. https://doi.org/10.1021/nn200573v.

(91) Seah, C. M.; Chai, S. P. & Mohamed, A. R., Mechanisms of graphene growth by chemical vapour deposition on transition metals, 2014, *Carbon* 70, 1-21. https://doi.org/10.1016/j.carbon.2013.12.073.

(92) Suk, J. W.; Kitt, A.; Magnuson, C. W.; Hao, Y.; Ahmed, S.; An, J.; Swan, A. K.; Goldberg, B. B. & Ruoff, R. S., Transfer of CVD-grown monolayer graphene onto arbitrary substrates, 2011, *ACS Nano* 5 (9), 6916-6924. https://doi.org/10.1021/nn201207c.

(93) Mishra, N.; Boeckl, J.; Motta, N. & Iacopi, F., Graphene growth on silicon carbide: a review, 2016, *Phys. Status Solidi A* 213 (9), 2277-2289. https://doi.org/10.1002/pssa.201600091.

(94) Mahato, N.; Parveen, N. & Cho, M. H., Graphene nanodiscs from electrochemical assisted micromechanical exfoliation of graphite: morphology and supramolecular behaviour, 2015, *Mater. Express* 5 (6), 471-479. https://doi.org/10.1166/mex.2015.1270.

(95) Toh, S. Y.; Loh, K. S.; Kamarudin, S. K. & Daud, W. R. W., Graphene production via electrochemical reduction of graphene oxide: synthesis and characterisation, 2014, *Chem. Eng. J.* 251, 422-434. https://doi.org/10.1016/j.cej.2014.04.004.

(96) Randviir, E. P.; Brownson, D. A. & Banks, C. E., A decade of graphene research: production, applications, and outlook, 2014, *Mater. Today* 17 (9), 426–432. https://doi.org/10.1016/j.mattod.2014.06.001.

(97) Backes, C.; Abdelkader, A. M.; Alonso, C.; Andrieux-Ledier, A.; Arenal, R.; Azpeitia, J.; Balakrishnan, N.; Banszerus, L.; Barjon, J.; Bartali, R.; Bellani, S.; Berger, C.; Berger, R.; Ortega, M. M. B.; Bernard, C.; Beton, P. H. *et al.,* Production and processing of graphene and related materials., 2020, 2*D Mater. 7, 022001*. https://doi.org/10.1088/2053-1583/ab1e0a.

(98) Li, X.; Cai, W.; An, J.; Kim, S.; Nah, J.; Yang, D.; Piner, R.; Velamakanni, A.; Jung, I. Tutuc, E.; Bannerjee, S. K.; Colombo, L. & Ruoff, R. S., Large-area synthesis of high-quality and uniform graphene films on copper foils, 2009, *Science* 324 (5932), 1312-1314. https://doi.org/10.1126/science.1171245.

(99) Yu, Q.; Lian, J.; Siriponglert, S.; Li, H.; Chen, Y. P. & Pei, S.-S., Graphene segregated on Ni surfaces and transferred to insulators, 2008, *Appl. Phys. Lett.* 93 (11), 113103. https://doi.org/10.1063/1.2982585.

(100) Shu, H.; Chen, X.; Tao, X. & Ding, F., Edge structural stability and kinetics of graphene chemical vapor deposition growth, 2012, *ACS Nano* 6 (4), 3243-3250. https://doi.org/10.1021/nn300726r.

(101) Li, X.; Cai, W.; Colombo, L. & Ruoff, R. S., Evolution of graphene growth on Ni and Cu by carbon isotope labelling, 2009, *Nano Lett*. 9 (12), 4268–4272. https://doi.org/10.1021/nl902515k.

(102) Hwang, C.; Yoo, K.; Kim, S.; Seo, E.; Yu, H. & Biró, L., Initial stage of graphene growth on a Cu substrate, 2011, *J. Phys. Chem. C* 115 (45), 22369-22374. https://doi.org/10.1021/jp205980d.

(103) Bhaviripudi, S.; Jia, X.; Dresselhaus, M. S. & Kong, J., Role of kinetic factors in chemical vapor deposition synthesis of uniform large area graphene using copper catalyst, 2010, *Nano Lett.* 10 (10), 4128-4133. https://doi.org/10.1021/nl102355e.

(104) Robertson, A. W. & Warner, J. H., Hexagonal single crystal domains of few-layer graphene on copper foils, 2011, *Nano Lett.* 11 (3), 1182-1189. https://doi.org/10.1021/nl104142k.

(105) Kalbac, M.; Frank, O. & Kavan, L., The control of graphene double-layer formation in copper-catalysed chemical vapor deposition, 2012, *Carbon* 50 (10), 3682-3687. https://doi.org/10.1016/j.carbon.2012.03.041.

(106) Guéret, C.; Daroux, M. & Billaud, F., Methane pyrolysis: thermodynamics, 1997, *Chem. Eng. Sci.* 52 (5), 815-827. https://doi.org/10.1016/S0009- 2509(96)00444-7.

(107) Vlassiouk, I.; Regmi, M.; Fulvio, P.; Dai, S.; Datskos, P.; Eres, G. & Smirnov, S., Role of hydrogen in chemical vapor deposition growth of large single-crystal graphene, 2011, *ACS Nano* 5 (7), 6069-6076. https://doi.org/10.1021/nn201978y.

(108) Bakr, N.; Funde, A.; Waman, V.; Kamble, M.; Hawaldar, R.; Amalnerkar, D.; Sathe, V.; Gosavi, S. & Jadkar, S., Role of argon in hot wire chemical vapor deposition of hydrogenated nanocrystalline silicon thin films, 2011, *Thin Solid Films* 519 (11), 3501-3508. https://doi.org/10.1016/j.tsf.2011.01.105.

(109) Strudwick, A. J.; Weber, N. E.; Schwab, M. G.; Kettner, M.; Weitz, R. T.; Wünsch, J. R.; Müllen, K. & Sachdev, H., Chemical vapor deposition of high-quality graphene films from carbon dioxide atmosphere, 2015, *ACS Nano* 9 (1), 31-42. https://doi.org/10.1021/nn504822m.

(110) Li, Q.; Chou, H.; Zhong, J.-H.; Liu, J.-Y.; Dolocan, A.; Zhang, J.; Zhou, Y.; Ruoff, R. S.; Chen, S. & Cai, W., Growth of adlayer graphene on Cu studied by carbon isotope labeling, 2013, *Nano Lett. 13* (2), 486-490. https://doi.org/10.1021/nl303879k.

(111) Bae, S.; Kim, H.; Lee, Y.; Xu, X.; Park, J.-S.; Zheng, Y.; Balakrishnan, J.; Lei, T.; Kim, H. R.; Song, Y. I., Kim, Y.-J.; Kim, K. S.; Ozyilmaz, B.; Ahn, J.- H.; Hong, B.H. & Iijima, S., Roll-to-roll production of 30-inch graphene films for transparent electrodes, 2010, *Nat. Nanotechnol.* 5 (8), 574. https://doi.org/10.1038/nnano.2010.132.

(112) Vlassiouk, I.; Fulvio, P.; Meyer, H.; Lavrik, N.; Dai, S.; Datskos, P. & Smirnov, S., Large scale atmospheric pressure chemical vapor deposition of graphene, 2013, *Carbon* 54, 58-67. https://doi.org/10.1016/j.carbon.2012.11.003.

(113) Polsen, E. S.; McNerny, D. Q.; Viswanath, B.; Pattinson, S. W. & Hart, A. J., High-speed roll-to-roll manufacturing of graphene using a concentric tube CVD reactor, 2015, *Sci. Rep.* 5 (1), 1-12. https://doi.org/10.1038/srep10257.

(114) Deng, B.; Hsu, P.-C.; Chen, G.; Chandrashekar, B.; Liao, L.; Ayitimuda, Z.; Wu, J.; Guo, Y.; Lin, L.; Zhou, Y.; Aisijiang, M.; Xie, Q.; Cui, Y.; Liu, Z. & Peng, H., Roll-to-roll encapsulation of metal nanowires between graphene and plastic substrate for high-performance flexible transparent electrodes, 2015, *Nano Lett.* 15 (6), 4206-4213. https://doi.org/10.1021/acs.nanolett.5b01531.

(115) Hernandez, Y.; Nicolosi, V.; Lotya, M.; Blighe, F. M.; Sun, Z.; De, S.; McGovern, I.; Holland, B.; Byrne, M.; Gun'Ko, Y. K., Boland, J.J.; Niraj, P.; Duesberg, G.; Krishnamurthy, S.; Goodhue, R.; Hutchison, J.; Scardaci, V.;

Ferrari, A. C. & Coleman, J. N., High-yield production of graphene by liquid-phase exfoliation of graphite, 2008, *Nat. Nanotechnol.* 3 (9), 563-568. https://doi.org/10.1038/nnano.2008.215.

(116) Phiri, J.; Gane, P. & Maloney, T. C., High-concentration shear-exfoliated colloidal dispersion of surfactant–polymer-stabilized few-layer graphene sheets, 2017, *J. Mater. Sci.* 52 (13), 8321-8337. https://doi.org/10.1007/s10853-017-1049-y.

(117) Shen, Z.; Li, J.; Yi, M.; Zhang, X. & Ma, S., Preparation of graphene by jet cavitation, 2011, *Nanotechnology* 22 (36), 365306. http://dx.doi.org/10.1088/0957-4484/22/36/365306.

(118) Karagiannidis, P. G.; Hodge, S. A.; Lombardi, L.; Tomarchio, F.; Decorde, N.; Milana, S.; Goykhman, I.; Su, Y.; Mesite, S. V.; Johnstone, D. N.; Leary, R. K.; Midgley, P. A.; Pugno, N. M.; Torrisi, F. & Ferrari, A.C., Microfluidisation of graphite and formulation of graphene-based conductive inks, 2017, *ACS Nano* 11 (3), 2742-2755. https://doi.org/10.1021/acsnano.6b07735.

(119) Varrla, E.; Paton, K. R.; Backes, C.; Harvey, A.; Smith, R. J.; McCauley, J. & Coleman, J. N., Turbulence-assisted shear exfoliation of graphene using household detergent, and a kitchen blender, 2014, *Nanoscale* 6 (20), 11810-11819. https://doi.org/10.1039/C4NR03560G.

(120) Xu, Y.; Cao, H.; Xue, Y.; Li, B. & Cai, W., Liquid-phase exfoliation of graphene: an overview on exfoliation media, techniques, and challenges, 2018, *Nanomaterials* 8 (11), 942. https://doi.org/10.3390/nano8110942.

(121) Paton, K. R.; Varrla, E.; Backes, C.; Smith, R. J.; Khan, U.; O'Neill, A.; Boland, C.; Lotya, M.; Istrate, O. M.; King, P.; Higgins, T.;Barwich, S.; May, P.; Puczkarski, P.; Ahmed, I., Moebius, M., Pettersson, H., Long, E.; Coelho, J.; O'Brian, S. E.; McGuire, E. K.; Sanvhez, B. M.; Duesberg, G. S.; McEvoy, N.; Pennycook, T. J.; Downing, C.; Crossley, A.; Nicolose, V. & Coleman, J. N., Scalable production of large quantities of defect-free few-layer graphene by shear exfoliation in liquids, 2014, *Nat. Mater.* 13 (6), 624-630. https://doi.org/10.1038/nmat3944.

(122) Tran, T. S.; Park, S. J.; Yoo, S. S.; Lee, T.-R. & Kim, T., High shear-induced exfoliation of graphite into high quality graphene by Taylor-Couette flow, 2016, *RSC Adv.* 6 (15), 12003-12008. https://doi.org/10.1039/C5RA22273G.

(123) Coleman, J. N., Liquid-phase exfoliation of nanotubes and graphene, 2009, *Adv. Funct. Mater.* 19 (23), 3680-3695. https://doi.org/10.1002/adfm.200901640.

(124) Coleman, J. N., Liquid exfoliation of defect-free graphene, 2013, *Acc. Chem. Res.* 46 (1), 14-22. https://doi.org/10.1021/ar300009f.

(125) Hamilton, C. E.; Lomeda, J. R.; Sun, Z.; Tour, J. M. & Barron, A. R., High-yield organic dispersions of unfunctionalized graphene, 2009, *Nano Lett.* 9 (10), 3460-3462. https://doi.org/10.1021/nl9016623.

(126) O'Neill, A.; Khan, U.; Nirmalraj, P. N.; Boland, J. & Coleman, J. N., Graphene dispersion and exfoliation in low boiling point solvents, 2011, *J. Phys. Chem. C* 115 (13), 5422-5428. https://doi.org/10.1021/jp110942e.

(127) Choi, E.-Y.; San Choi, W.; Lee, Y. B. & Noh, Y.-Y., Production of graphene by exfoliation of graphite in a volatile organic solvent, 2011, *Nanotechnology* 22 (36), 365601. http://dx.doi.org/10.1088/0957-4484/22/36/365601.

(128) Ma, Z.; Yu, J. & Dai, S., Preparation of inorganic materials using ionic liquids, 2010, *Adv. Mater.* 22 (2), 261-285. https://doi.org/10.1002/adma.200900603.

(129) Liu, W.; Zhou, R.; Zhou, D.; Ding, G.; Soah, J. M.; Yue, C. Y. & Lu, X., Lignin-assisted direct exfoliation of graphite to graphene in aqueous media and its application in polymer composites, 2015, *Carbon* 83, 188-197. https://doi.org/10.1016/j.carbon.2014.11.036.

(130) Ismail, Z.; Kassim, N. F. A.; Abdullah, A. H.; Abidin, A. S. Z.; Ismail, F. S. & Yusoh, K., Black tea assisted exfoliation using a kitchen mixer allowing one-step production of graphene, 2017, *Mater. Res. Express* 4 (7), 075607. http://dx.doi.org/10.1088/2053-1591/aa7ae2.

(131) Ma, H.; Shen, Z.; Yi, M.; Ben, S.; Liang, S.; Liu, L.; Zhang, Y.; Zhang, X. & Ma, S., Direct exfoliation of graphite in water with addition of ammonia solution, 2017, *J. Colloid Interface Sci.* 503, 68-75. https://doi.org/10.1016/j.jcis.2017.04.070.

(132) Yi, M.; Shen, Z.; Liang, S.; Liu, L.; Zhang, X. & Ma, S., Water can stably disperse liquid-exfoliated graphene, 2013, *Chem. Commun.* 49 (94), 11059-11061. https://doi.org/10.1039/c3cc46457a.

(133) Lotya, M.; Hernandez, Y.; King, P. J.; Smith, R. J.; Nicolosi, V.; Karlsson, L. S.; Blighe, F. M.; De, S.; Wang, Z.; McGovern, I. T.; Duesberg, G. S. & Coleman, J. N., Liquid phase production of graphene by exfoliation of graphite in surfactant/water solutions, 2009, *J. Am. Chem. Soc.* 131 (10), 3611-3620. https://doi.org/10.1021/ja807449u.

(134) Kim, J.; Kwon, S.; Cho, D.-H.; Kang, B.; Kwon, H.; Kim, Y.; Park, S. O.; Jung, G. Y.; Shin, E.; Kim, W.-G. Lee, H., Ryu, G.H.; Choi, M.; Kim, T.H.; Oh, J., Park, S.; Kwak, S. K.; Yoon, S. W.; Byun, D.; Lee, Z. & Lee, C, Direct exfoliation, and dispersion of two-dimensional materials in pure water via temperature control, 2015, *Nat. Commun.* 6 (1), 1-9. https://doi.org/10.1038/ncomms9294.

(135) Li, X.; Zhu, Y.; Cai, W.; Borysiak, M.; Han, B.; Chen, D.; Piner, R. D.; Colombo, L. & Ruoff, R. S., Transfer of large-area graphene films for high-performance transparent conductive electrodes, 2009, *Nano Lett.* 9 (12), 4359-4363. https://doi.org/10.1021/nl902623y.

(136) Kim, K. S.; Zhao, Y.; Jang, H.; Lee, S. Y.; Kim, J. M.; Kim, K. S.; Ahn, J.-H.; Kim, P.; Choi, J.-Y. & Hong, B. H., Large-scale pattern growth of graphene films for stretchable transparent electrodes, 2009, Nature 457 (7230), 706-710. https://doi.org/10.1038/nature07719.

(137) Broderick, A. H.; Manna, U. & Lynn, D. M., Covalent layer-by-layer assembly of water-permeable and water-impermeable polymer multilayers on highly water-soluble and water-sensitive substrates, 2012, *Chem. Mater.* 24 (10), 1786-1795. https://doi.org/10.1021/cm300307g.

(138) Chen, M.; Li, G.; Li, W.; Stekovic, D.; Arkook, B.; Itkis, M. E.; Pekker, A.; Bekyarova, E. & Haddon, R. C., Large-scale cellulose-assisted transfer of graphene toward industrial applications, 2016, *Carbon* 110, 286-291. https://doi.org/10.1016/j.carbon.2016.09.029.

(139) Chen, M.; Stekovic, D.; Li, W.; Arkook, B.; Haddon, R. C. & Bekyarova, E., Sublimation-assisted graphene transfer technique based on small polyaromatic hydrocarbons, 2017, *Nanotechnology* 28 (25), 255701. http://dx.doi.org/10.1088/1361-6528/aa72d5.

(140) Zhang, G.; Güell, A. G.; Kirkman, P. M.; Lazenby, R. A.; Miller, T. S. & Unwin, P. R., Versatile polymer-free graphene transfer method and applications, 2016, *ACS Appl. Mater. Interfaces* 8 (12), 8008-8016. https://doi.org/10.1021/acsami.6b00681.

(141) Wang, S.; Qiao, L.; Zhao, C.; Zhang, X.; Chen, J.; Tian, H.; Zheng, W. & Han, Z., A growth mechanism for graphene deposited on polycrystalline co film by plasma enhanced chemical vapor deposition, 2013, *New J Chem* 37 (5), 1616-1622. http://dx.doi.org/10.1039/C3NJ41136B.

(142) Chen, M.; Haddon, R. C.; Yan, R. & Bekyarova, E., Advances in transferring chemical vapour deposition graphene: a review, 2017, *Mater. Horiz.* 4 (6), 1054-1063. http://dx.doi.org/10.1039/C7MH00485K.

(143) Lin, Y.-C.; Lu, C.-C.; Yeh, C.-H.; Jin, C.; Suenaga, K. & Chiu, P.-W., Graphene annealing: how clean can it be?, 2012, *Nano Lett.* 12 (1), 414-419. https://doi.org/10.1021/nl203733r.

(144) Jia, Y.; Gong, X.; Peng, P.; Wang, Z.; Tian, Z.; Ren, L.; Fu, Y. & Zhang, H., Toward high carrier mobility and low contact resistance: laser cleaning of PMMA residues on graphene surfaces, 2016, *Nano-Micro Lett.* 8 (4), 336-346. https://doi.org/10.1007/s40820-016-0093-5.

(145) Sun, J.; Finklea, H. O. & Liu, Y., Characterisation, and electrolytic cleaning of poly (methyl methacrylate) residues on transferred chemical vapor deposited graphene, 2017, *Nanotechnology* 28 (12), 125703. http://dx.doi.org/10.1088/1361-6528/aa5e55.

(146) Lin, W.-H.; Chen, T.-H.; Chang, J.-K.; Taur, J.-I.; Lo, Y.-Y.; Lee, W.-L.; Chang, C.-S.; Su, W.-B. & Wu, C.-I., A direct and polymer-free method for transferring graphene grown by chemical vapor deposition to any substrate, 2014, *ACS Nano* 8 (2), 1784-1791. https://doi.org/10.1021/nn406170d.

(147) Oren, S.; Ceylan, H.; Schnable, P. S. & Dong, L., High-resolution patterning and transferring of graphene-based nanomaterials onto tape toward roll-to-roll production of tape-based wearable sensors, 2017, *Adv. Mater. Technol.* 2, 1700223.https://doi.org/10.1002/admt.201700223.

(148) Pu, N.-W.; Wang, C.-A.; Liu, Y.-M.; Sung, Y.; Wang, D.-S. & Ger, M.-D., Dispersion of graphene in aqueous solutions with different types of surfactants and the production of graphene films by spray or drop coating, 2012, *J. Taiwan Inst. Chem. Eng.* 43 (1), 140-146. https://doi.org/10.1016/j.jtice.2011.06.012.

(149) Kymakis, E.; Stratakis, E.; Stylianakis, M.; Koudoumas, E. & Fotakis, C., Spin coated graphene films as the transparent electrode in organic photovoltaic devices. 2011, *Thin Solid Films*, 520 (4), 1238-1241. https://doi.org/10.1016/j.tsf.2011.04.208

(150) Liu, J.; Hua, L.; Li, S. & Yu, M., Graphene dip coatings: an effective anticorrosion barrier on aluminium, 2015, *Appl. Surf. Sci.* 327, 241-245. https://doi.org/10.1016/j.apsusc.2014.11.187.

(151) Gao, W. & Kono, J., Science and applications of wafer-scale crystalline carbon nanotube films prepared through controlled vacuum filtration, 2019, *R. Soc. Open Sci.* 6 (3), 181605. https://doi.org/10.1098/rsos.181605.

(152) Long, D. A., The Raman effect: a unified treatment of the theory of Raman scattering by molecules, 2002, Wiley, 1st ed., ISBN: 9780471490289.

(153) Raman, C. & Krishnan, K. A., New Type of Secondary Radiation, 1928, *Nature* 121, 501-502. https://doi.org/10.1038/121501c0.

(154) Malard, L. M.; Pimenta, M. A.; Dresselhaus, G. & Dresselhaus, M. S., Raman spectroscopy in graphene, 2009, *Phys Rep* 473, 51-87. https://doi.org/10.1016/j.physrep.2009.02.003.

(155) Ferrari, A. C. & Basko, D. M., Raman spectroscopy as a versatile tool for studying the properties of graphene, 2013, *Nat. Nanotechnol*., 235-246. https://doi.org/10.1038/nnano.2013.46.

(156) Ferrari, A. C.; Meyer, J.; Scardaci, V.; Casiraghi, C.; Lazzeri, M.; Mauri, F.; Piscanec, S.; Jiang, D.; Novoselov, K.; Roth, S. & Geim, A. K., Raman spectrum of graphene and graphene layers, 2006, *Phys. Rev. Lett.* 97 (18), 187401. https://doi.org/10.1103/PhysRevLett.97.187401.

(157) Pollard, A. J.; Paton, K. R.; Clifford, C. A. & Legge, E., Good Practice Guide No. 145 - Characterisation of the Structure of Graphene, 1st ed. National Physical Laboratory, 2017.

(158) Das, A.; Chakraborty, B. & Sood, A. K., Raman spectroscopy of graphene on different substrates and influence, 2008, 31, 579-584. https://doi.org/10.1007/s12034-008-0090-5.

(159) Ring, E.F.J., Progress in the measurement of human body temperature, 1998, *IEEE Eng. Med. Biol. Mag.* 17 (4), 19-24. https://doi.org/10.1109/51.687959.

(160) Bentley, J. P., Principles of measurement systems, 2005, Pearson education, 4th ed., ISBN: 0130430285.

(161) Ali, S.; Hassan, A.; Bae, J.; Lee, C. H. & Kim, J., All-printed differential temperature sensor for the compensation of bending effects, 2016, *Langmuir* 32, 11432-11439. https://doi.org/10.1021/acs.langmuir.6b02885.

(162) Rogers, J. A.; Someya, T. & Huang, Y., Materials, and mechanics for stretchable electronics, 2010, *Science* 327 (5973), 1603-1607. https://doi.org/10.1126/science.1182383.

(163) Kuzubasoglu, B. A. & Bahadir, S. K., Flexible temperature sensors: a review, 2020, *Sens. Actuators Phys.* 112282. https://doi.org/10.1016/j.sna.2020.112282.

(164) Tsao, L.-C.; Cheng, M.-Y.; Chen, I.-L.; Shih, W.-P.; Yang, Y.-J.; Chang, F.-Y.; Fan, K.-C. & Chang, S.-H., Flexible temperature sensor array using electro-resistive polymer for humanoid artificial skin, 2007, *TRANSDUCERS 2007-2007 International Solid-State Sensors, Actuators and Microsystems Conference, IEEE,* 2287-2290. https://doi.org/10.1109/SENSOR.2007.4300626.

(165) Yang, J.; Wei, D.; Tang, L.; Song, X.; Luo, W.; Chu, J.; Gao, T.; Shi, H. & Du, C., Wearable temperature sensor based on graphene nanowalls, 2015, *RSC Adv.* 5 (32), 25609-25615. https://doi.org/10.1039/C5RA00871A.

(166) Tian, H.; Shu, Y.; Cui, Y.-L.; Mi, W.-T.; Yang, Y.; Xie, D. & Ren, T.-L., Scalable fabrication of high-performance and flexible graphene strain sensors, 2014, *Nanoscale* 6 (2), 699-705. https://doi.org/10.1039/c3nr04521h.

(167) da Costa, T. H.; Song, E.; Tortorich, R. P. & Choi, J.-W., A paper-based electrochemical sensor using inkjet-printed carbon nanotube electrodes, 2015, *ECS J Solid State Sci Technol* 4, 3044-3047. http://dx.doi.org/10.1149/2.0121510jss.

(168) Stempien, Z.; Rybicki, E.; Rybicki, T. & Lesnikowski, J., Inkjet-printing deposition of silver electro-conductive layers on textile substrates at low sintering temperature by using an aqueous silver ions-containing ink for textronic applications, 2016, *Sens. Actuators B Chem.* 224, 714-725. https://doi.org/10.1016/j.snb.2015.10.074.

(169) Turkani, V. S.; Narakathu, B. B.; Maddipatla, D.; Altay, B. N.; Fleming, P. D.; Bazuin, B. J. & Atashbar, M. Z., Nickel based printed resistance temperature detector on flexible polyimide substrate, 2018, *IEEE Sensors,* 1-4. https://doi.org/10.1109/ICSENS.2018.8589549.

(170) Leppävuori, S.; Väänänen, J.; Lahti, M.; Remes, J. & Uusimäki, A., A novel thick-film technique, gravure offset printing, for the realization of fine-line sensor structures, 1994, *Sens. Actuators A Phys.* 42 (1-3), 593-596. https://doi.org/10.1016/0924-4247(94)80060-X.

(171) Courbat, J.; Kim, Y.; Briand, D. & de Rooij, N., Inkjet printing on paper for the realization of humidity and temperature sensors, 2011, 16th International Solid-State Sensors, Actuators and Microsystems Conference, *IEEE*, 1356-1359. https://doi.org/10.1109/TRANSDUCERS.2011.5969506.

(172) Dankoco, M. D.; Tesfay, G. Y.; Benevent, E. & Bendahan, M., Temperature sensor realized by inkjet printing process on flexible substrate, 2015, *Mater Sci Eng B Solid State Mater Adv Technol* 205, 1-5. https://doi.org/10.1016/j.mseb.2015.11.003.

(173) Li, D.; Sutton, D.; Burgess, A.; Graham, D. & Calvert, P. D., Conductive copper, and nickel lines via reactive inkjet printing, 2009, *J. Mater. Chem* 19 (22), 3719-3724. https://doi.org/10.1039/B820459D.

(174) Lee, J.-W.; Choi, Y.; Jang, J.; Yeom, S.-H.;. Lee, W. & Ju., B.-K., High sensitivity flexible paper temperature sensor and body-attachable patch for thermometers, 2020, *Sens. Actuators A: Phys*. 333, 112205. https://doi.org/10.1016/j.sna.2020.112205

(175) Jeon, J.; Lee, H.; Bao, Z., Flexible wireless temperature sensors based on Ni microparticle-filled binary polymer composites, 2013, *Adv. Mater.*, 25, 850-855. https://doi.org/10.1002/adma.201204082.

(176) Shih, W.-P.; Tsao, L.-C.; Lee, C.-W.; Cheng, M.-Y.; Chang, C.; Yang, Y.-J.& Fan, K.-C., Flexible temperature sensor array based on a graphite-

polydimethylsiloxane composite, 2010, *Sensors* 10 (4), 3597-3610. https://doi.org/10.3390/s100403597.

(177) Polanský, R.; Soukup, R.; Řeboun, J.; Kalčík, J.; Moravcová, D.; Kupka, L.; Švantner, M.; Honnerová, P. & Hamáček, A., A novel large-area embroidered temperature sensor based on an innovative hybrid resistive thread, 2017, *Sens. Actuators A Phys.* 265, 111-119. https://doi.org/10.1016/j.sna.2017.08.030.

(178) Bae, G. Y.; Han, J. T.; Lee, G.; Lee, S.; Kim, S. W.; Park, S.; Kwon, J.; Jung, S. & Cho, K., Pressure/temperature sensing bimodal electronic skin with stimulus discriminability and linear sensitivity, 2018, *Adv. Mater.* 30 (43), 1803388. https://doi.org/10.1002/adma.201803388.

(179) Neella, N.; Gaddam, V.; Rajanna, K. & Nayak, M. M., Negative temperature coefficient behaviour of graphene – silver nanocomposite films for temperature sensor applications, 2016, 11th Annual International Conference on Nano/Micro Engineered and Molecular Systems (NEMS), IEEE, 329-332. https://doi.org/10.1109/NEMS.2016.7758260.

(180) Hughes-Riley, T.; Lugoda, P.; Dias, T.; Trabi, C. L. & Morris, R. H., A study of thermistor performance within a textile structure, 2017, *Sensors* 17 (8), 1804. https://doi.org/10.3390/s17081804.

(181) Husain, M. D. & Kennon, R., Preliminary investigations into the development of textile-based temperature sensor for healthcare applications, 2013, *Fibres* 1 (1), 2-10. https://doi.org/10.3390/fib1010002.

(182) Ziegler, S. & Frydrysiak, M., Initial research into the structure and working conditions of textile thermocouples, 2009, *Fibres Text. East. Eur*, 17, 84-88.

(183) Rosace, G.; Trovato, V.; Colleoni, C.; Caldara, M.; Re, V.; Brucale, M.; Piperopoulos, E.; Mastronardo, E.; Milone, C.; De Luca, G. & Plutino, M. R., Structural and morphological characterizations of MWCNTs hybrid coating onto cotton fabric as potential humidity and temperature wearable sensor, 2017, *Sens. Actuators B Chem.* 252, 428-439. https://doi.org/10.1016/j.snb.2017.05.175.

(184) Hilal, M. & Han, J. I., Development of a highly flexible and durable fibre-shaped temperature sensor based on graphene/Ni double-decked layer for wearable devices, 2020, *IEEE Sens. J.* 20 (10), 5146-5154. https://doi.org/10.1109/JSEN.2020.2967347.

(185) Lowen, A. C.; Mubareka, S.; Steel, J. & Palese, P. Influenza virus transmission is dependent on relative humidity and temperature, 2007, *PLOS Pathog.* 3 (10): e151. https://doi.org/10.1371/journal.ppat.0030151.

(186) Hanhijärvi, A., Advances in the knowledge of the influence of moisture changes on the long-term mechanical performance of timber structures, 2000, *Mat. Struct.* 33, 43. https://doi.org/10.1007/bf02481695.

(187) Chen, Z. & Lu, C., Humidity sensors: a review of materials and mechanisms, , 2005, *Sens. Lett.* 3, 274-295. https://doi.org/10.1166/sl.2005.045.

(188) Khanna, V. & Nahar, R., Carrier-transfer mechanisms and Al_2O_3 sensors for low and high humidity, 1986, *J. Phys. Appl. Phys.* 19 (7), L141. https://doi.org/10.1088/0022-3727/19/7/004.

(189) Ahmad, S.; Husain, A.; Khan, M. M. A.; Khan, I.; Khan, A.; Khan, I.; Verpoort, F.; Khan, S.; Umar, A & Asiri, A. M., Perovskite-based material for sensor applications. In: Hybrid perovskite composite materials*, Woodhead Publishing,* 135-145, ISBN: 978-0-12-819977-0. https://doi.org/10.1016/B978-0-12-819977-0.00005-6.

(190) Korotcenkov, G. Humidity-sensitive materials. In: Handbook of gas sensor materials, 2013, *Springer* 389-408. ISBN: 978-1-4614-7165-3. https://doi.org/10.1007/978-1-4614-7165-3_18.

(191) Park, S. Y.; Lee, J. E.; Kim, Y. H.; Kim, J. J.; Shim, Y.-S.; Kim, S. Y.; Lee, M. H. & Jang, H. W., Room temperature humidity sensors based on rGo/MoS_2 hybrid composites synthesized by hydrothermal method, 2018, *Sens. Actuators B Chem.* 258, 775-782. https://doi.org/10.1016/j.snb.2017.11.176.

(192) Cao, C.; Hu, C.; Fang, L.; Wang, S.; Tian, Y. & Pan, C., Humidity sensor based on multi-walled carbon nanotube thin films, 2010, *J. Nanomater.* 2011, 707303. https://doi.org/10.1155/2011/707303.

(193) Popov, V. I.; Nikolaev, D. V.; Timofeev, V. B.; Smagulova, S. A. & Antonova, I. V., Graphene-based humidity sensors: the origin of alternating resistance change, 2017, *Nanotechnology* 28, 355501. https://doi.org/10.1088/1361-6528/aa7b6e.

(194) Feng, Y.; Gong, S.; Du, E.; Yu, K.; Ren, J.; Wang, Z. & Zhu, Z., TaS_2 nanosheet-based ultrafast response and flexible humidity sensor for multifunctional applications, 2019, *J. Mater. Chem. C* 7(30), 9284-9292. https://doi.org/10.1039/c9tc02785h.

(195) Zhou, C.; Zhang, X.; Tang, N.; Fang, Y.; Zhang, H. & Duan, X., Rapid response flexible humidity sensor for respiration monitoring using nano-confined strategy, 2020, *Nanotechnology* 31, 125302. https://doi.org/10.1088/1361-6528/ab5cda.

(196) Li, L.; Zhuang, C.; Ban, C.; Zhou, W. & Liu, X., Effective growth of pure long-straight boron nitride nanowires strain and application as flexible humidity

sensor, 2020, *IEEE Sens. J.* 20, 4063-4071. https://doi.org/10.1109/jsen.2019.2963684.

(197) Zhang, D.; Zong, X. & Wu, Z., Fabrication of tin disulfide/graphene oxide nanoflower on flexible substrate for ultrasensitive humidity sensing with ultralow hysteresis and good reversibility, 2019, *Sens. Actuators B Chem.* 287, 398-407. https://doi.org/10.1016/j.snb.2019.01.123.

(198) Soomro, A. M.; Jabbar, F.; Ali, M.; Lee, J. W.; Mun, S. W. & Choi, K. H., All-range flexible, and biocompatible humidity sensor based on poly lactic glycolic acid (PLGA) and its application in human breathing for wearable health monitoring, 2019, *J. Mater. Sci. Mater. Electron*. 30, 9455-9465. https://doi.org/10.1007/s10854-019-01277-1.

(199) Tang, H.; Li, Y.; Ye, H.; Hu, F.; Gao, C.; Tao, L.; Tu, T.; Gou, G.; Chen, X.; Fan, X.; Ren, T. & Zhang, G. High-performance humidity sensor using Schottky-contacted SNS nanoflakes for noncontact healthcare monitoring, 2020, *Nanotechnology* 31 (5), 055501. https://doi.org/10.1088/1361-6528/ab414e.

(200) Hajian, S.; Zhang, X.; Khakbaz, P.; Tabatabaei, S.-M.; Maddipatla, D.; Narakathu, B. B.; Blair, R. G. & Atashbar, M. Z., Development of a fluorinated graphene-based resistive humidity sensor, 2020, *IEEE Sens. J.* 20 (14), 7517-7524. https://doi.org/10.1109/JSEN.2020.2985055.

(201) Li, T.; Li, L.; Sun, H.; Xu, Y.; Wang, X.; Luo, H. & Liu, Z., Porous ionic membrane based flexible humidity sensor and its multifunctional applications, 2017, *Adv. Sci.* 4, 1600404. https://doi.org/10.1002/advs.201600404.

(202) Duan, Z.; Jiang, Y.; Yan, M.; Wang, S.; Yuan, Z.; Zhao, Q.; Sun, P.; Xie, G.; Du, X. & Tai, H., Facile, flexible, cost-saving, and environment-friendly paper-based humidity sensor for multifunctional applications, 2019, *ACS Appl. Mater. Interfaces* 11 (24), 21840-21849. https://doi.org/10.1021/acsami.9b05709.

(203) Yang, J.; Shi, R.; Lou, Z.; Chai, R.; Jiang, K. & Shen, G., Flexible smart noncontact control systems with ultrasensitive humidity sensors, 2019, *Small* 15 (38), 1902801. https://doi.org/10.1002/smll.201902801.

(204) Turkani, V. S.; Maddipatla, D.; Narakathu, B. B.; Saeed, T. S.; Obare, S. O.; Bazuin, B. J. & Atashbar, M. Z., A highly sensitive printed humidity sensor based on a functionalized MWCNT/HEC composite for flexible electronics application, 2019, *Nanoscale Adv.* 1 (6), 2311-2322. https://doi.org/10.1039/C9NA00179D.

(205) Wu, J.; Wu, Z.; Tao, K.; Liu, C.; Yang, B.-R.; Xie, X. & Lu, X. Rapid-response, reversible and flexible humidity sensing platform using a hydrophobic and

porous substrate, 2019, *J. Mater. Chem. B* 7 (12), 2063-2073. https://doi.org/10.1039/C8TB02963F.

(206) Wu, J.; Sun, Y. M.; Wu, Z.; Li, X.; Wang, N.; Tao, K. & Wang, G. P. Carbon nanocoil-based fast-response and flexible humidity sensor for multifunctional applications, 2019, *ACS Appl. Mater. Interfaces*, 11, 4242-4251. https://doi.org/10.1021/acsami.8b18599.

(207) Park, H.; Lee, S.; Jeong, S. H.; Jung, U. H.; Park, K.; Lee, M. G.; Kim, S. & Lee, J. Enhanced moisture-reactive hydrophilic-PTFE-based flexible humidity sensor for real-time monitoring, 2018, *Sensors* 18 (3), 921. https://doi.org/10.3390/s18030921.

(208) Zhu, P.; Liu, Y.; Fang, Z.; Kuang, Y.; Zhang, Y.; Peng, C. & Chen, G., Flexible and highly sensitive humidity sensor based on cellulose nanofibres and carbon nanotube composite film, 2019, *Langmuir* 35, 4834-4842. https://doi.org/10.1021/acs.langmuir.8b04259.

(209) Ma, L.; Wu, R.; Patil, A.; Zhu, S.; Meng, Z.; Meng, H.; Hou, C.; Zhang, Y.; Liu, Q.; Yu, R. Wang, J.; Lin, N. & Liu, X. Y., Full-textile wireless flexible humidity sensor for human physiological monitoring, 2019, *Adv. Funct. Mater.* 29 (43), 1904549. https://doi.org/10.1002/adfm.201904549.

(210) Razmand, R.; Dehkharghani, M. N.; Karimpour, A. & Hossein-Babaei, F., A graphene oxide-based humidity sensor for wearable electronic, 2019, *27th Iranian Conference on Electrical Engineering*, 423-426. https://doi.org/10.1109/IranianCEE.2019.8786557.

(211) Devaux, E.; Aubry, C.; Campagne, C. & Rochery, M., PLA / carbon nanotubes multifilament yarns for relative humidity textile sensor, 2011, *J. Eng. Fiber Fabr.* 6 (3), 13-24. http://dx.doi.org/10.1177/155892501100600302.

(212) Mattana, G.; Kinkeldei, T.; Leuenberger, D.; Ataman, C.; Ruan, J. J.; Molina-lopez, F.; Quintero, A. V.; Nisato, G.; Troster, G.; Briand, D. & de Rooji, N. F., Woven temperature and humidity sensors on flexible plastic substrates for e-textile applications, 2013, *IEEE Sens. J.* 13 (10), 3901-3909. https://doi.org/10.1109/JSEN.2013.2257167.

(213) Lv, C.; Hu, C.; Luo, J.; Liu, S.; Qiao, Y.; Zhang, Z.; Song, J.; Shi, Y.; Cai, J. & Watanabe, A., Recent advances in graphene-based humidity sensors., 2019, *Nanomaterials* 9 (3), 422. https://doi.org/10.3390/nano9030422.

(214) Li, X.; Zong, L.; Wu, X.; You, J.; Li, M. & Li, C., Biomimetic engineering of spider silk fibres with graphene for electric devices with humidity and motion sensitivity, 2018, *J. Mater. Chem. C* 6 (13), 3212-3219. https://doi.org/10.1039/C8TC00265G.

(215) Tarapata, G. & Jachowicz, R., Humidity sensor printed on textile with use of ink-jet technology humidity sensor printed on textile with use of ink-jet technology, 2012. https://doi.org/10.1016/j.proeng.2012.09.410.

(216) Zhang, J.; Shen, G.; Wang, W.; Zhou, X. & Guo, S., Individual nanocomposite sheets of chemically reduced graphene oxide and poly(N-vinyl pyrrolidone): preparation and humidity sensing characteristics, 2010, *J. Mater. Chem.* 20 (48), 10824-10828. https://doi.org/10.1039/C0JM02440F.

(217) Jha, R. K.; Burman, D.; Santra, S. & Guha, P. K., WS_2/GO nanohybrids for enhanced relative humidity sensing at room temperature, 2017, *IEEE Sens. J.* 17 (22), 7340-7347. https://doi.org/10.1109/JSEN.2017.2757243.

(218) https://Graphene-Supermarket.Com/Ten-Pack-100mm-4-in-Graphene-Film-on-Nickel.html (accessed on 20th January 2021).

(219) Biccai, S.; Barwich, S.; Boland, D.; Harvey, A.; Hanlon, D.; McEvoy, N. & Coleman, J. N., Exfoliation of 2D materials by high shear mixing, 2018, *2D Mater.* 6 (1), 015008. http://dx.doi.org/10.1088/2053-1583/aae7e3.

(220) https://www.Graphenea.Com/Collections/Graphene-Oxide/Products/Graphene-Oxide-Powder (accessed on 28th March 2021).

(221) Klapetek, P., Quantitative data processing in scanning probe microscopy: SPM applications for nanometrology, 2018, *Elsevier*, 2nd ed. ISBN: 9780128133484.

(222) Horcas, I. & Fernández, R., A. WSXM: a software for scanning probe microscopy and a tool for nanotechnology, 2007, *Rev. Sci. Instrum.* 78 (1), 013705. https://doi.org/10.1063/1.2432410.

(223) https://www.Azooptics.Com/Article.Aspx?ArticleID=823 (accessed on 6th February 2021).

(224) Zhu, S.-E.; Yuan, S. & Janssen, G. Optical transmittance of multilayer graphene, 2014, *EPL (Europhys. Lett.)* 108 (1), 17007. https://doi.org/10.1209/0295-5075/108/17007.

(225) De Sanctis, A.; Jones, G. F.; Townsend, N. J.; Craciun, M. F. & Russo, S., An integrated and multi-purpose microscope for the characterization of atomically thin optoelectronic devices, 2017, *Rev. Sci. Instrum.* 88 (5), 055102. https://doi.org/10.1063/1.4982358.

(226) Bointon, T. H.; Barnes, M. D.; Russo, S. & Craciun, M. F., High quality monolayer graphene synthesized by resistive heating cold wall chemical vapour deposition, 2015, *Adv. Mater.* 27, 4200-4206. https://doi.org/10.1002/adma.201501600.

(227) Ta, H. Q.; Perello, D. J.; Duong, D. L.; Han, G. H.; Gorantla, S.; Nguyen, V. L.; Bachmatiuk, A.; Rotkin, S. V.; Lee, Y. H. & Rümmeli, M. H., Stranski-Krastanov and Volmer-Weber CVD growth regimes to control the stacking order in bilayer graphene, 2016, *Nano Lett.* 16 (10), 6403-6410. https://doi.org/10.1021/acs.nanolett.6b02826.

(228) Koh, Y. K.; Bae, M. H.; Cahill, D. G. & Pop, E., Reliably counting atomic planes of few-layer graphene (n > 4) , 2011, *ACS Nano* 5, 269-274. https://doi.org/10.1021/nn102658a.

(229) Rajan, G.; Morgan, J. J.; Murphy, C.; Torres Alonso, E.; Wade, J.; Ott, A. K.; Russo, S.; Alves, H.; Craciun, M. F. & Neves, A. I. S., Low operating voltage carbon-graphene hybrid e-textile for temperature sensing, 2020, *ACS Appl. Mater. Interfaces* 12 (26), 29861-29867. https://doi.org/10.1021/acsami.0c08397.

(230) Jhang, S. H.; Craciun, M. F.; Schmidmeier, S.; Tokumitsu, S.; Russo, S.; Yamamoto, M.; Skourski, Y.; Wosnitza, J.; Tarucha, S.; Eroms, J.; Strunk, C., Stacking-order dependent transport properties of trilayer graphene, 2011, *Phys. Rev. B* 84, 161408. https://doi.org/10.1103/PhysRevB.84.161408.

(231) Russo, S.; Craciun, M.; Yamamoto, M.; Morpurgo, A. & Tarucha, S. Contact resistance in graphene-based devices, 2010, *Phys. E Low-Dimens. Syst. Nanostructures* 42 (4), 677-679. https://doi.org/10.1016/j.physe.2009.11.080.

(232) https://www.Hallcrest.Com/Products/Healthcare-Thermometers/Forehead-Anesthesia/Clinitrend (accessed on 5th March 2021).

(233) Press, S & Quinn, B.J., The pacifier thermometer: comparison of supralingual with rectal temperatures in infants and young children, 1997, *Arch Pediatr Adolesc Med.* 151:551-4. https://doi.org/10.1001/archpedi.1997.02170430017003.

(234) https://www.Cardinalhealth.Com/En/Product-Solutions/Medical/Patient-Monitoring/Thermometry/Genius-3/Genius-3-Tympanic-Thermometer.Html (accessed on 5th March 2021).

(235) Arman Kuzubasoglu, B. & Kursun Bahadir, S., Flexible temperature sensors: a review, 2020, *Sens. Actuator A Phys.* 315, 112282. https://doi.org/10.1016/j.sna.2020.112282.

(236) Pasquini, N., Polypropylene handbook, 2015, 2nd ed., *Hanser,* ISBN 3446229787.

(237) Maier, C., & Calafut, T., *Polypropylene: the definitive user's guide and databook*, revised ed., 1996, William Andrew, ISBN: 9780815518716.

(238) Kanzaki, K.; Hibino, H. & Makimoto, T., Graphene layer formation on polycrystalline nickel grown by chemical vapor deposition, 2013, *JJAP* 52 (3), 5103. http://dx.doi.org/10.7567/JJAP.52.035103.

(239) Shao, Q.; Liu, G.; Teweldebrhan, D. & Balandin, A. A., High-temperature quenching of electrical resistance in graphene, 2008, *Appl. Phys. Lett.* 92, 202108. https://doi.org/10.1063/1.2927371.

(240) Di Bartolomeo, A.; Sarno, M.; Giubileo, F.; Altavilla, C.; Iemmo, L.; Piano, S.; Bobba, F.; Longobardi, M.; Scarfato, A.; Sannino, D. Cucolo, A. M. & Ciambelli, P., Multiwalled carbon nanotube films as small-sized temperature sensors, 2009, *J. Appl. Phys.* 105 (6), 064518. https://doi.org/10.1063/1.3093680.

(241) Kong, D.; Le, L. T.; Li, Y.; Zunino, J. L. & Lee, W., Temperature-dependent electrical properties of graphene inkjet-printed on flexible materials, 2012, *Langmuir* 28, 13467-13472. https://doi.org/10.1021/la301775d.

(242) Kumar, S.; Bhatt, K.; Kumar, P.; Sharma, S.; Kumar, A. & Tripathi, C. C., Laser patterned, high-power graphene paper resistor with dual temperature coefficient of resistance, 2019, *RSC Adv.* 2019, 8262−8270. https://doi.org/10.1039/C8RA10246E.

(243) Calizo, I.; Balandin, A. A.; Bao, W.; Miao, F. & Lau, C. N., Temperature dependence of the Raman spectra of graphene and graphene multilayers, 2007, *Nano Lett.* 7 (9), 2645-2649. https://doi.org/10.1021/nl071033g.

(244) Dai, J.; Zhao, H.; Lin, X.; Liu, S.; Liu, Y.; Liu, X.; Fei, T. & Zhang, T., Ultrafast response polyelectrolyte humidity sensor for respiration monitoring, 2019, *ACS Appl. Mater. Interfaces* 2019, 11 (6), 6483-6490. https://doi.org/10.1021/acsami.8b18904.

(245) Liang, R.; Luo, A.; Zhang, Z.; Li, Z.; Han, C. & Wu, W. Progress of graphene-based flexible humidity sensor, 2020, *Sensors* 20 (19), 5601. https://doi.org/10.3390/s20195601. Research

(246) Chen, M. C.; Hsu, C. L. & Hsueh, T. J. Fabrication of humidity sensor based on bilayer graphene, 2014, *IEEE Electron. Device Lett.* 35, 590-592. https://doi.org/10.1109/LED.2014.2310741.

(247) Son, Y. J.; Chun, K. Y.; Kim, J. S.; Lee, J. H. & Han, C. S., Effects of chemical and physical defects on the humidity sensitivity of graphene surface, 2017, *Chem. Phys. Lett.* 689, 206-211. https://doi.org/10.1016/j.cplett.2017.10.028.

(248) Liu, L.; Qing, M.; Wang, Y. & Chen,S., Defects in Graphene: Generation, Healing, and Their Effects on the Properties of Graphene: A Review, 2015, *J. mater. sci. technol.* https://doi.org/10.1016/j.jmst.2014.11.019.

(249) Pu, J. et al. Chemical Vapor Deposition of Few-Layer Graphene for Transparent Conductive Films, 2015, *RSC Adv.* 5, 44142–44148. https://doi.org/10.1039/C5RA03919C

(250)

(251) https://www.analog.com/en/index.html (accessed on 11th December 2021)

(252) https://www.ti.com/product/LM94021 (accessed on 11th December 2021)

(253) https://sps.honeywell.com/us/en/products/sensing-and-iot/sensors/humidity-with-temperature-sensors/hih-5030-5031-series (accessed on 11th December 2021)

(254)https://www.ti.com/lit/ds/symlink/hdc3020.pdf?ts=1639238779928&ref_url=https%253A%252F%252Fwww.ecosia.org%252F (accessed on 11th December 2021)

(255) Maier,G. and Calafut T., Polypropylene: The Definitive User's Guide and Databook, ISBN 978-1-884207-58-7

(256) Xu, J.; Dang, D.K.; Tran, V.T. *et al.* Liquid-phase exfoliation of graphene in organic solvents with addition of naphthalene, 2014, *Journal of Colloid and Interface Science* 418, 37-42

(257) Smallwood, I.M., Handbook of Organic Solvent Properties, 1996*, Butterworth-Heinemann,* ISBN- 978-0-08-052378-1. https://doi.org/10.1016/C2009-0-23646-4

(258) Kozbial, A.; Zhou, F.; Li, Z.; Liu, H. & Li, L. Are Graphitic Surfaces Hydrophobic? 2016, *Acc Chem Res* 20;49 (12):2765-2773. https://doi.org/10.1021/acs.accounts.6b00447.

(259) Hansora, D.P.; Shimpi, N.G. & Mishra, S. Graphite to Graphene via Graphene Oxide: An Overview on Synthesis, Properties, and Applications, 2015, *JOM* 67, 2855–2868. https://doi.org/10.1007/s11837-015-1522-5.

(260) Shibayama, M.; Imamura, K.; Katoh, K. & Nomura S. Transparency of recycled polypropylene film, 1991, *J. Appl. Polym. Sci.* 42(5), 1451-1458.

(261) Fang, Jian & Zhang, Li & Sutton, David & Wang, Xungai & Lin, Tong, Needleless Melt-Electrospinning of Polypropylene Nanofibres, 2012, *J. Nanomater* https://doi.org/10.1155/2012/382639.

(262) Fatemeh, F. *et al. Recent Developments in Graphene and Graphene Oxide: Properties, Synthesis, and Modifications: A Review. ChemistrySelect.* 5(33), *10200-10219.* https://doi:10.1002/slct.202002501.

(263) Çakır, O., Temel, H. and Murat, K., Chemical etching of Cu-ETP copper, *J Mater Process tech.* 162, 275-279. https://doi.org/10.1016/j.jmatprotec.2005.02.035.

(264) Bae, J-W.; Kim, M-J. & Seo, J-H., Wet Etching Behavior of Amorphous CuZr Thin Film in Hydrogen Peroxide Solution for Stretchable Display, 2021, *ECS J. Solid State Sci. Technol.* 10 056005.

(265) Çakır, O., Review of Etchants for Copper and its Alloys in Wet Etching Processes, 2008, *Key Eng Mater,* 364-366, 460-465. https://doi.org/10.4028/www.scientific.net/kem.364-366.460.

(266) Liu, Y., Liu, Z., Lew, W.S. et al. Temperature dependence of the electrical transport properties in few-layer graphene interconnects, 2013, *Nanoscale Res Lett* 8, 335. https://doi.org/10.1186/1556-276X-8-335

(267) Liu, L.; Qing, M.; Wang, Y.; Chen, S. Defects in Graphene: Generation, Healing, and Their Effects on the Properties of Graphene: A Review 2015*, J. mater. sci. technol.*, 31(6), 599-606. https://doi/10.1016/j.jmst.2014.11.019.